Development and application of a selected configuration interaction method : from dispersive interactions to photo-induced magnetism in Prussian blue analogues

Tim Krah

UNIVERSITÉ DE STRASBOURG

ÉCOLE DOCTORALE DE SCIENCES CHIMIQUES

Institut de Chimie UMR 7177

THÈSE présentée par :

Tim KRAH

soutenue le : **24 septembre 2014**

pour obtenir le grade de : **Docteur de l'université de Strasbourg**

Discipline / Spécialité : Chimie / Chimie Théorique

Development and application of a selected Configuration Interaction method : from dispersive interactions to photo-induced magnetism in Prussian Blue Analogues

THÈSE dirigée par :

M. ROBERT Vincent	Professeur, Université de Strasbourg

RAPPORTEURS :

M. ANGELI Celestino	Assistant Professor, Università di Ferrara, Italie
Mme CALZADO Carmen	Professeur, Universidad de Sevilla, Espagne

AUTRES MEMBRES DU JURY :

M. FERRE Nicolas	Professeur, Aix-Marseille Université
M. DE GRAAF Coen	Professeur, Universitat Rovira i Virgili, Tarragona, Espagne
M. MARQUARDT Roberto	Professeur, Université de Strasbourg

Mme BEN AMOR Nadia	Chargée de recherches, Université Paul Sabatier, Toulouse

Contents

Résumé - French abstract

Cette thèse comporte deux aspects principaux. D'un côté, elle utilise des méthodes de calcul ab initio existantes afin de fournir des éléments de résultats pour les problèmes de structure électronique difficilement accessibles aux expériences. De l'autre côté, elle propose une méthode, implémentée et évaluée, dans le but de surmonter certaines difficultés informatique et de gagner une vision claire des phénomènes physiques.

1 Méthodes

Au centre d'un grand nombre d'approches théoriques de chimie quantique est l'équation de Schrödinger non-relativiste et indépendante du temps

$$\hat{H}\left|\Psi\right\rangle = \varepsilon\left|\Psi\right\rangle \tag{0.1}$$

où Ψ est la fonction d'onde décrivant un système à N électrons et M noyaux. L'opérateur hamiltonien $\hat{H}$ s'écrit

$$\hat{H} = -\sum_{i=1}^{N}\frac{1}{2}\nabla_i^2 - \sum_{i=1}^{N}\sum_{A=1}^{M}\frac{Z_A}{r_{iA}} + \sum_{i=1}^{N}\sum_{j>i}^{N}\frac{1}{r_{ij}} - \sum_{A=1}^{M}\frac{1}{2M_A}\nabla_A^2 + \sum_{A=1}^{M}\sum_{B>A}^{M}\frac{Z_A Z_B}{R_{AB}} \tag{0.2}$$

où Z_A est le numéro atomique du noyau A, r_{iA} la distance entre l'électron i et le noyau A et r_{ij} la distance entre les électrons i et j, M_A est la masse du noyau A par rappport à la masse d'un électron et R_{AB} est la distance entre les noyaux A et B. Le premier terme concerne l'énergie cinétique des électrons, le deuxième son attraction coulombienne au noyau A et le troisième la répulsion électron-électron. Les deux derniers sont analogues aux termes 1 et 3 pour les noyaux. L'approximation de *Born-Oppenheimer* permet la suppression de l'énergie cinétique des noyaux dans

eq. (0.1). La répulsion noyau-noyau est ensuite rajoutée comme une constante à l'énergie électronique pour un jeu de coordonnées nucléaires donné.

Malgré cette simplification, le problème électronique à N électrons n'a pas de solution analytique sauf pour les hydrogénoïdes en raison du terme r_{ij}^{-1} qui décrit l'interaction explicite des électrons. Cette interaction est telle que, *à chaque instant* l'énergie d'un électron dépend des positions des autres électrons, et non pas de leur position moyenne. Cette interaction dite "*corrélation électronique*" est un élément crucial. Les méthodes utilisées et implémentées dans ce travail cherchent à décrire la corrélation électronique de manière approximative.

1.1 La méthode *Hartree-Fock*

L'objectif de la plupart des méthodes *ab initio* est d'obtenir une approximation aussi bonne que possible à la fonction d'onde Ψ dans eq. (0.1). La méthode de Hartree-Fock (HF) ou du *champ auto-cohérent* (*self-consistent field, SCF*) est une méthode de champ moyen, c'est-à-dire que chaque électron est considéré comme évoluant dans le champ moyen des autres. Les fluctuations instantanées autour de ce champ moyen ne sont pas prises en compte.

Dans la méthode Hartree-Fock, la fonction d'onde est construite comme un seul déterminant de *Slater*. Celui-ci est un produit de spin-orbitales, anti-symmétrisé pour respecter le principe de *Pauli*. Les spin-orbitales φ^a constituant le déterminant Ψ^{HF} sont développées sur les orbitales atomiques ϕ_i avec des coefficients c_i^a de l'orbitale atomique i dans la spin-orbitale a,

$$\varphi^{\mathrm{a}} = \sum_i c_i^a \phi_i \tag{0.3}$$

L'approche de Hartree et Fock vise à optimiser la fonction d'onde à travers les coefficients c_i^a de manière itérative à partir d'un jeu d'orbitales d'essai. Dans ce processus, chaque électron est considéré dans le champ moyen des $(N-1)$ autres électrons. La fonction d'onde ainsi optimisée décrit l'état fondamental par un seul déterminant.

1.2 Interaction de configurations

Les méthodes post-HF prennent en compte la corrélation électronique qui se distingue formellement en deux types : la corrélation *dynamique* provient de l'interaction instantanée des électrons discutée en sec. 1 et la corrélation *non-dynamique* ou *statique* a son origine dans une vraie ou quasi-dégénérescence des orbitales.

L'approche d'*interaction de configurations* (IC) prend en compte la corrélation dynamique par développement de la fonction d'onde Ψ,

$$\Psi = c_0\Psi^0 + \sum_{pa} c_a^p \Psi_a^p + \sum_{\substack{a<b\\p<q}} c_{ab}^{pq}\Psi_{ab}^{pq} + \sum_{\substack{a<b<c\\p<q<r}} c_{abc}^{pqr}\Psi_{abc}^{pqr} + \dots \tag{0.4}$$

sur les déterminants mono- (Ψ_a^p), di- (Ψ_{ab}^{pq}), tri-excités (Ψ_{abc}^{pqr}) par rapport à une fonction de référence Ψ^0. La fonction d'onde est optimisée à travers les coefficients $\{ c_0, c_a^p, c_{ab}^{pq}, \dots \}$.

Si tous les déterminants possibles sont inclus dans l'expansion de la fonction d'onde, on parle de l'IC complète (*full* CI, FCI). L'énergie totale E_{FCI} associée à cette fonction d'onde, $E_{\mathrm{FCI}} = \langle \Psi^{\mathrm{FCI}} | \hat{H} | \Psi^{\mathrm{FCI}} \rangle$, est la plus basse possible pour une base d'orbitales donnée. La fonction d'onde connaît donc deux descriptions extrêmes : par un seul déterminant (SCF) ou par tous les déterminants possibles (FCI).

L'IC est une méthode variationelle, c'est-à-dire que l'énergie d'une fonction d'onde tronquée sera toujours plus haute que l'énergie exacte.

IC mono-référentielle.

L'espace de référence Ψ^0 dans l'eq. (0.4) peut avoir différents contenus. Si il s'agit de la fonction mono-déterminantale d'un calcul HF, l'IC est de type *mono-référentielle*. Des descriptions intermédiaires entre les deux extrêmes SCF et FCI sont obtenues si un degré maximal d'excitation est imposé. Par exemple, dans l'IC des mono-excitations (IC des simples, ICS) les déterminants mono-excités par rapport à Ψ_0 sont ajoutés à l'espace de référence. Il s'agit des mono- et di-excitations dans le cas de l'ICSD et ainsi de suite. L'énergie totale E_{SD}, par exemple, de la fonction d'onde ICSD est $E_{SD} = \langle \Psi^{\mathrm{SD}} | \hat{H} | \Psi^{\mathrm{SD}} \rangle$.

IC multi-référentielle.

Il existe également la possibilité d'utiliser un espace de référence Ψ_0 autre que l'espace mono-déterminantal Ψ_{HF}. Les considérations sur l'énergie et la troncature des excitations restent inchangées sauf que maintenant l'espace de référence est lui-même multi-déterminantal. Dans ce cas, on parle d'un calcul d'IC multi-référence (*multi-reference CI*, MR-CI).

Au delà d'un espace de références complet (complete active space, CAS), la sélection de déterminants de référence peut être divers. Il est également possible d'inclure les déterminants de l'IC individuellement. Dans ce travail, c'est la proximité spatiale des orbitales qui sera utilisée pour générer l'espace de l'IC.

Difference dedicated CI.

L'investigation des systèmes magnétiques a stimulé l'implémentation d'une méthode MR-CI appelée *Difference dedicated CI* (DDCI) [1]. Elle correspond à une méthode ICSD d'un coût de calcul réduit grâce à une exclusion judicieuse de la classe d'excitations 2h2p (double excitation des orbitales inactives vers les virtuelles).

Malrieu *et al.* ont montré au deuxième ordre des perturbations, que les énergies de l'état fondamental et de l'état excité sont abaissées de la même manière par les excitations 2h2p. Néanmoins, la suppression systématique des excitations nombreuses suppose un même jeu d'orbitales pour décrire l'état fondamental et l'état excité.

1.3 Complete Active Space SCF

Dans la méthode de l'*espace actif complet SCF* (*complete active space SCF*, CASSCF),[2] la fonction d'onde, Ψ^{CASSCF} est développée sur tous les déterminants Ψ^I appartenant à l'espace actif complet et associés aux coefficients c_I,

$$\Psi^{\text{CASSCF}} = \sum_{I \epsilon CAS} c_I \Psi^I \tag{0.5}$$

L'ensemble des orbitales est divisé en trois groupes qui se distinguent par les nombres d'occupation n qui leur sont imposés : orbitales *inactives* ($n = 2$), *virtuelles* ($n = 0$) et *actives* ($0 \leq n \leq 2$). L'espace actif complet (CAS), correspond à l'ensemble des possibles déterminants des électrons actives dans les orbitales actives qui respectent une multiplicité de spin et une symétrie spatiale données. Dans *tous* les déterminants du CAS, les orbitales *inactives* seront doublement occupées et les *virtuelles* seront vacantes. Un bon choix du CAS est nécessaire afin de capturer la physique du phénomène inspecté.

Le calcul CASSCF optimise à la fois les coefficients c_I des déterminants du CAS selon l'approche d'IC et les coefficients c_i^a des orbitales actives selon l'approche SCF.

Par le calcul CASSCF, la corrélation non-dynamique, est introduite dans la fonction d'onde. Le traitement de la corrélation dynamique nécessite un calcul ultérieur, tel que l'IC.

1.4 CAS + théorie de perturbations de deuxième ordre

Dans les théories de perturbation, l'hamiltonien exact $\hat{H}$ est découpé en un hamiltonien d'ordre zéro $\hat{H}_0$, dont les fonctions et valeurs propres sont connues et une perturbation $\hat{V}$,

$$\hat{H} = \hat{H}_0 + \hat{V} \tag{0.6}$$

Ce découpage est valable tant que la perturbation reste petite par rapport à la solution exacte connue. La fonction d'ordre zéro peut être une fonction mono-déterminantale de type SCF ou multi-configurationelle (*i.e.* CASSCF). Dans le dernier cas on parle de

théorie des perturbations de deuxième ordre avec une fonction de référence CAS : *second order perturbation theory with a CAS reference function*, (CASPT2) [3, 4] ou *n-electron valence state PT2*, (NEVPT2). [5–7] Contrairement aux autres méthodes présentées précédemment, les méthodes CASPT2 et NEVPT2 ne sont pas variationelles mais elles présentent des contraintes moins fortes vis-à-vis de la taille du système traité.

2 Développement et implémentation d'un code MR-CI

Les méthodes *ab initio* répandues atteignent rapidement les limites computationelles face à certains systèmes moléculaires étendus, tel que par exemple l'architecture polymétallique des Analogues de Bleu de Prusse (*Prussian Blue Analogues*, PBA).

Pour le représentant CoFe de cette famille, par exemple, un espace actif de l'ordre de 24 électrons dans 28 orbitales est nécessaire pour un traitement CASSCF/CASPT2 de la partie bi-métallique physiquement importante. Un traitement d'un espace actif de cette taille est ingérable. Ce constat, réalisé sur d'autres systèmes, a motivé la quête méthodologique aux alternatives.

Les méthodes de type MRCI se basent sur le constat que la matrice hamiltonienne du full CI contient beaucoup d'éléments de matrice $\langle \phi_i | \hat{H} | \phi_j \rangle$ d'une valeur proche de zéro. Autrement dit, une majorité des déterminants inclus dans le calcul a un poids négligeable dans l'expansion de la fonction d'onde. Les méthodes MRCI visent donc à limiter le nombre de déterminants à ceux d'un poids non-négligeable et donc d'une certaine importance pour le phénomène étudié. Afin de judicieusement trier les déterminants, on peut utiliser la nature locale de la corrélation électronique. Dans ce sens, les excitations entre des orbitales lointaines auront un poids plus faible que celles impliquant des orbitales spatialement proches. Une distinction spatiale est facile quand on utilise des orbitales moléculaires localisées (*localized molecular orbitals*, LMO).

La méthode implémentée et appliquée avec succès dans ce travail exploite le caractère spatial restreint des LMOs dans une approche MRCI afin de (*i*) réduire le coût de calcul pour pouvoir traiter des grands systèmes moléculaires tels que les PBA, et (*ii*) analyser systématiquement la contribution énergétique de différents types d'excitations et ainsi déduire leur importance physique dans le système inspecté.

En pratique, les déterminants moléculaires sont construits comme des combinaisons de déterminants de *fragments*. Un fragment correspond à un groupement de LMOs et à chacun sont associés un certain nombre d'électrons et un nombre maximal d'excitations *à l'intérieur* de ce fragment. Les déterminants moléculaires de référence sont des combinaisons de déterminants de fragments qui respectent les nombres d'excitations *entre* les fragments et une multiplicité de spin et une symétrie spatiale préalablement définis. Les différentes restrictions qui définissent l'espace de références, à savoir le nombre de fragments et les nombres d'excitations *intra*-et *inter*-fragment, peuvent être librement choisis en fonction du système inspecté.

Dans cet espace de déterminants de référence, tous les éléments de matrice de type

$\langle \phi_i | \hat{H} | \phi_j \rangle$ entre deux déterminants i et j sont évalués et la matrice est diagonalisée afin de trouver les coefficients c_i dans l'expansion $\Psi = \sum_i c_i \phi_i$ de la fonction d'onde en déterminants ϕ_i.

Une procédure d'adressage a été mise en place afin d'accélérer l'évaluation des éléments de matrice. Cette procédure permet d'adresser de manière ciblée les déterminants nécessaires.

3 Transition de spin dans le CoFe Analogue de Bleu de Prusse

Depuis les années 90 la famille des analogues du Bleu de Prusse (PBA) attire l'attention par ces propriétés électroniques intéressantes. Les membres de cette famille sont constitués de métaux M et M' (M,M'=V,Cr,Mn,Fe,Co,Ni) liés par des ponts cyano dans un réseau cubique faces centrées. Des ions alcalins sont intercalés dans la structure sur les sites tétraédriques et mènent à la présence de lacunes en $[Fe(CN)_6]^{-4}$, comblées par des molécules d'eau cristallines. Au même titre que la distribution des lacunes, celle des ions alcalins dans le cristal entier semble aléatoire.

Le composé dans lequel M=Co et M'=Fe présente un effet dit *photomagnétique* qui consiste en une transition d'un état fondamental *diamagnétique* [Co(t_{2g}^6)-NC-Fe(t_{2g}^6)] à un état *ferrimagnétique* [Co($t_{2g}^5 e_g^2$)-NC-Fe(t_{2g}^5)]. [8] Ce processus complexe peut être formellement décomposé en (*i*) un transfert d'électron du Fe(d^6) au Co(d^6), et (*ii*) une transition bas-spin (BS) → haut-spin (HS) sur l'ion métallique cobalt. Néanmoins, cette distinction est uniquement formelle et les deux processus physiques sont liés, voire même déclencheurs mutuels. De plus, des effets chimiques sont présents, telle que la composition variable de la sphère de coordination en fonction du nombre de lacunes, ou le nombre variable d'ions alcalins dans les sites tétraédriques. Un traitement de l'unité bi-métallique Co-NC-Fe et ses ligands respectifs est en dehors des possibilités computationelles. Un découpage du système et des effets inspectés est donc incontournable. Dans cet esprit, j'ai mené une inspection de la transition BS-HS sur l'ion Co(III) et des dépendances chimico-structurales. [9]

La corrélation non-dynamique et dynamique ont été traitées par des calculs CAS(10,12)SCF et des calculs PT2 consécutifs.

L'approche répandue *embedded cluster* a été employée : l'unité $[Co(NC)_5(OH_2)]^{-2}$ a été définie comme cluster et traité de manière précise. Celui-ci a été émergé dans un bain de *potentiels ioniques complets* (total ion potentials, TIP) [10, 11] et de charges ponctuelles formelles [*i.e.* Co(+3),Fe(+2),N/C(-0.5)] afin de prendre en compte les principaux effets cristallins de longue et courte portée. Des études expérimentales estiment que, en moyenne, deux sites tétraédriques par maille sont occupés par des ions alcalins Rb^+. Néanmoins, leur distribution à travers la totalité du cristal est aléatoire. Dans un premier temps, les ions Rb^+ ont donc été représentés par des charges partielles de +0,25 dans *tous* les sites tétraédriques afin de prendre en compte

l'effet d'une moyenne de 2 ions par maille.

Dans une première partie, deux paramètres de modélisation de l'environnement ont été optimisés, à savoir l'extension des charges ponctuelles et la distance de liaison Co-N. Ce deuxième a été considéré comme une variation géométrique pertinente car il a été montré expérimentalement que les changements géométriques de l'unité $[Fe(CN)_6]^{-4}$ pendant le processus photomagnétique sont négligeables. La modélisation des charges de l'environnement a été convergé par rapport aux énergies spectroscopiques (jusqu'à environ 20000 cm^{-1}) pour un cube de charges de 40Å de longueur (*i.e.* 4 fois le paramètre de maille a_0) autour du modèle central. Ensuite, la distance d(Co-N) a été modifiée à travers l'environnement complet en gardant une structure cubique faces centrées et des unités $[Fe(CN)_6]^{-4}$ rigides. Cette variation correspond ainsi à une variation du paramètre de maille a_0. Il a été optimisé par rapport aux énérgies des états BS et HS. La différence de $0,26$Å des valeurs obtenu pour l'état BS (d(Co-N)= $1,975$Å ; $a_0(BS)$ = $10,11$Å) et l'état HS (d(Co-N)= $2,11$Å ; $a_0(HS)$ = $10,37$Å) est en adéquation avec l'observation expérimentale d'une extension de la maille d'environ $0,33$Å au cours du processus photomagnétique.

Dans la deuxième partie de cette inspection j'ai mis en évidence une déformation du cluster $[Co(NC)_5(OH_2)]^{-2}$ induite par la lacune voisine. Celle-ci est supposée permettre une relaxation géométrique du cluster lors de la transition de spin. Deux paramètres structuraux dans l'axe Co-O ont donc été jugés pertinents : la distance d de liaison cobalt oxygène et la hauteur z de l'ion métallique par rapport au plan équatorial. Les minima en z des deux états ont été trouvés à des valeurs négatives de z=-0,15Å, ainsi le cobalt est dans sa position d'équilibre hors du plan équatorial près du ligand cyano axial. Dans une interprétation électrostatique, cette déviation de la structure octaédrique est le résultat de la présence de la lacune et de la distribution asymmétrique de charge associée. L'allongement de la distance d (BS : $1,97$Å → HS : $2,27$Å) reflète l'expansion de la sphère de coordination dans un environnement gelé.

Finalement, j'ai étudié l'influence de différentes distributions d'ions Rb^+ dans les sites tétraédriques à proximité immédiate du Co(III). Au total, huit distributions ont été choisies pour des raisons de symétrie et de répulsion minimale entre les Rb^+. Les valeurs des charges ponctuelles [+0,25 ;+0,5 ;+1,0] ont toujours été adaptées aux nombres d'ions Rb^+ [8 ;4 ;2] pour simuler une charge totale de +2 dans la maille. L'analyse des minima de d et z pour chaque distribution montre la même préférence du Co(III) pour le régime $z < 0$ dans les deux états BS et HS. Toutes les valeurs énergétiques et structurales sont qualitativement indépendantes du nombre et des positions des Rb^+.

Une déformation de la structure octaédrique induite par la lacune est supposée lever l'orthogonalité des orbitales e_g vacantes du Co(III) et les orbitales π/π^* du ligand pontant. Ainsi, la déformation jouerait un rôle déclencheur dans le transfert d'électron (Fe→Co).

4 Changement d'interaction magnétique dans le NiFe PBA

La complexité de l'analogue CoFe photomagnétique est nettement réduit dans l'analogue NiFe de même structure cristalline mais avec M=Ni et M'=Fe. Contrairement à son grand frère, ce composé présente uniquement un phénomène d'interaction magnétique entre les centres métalliques. Les deux électrons célibataires du site $Ni^{II}(d^8)$ et le seul électron célibataire sur le site $Fe^{III}(d^5)$ interagissent de manière ferromagnétique. La vision plus claire des effets physiques dans cet analogue et des études récentes sur sa potentielle utilisation comme cathode des batteries à base de Na^+ en font l'objet idéal d'une étude magnéto-structurale.

Une ouverture du ligand pontant entre Ni(II) et Fe(III) a été choisi comme déformation pertinente au vu de la rigidité de l'unité $[Fe(CN)_6]^{-3}$. [12, 13] De plus, ce type de déformation est susceptible de modifier l'interaction magnétique à travers un changement du recouvrement entre les orbitales 3*d* magnétiques et les orbitales σ,π et π^* du ligand pontant CN^-. La déformation est décrite par l'angle $\beta = \angle(\text{Ni-Fe-CN})$, un angle de $\beta = 0°$ correspond ainsi à la structure parfaitement octaédrique.

L'approche *embedded cluster* a été à nouveau employée. Le cluster de $[Ni(NC)_5\text{-}NC\text{-}Fe(NC)_5]^{-6}$ a été traité au niveau CAS-CI et DDCI. L'environnement de dimensions 10Å × 10Å × 15Å a contenu les TIP et charges ponctuelles sur les positions cristallographiques et est resté gelé pendant la déformation.

L'hamiltonien de spin de *Heisenberg-Van-Vleck*, [14, 15]

$$H = -JS_{Ni} \cdot S_{Fe} \tag{0.7}$$

introduit un seul paramètre, la constante d'échange-couplage J, afin de décrire l'interaction entre les deux spins sur les centre métalliques, $S_{Ni} = 1$ et $S_{Fe} = 1/2$. Conceptuellement, ce paramètre est souvent découpé en une contribution ferromagnétique J_{FM} et antiferromagnétique J_{AFM},

$$J = J_{FM} + J_{AFM} = f\,K_{eff} - f'\frac{t_{eff}^2}{U_{eff}} \tag{0.8}$$

qui sont proportionelles à l'intégrale d'échange K_{eff}, l'intégrale de saut t_{eff} et la répulsion U_{eff} entre deux électrons sur le même site métallique. Ces trois paramètres sont effectifs, f et f' sont des facteurs constants. En vue du caractère fortement atomique des orbitales 3d, j'ai également fait la supposition d'une répulsion U_{eff} constante lors de la déformation.

Les valeurs de J ont été calculées pour des angles entre $0° < \beta < 25°$ par intervalles de 5° au niveau CAS-CI et DDCI. Pour les deux niveaux de calcul, un régime ferromagnétique ($0° < \beta < 9,5°$) peut être clairement distingué de l'antiferromagnétique ($9,5° < \beta < 25°$). Ce basculement reflète la dépendance du terme antiferromagné-

tique J_{AFM} du recouvrement orbitalaire à travers l'intégrale de saut t_{eff} avec une contribution négligeable pour $\beta = 0°$. [16] Lors de l'ouverture de l'angle β, le recouvrement et donc la contribution anti-ferromagnétique augmentent et provoquent un changement de régime magnétique.

L'amplitude de changement de J entre maximum et minimum est beaucoup plus grande aux niveau DDCI (+11,4 → -12,5) cm^{-1} qu'au niveau CAS-CI (+1,8 → -2,1) cm^{-1}. Autrement dit, l'effet de corrélation au niveau DDCI semble stabiliser le comportement magnétique dominant quelqu'il soit dans la fonction d'onde au niveau CAS-CI.

Sur la base des valeurs de J=11,4 ; 0 et -12,5 cm^{-1} à β =0 ;9,5 et 19°, l'intégrale de saut t_{eff} a été quantifiée. Son augmentation est d'un facteur 1,5 entre β =9,5 et 19°. Cette augmentation de l'amplitude de transfert d'électron pourrait être couplée au transfert de Na^+ dans un NiFe PBA.

5 Les systèmes modèles : dimère de dihydrogène et *1,3*-butadiène

La méthode présentée en sec. 2 a été implémentée et appliquée au dimère de dihydrogène $(H_2)_2$ et au *1,3*-butadiène (C_4H_6). Les interactions dispersives sont l'élément clé dans la liaison de $(H_2)_2$ et un grand nombre d'excitations est supposé nécessaire pour leur bonne description. L'approche sélective semble donc idéale pour analyser systématiquement la contribution des différentes excitations. Le butadiène comme analogue covalent à 4 électrons π est un représentant modèle de la famille intéressante des polyènes. Grâce à leurs petites tailles, les systèmes choisis permettent une comparaison avec des valeurs précises obtenues par des méthodes de référence (full CI, coupled cluster). Cependant, il est à noter que l'objectif de cette étude ne consistait pas uniquement en une reproduction des valeurs de référence mais en une analyse de l'importance physique des différentes excitations habituellement incluses dans l'expansion de la fonction d'onde. Les contributions à l'énergie de dissociation D_e de $(H_2)_2$ et à la barrière de rotation D_{rot} de C_4H_6 ont été examinées.

Les *orbitales moléculaires localisées* (localized molecular orbitals, LMOs) ont été obtenues selon la procédure de localisation de Maynau *et al.*.[17] Cette procédure permet la génération de LMO de niveau SCF ou CASSCF, les premiers étant choisies dans les présentes études. Elles ont permis l'identification facile mentionnée dans sec. 2.

Dans le cas du dimère de dihydrogène, la distance intermoléculaire H_2–H_2 entre les molécules parallèles a été variée entre 2,5 et 20 Å en gardant la distance intramoléculaire H-H fixe à 0,74Å. Les valeurs FCI de D_e =12,3 meV et R_{eq} =3,4 Å pour la distance d'équilibre ont été obtenues dans un espace IC de 36100 déterminants dans des contractions 2s1p de la base ANO-L. Par la suite, différents découpages en fragments et restrictions sur les excitations ont été testés.

Dans un premier temps, le système entier a été formellement découpé en deux fragments, chacun contenant les LMOs d'une unité H-H. En interdisant toutes les excitations entre les deux fragments, 65% de D_e ont été récupérés dans un espace d'IC de 39% de l'espace FCI. L'apport énergétique des doubles transferts de charge a été trouvé négligeable. Néanmoins, même après exclusion de ce type d'excitation, les dimensions de l'espace IC par rapport au FCI restent grandes (89%).

Dans un second temps, sur chaque unité H-H le seul fragment a été découpé plus finement en trois fragments contenant les orbitales de type $[\sigma]$, $[\sigma^*, 2s, 2p_z]$, et $[2p_x, 2p_y]$. Les excitations permises ont été choisies de fa**c** con à décrire au maximum la corrélation locale et la dispersion principalement le long de l'axe entre les deux unités H-H (*i.e.* $\overset{\mathrm{H}}{\mathrm{H}} \cdots \overset{\mathrm{H}}{\mathrm{H}}$), et à négliger les doubles transferts de charge. Cet espace d'IC a permis à la fois une réduction de taille considérable (3% de l'espace FCI) en gardant la précision chimique (90% de D_e) et une analyse de l'interaction dispersive par rapport à la directionalité des orbitales 2p.

Dans le cas du butadiène, un calcul d'IC dans un sous-espace (4,36) contenant les orbitales π/π^*, 3p et 3d a donné une valeur de référence $D_{rot} = E_{cis} - E_{trans} = 14.7^{kJ}/_{mol}$ en bon accord avec des résultats précis de type CCSD(T).

Par analogie avec le système dispersif $(H_2)_2$, le système entier a été considéré comme une combinaison de deux sous-unités C_1-C_2 et C_3-C_4. Sur chacune, six fragments contenant les LMOs suivantes ont été définis : $[\pi]$, $[\pi^*]$ et $[3p]$, $[3d]$ sur chaque atome de carbone.

Suite à des tests de divers espaces d'IC, le meilleur compromis entre taille et précision a été trouvé en incluant quatres types d'excitations : (*i*) FCI au sein de chaque sous-unité, (*ii*) FCI au sein du système π (*i.e.* 4 e^-/4 LMOs π), (*iii*) simples transferts de charge entre les deux unités et la repolarisation associée du système π, et (*iv*) double-, triple-, et quadruples excitations dispersives couplant des excitations $(\pi)^2 \rightarrow(\pi^*)^2$ sur une unité et des excitations $(\pi)^2 \rightarrow(3p/3d)^2$ sur l'autre. A nouveau, j'ai pû conclure que les excitations doubles entre sous-unités (*i.e.* transferts de charge) n'ont qu'un apport énergétique négligeable. Avec cet espace, un excellent rapport entre la taille (0,8% de l'espace FCI) et la précision du calcul (97% de D_{rot}) a été atteint.

6 Conclusion et Perspectives

La transition de spin de l'analogue CoFe de Bleu de Prusse a été inspectée au niveau CAS(10,12)PT2 dans un environnement préalablement optimisé. Le déplacement observé de l'ion Co(III) en dehors de la géométrie octaédrique semble qualitativement indépendant de l'environnement immédiat d'ions Rb^+. Un tel déplacement est supposé jouer un rôle déclencheur dans le transfert d'électron (Fe→Co) en allumant un recouvrement entre orbitales métalliques et celles du ligand cyano.

Des travaux sont en cours afin d'étendre la région d'inspection au système complet bi-métallique et ainsi inclure explicitement l'état à transfert d'électron dans la

spectroscopie évaluée.

Dans l'analogue NiFe, des calculs DDCI de type embedded cluster ont été effectués afin d'étudier les propriétés magnétiques. Un changement ferromagnétique→antiferromagnétique est observé alors que la géométrie s'éloigne de la structure purement octaédrique par une ouverture du pont CN entre les deux sites métalliques. La constante de couplage J baisse considérablement (*i.e.* 23,9cm^{-1}) lors d'une ouverture de 20° du ligand pontant.

Dans le cadre du développement méthodologique, une méthode de type MR-CI a été mise en place. Contrairement à d'autres méthodes de ce type, elle est destinée à un traitement de la corrélation électronique dans des régions spatiales du système clairement définies (*i.e. fragments*). Elle profite, dans ce sens, pleinement des avantages des orbitales moléculaires localisées et permet une sélection rationelle des excitations à inclure dans l'expansion de la fonction d'onde. En même temps, une telle sélection constitue un outil d'analyse de l'apport énergétique des différentes excitations.

Les systèmes modèles $(H_2)_2$ et C_4H_6 ont été les premières applications de la méthode sélective. L'inclusion systématique des excitations physiquement importantes a permis des réductions remarquables de la taille de l'espace d'IC. Pour le dimère de dihydrogène, l'espace est réduit à 3% de l'espace complet en gardant une précision de 90% sur l'énergie de dissociation. Cependant, il s'avère qu'une augmentation de la base orbitalaire est accompagné d'une perte de localité. Dans ce cas, une identification claire des excitations n'est plus possible. La méthode se prête donc à l'inspection des systèmes moléculaires larges et des bases limitées aux doubles ou triples zeta avec polarisation.

La réduction de l'espace d'IC est encore plus importante dans le cas du butadiène puisque avec moins de 1% des déterminants 97% de la barrière de rotation *cis-trans* sont reproduits.

Bibliographie

[1] Miralles, J. ; Castell, O. ; Caballol, R. ; Malrieu, J.-P. *Chemical Physics* **1993**, *172*, 33 − 43.

[2] Roos, B. O. ; Taylor, P. R. ; Siegbahn, P. E. *Chemical Physics* **1980**, *48*, 157 − 173.

[3] Andersson, K. ; Malmqvist, P. A. ; Roos, B. O. ; Sadlej, A. J. ; Wolinski, K. *J. Phys. Chem.* **1990**, *94*, 5483–5488.

[4] Andersson, K. ; Malmqvist, P.-A. ; Roos, B. O. *J. Chem. Phys.* **1992**, *96*, 1218–1226.

[5] Angeli, C. ; Cimiraglia, R. ; Evangelisti, S. ; Leininger, T. ; Malrieu, J.-P. *The Journal of Chemical Physics* **2001**, *114*, 10252–10264.

[6] Angeli, C. ; Cimiraglia, R. ; Malrieu, J.-P. *Chemical Physics Letters* **2001**, *350*, 297 − 305.

[7] Angeli, C. ; Cimiraglia, R. ; Malrieu, J.-P. *The Journal of Chemical Physics* **2002**, *117*, 9138–9153.

[8] Sato, O. ; Iyoda, T. ; Fujishima, A. ; Hashimoto, K. *Science* **1996**, *272*, 704–705.

[9] Krah, T. ; Suaud, N. ; Zanchet, A. ; Robert, V. ; Ben Amor, N. *European Journal of Inorganic Chemistry* **2012**, *2012*, 5777–5783.

[10] Sadoc, A. ; de Graaf, C. ; Broer, R. *Phys. Rev. B* **2007**, *75*, 165116.

[11] Barandiaran, Z. ; Seijo, L. *J. Chem. Phys.* **1988**, *89*, 5739–5746.

[12] Yokoyama, T. ; Ohta, T. ; Sato, O. ; Hashimoto, K. *Phys. Rev. B* **1998**, *58*, 8257–8266.

[13] Cafun, J.-D. ; Lejeune, J. ; Itié, J.-P. ; Baudelet, F. ; Bleuzen, A. *The Journal of Physical Chemistry C* **2013**, *117*, 19645–19655.

[14] Heisenberg, W. *Z. Phys* **1928**, *49*, 619.

[15] Dirac, P. A. M. *The Principles of Quantum Mechanics*, 3rd ed. ; Clarenden, Oxford, 1947 ; Vol. Chap. IX.

[16] Kahn, O. *Molecular Magnetism* ; Wiley-VCH Verlag GmbH, 1993.

[17] Maynau, D. ; Evangelisti, S. ; Guihéry, N. ; Calzado, C. J. ; Malrieu, J.-P. *J. Chem. Phys.* **2002**, *116*, 10060–10068.

1
Introduction

Quantum chemistry has undergone a remarkable evolution over the last century in several respects. The very first considerations in the field have mostly been concerned with atomic species. The interpretation of their experimentally measured properties stimulated the development of fundamental concepts such as Bohr's assignment of atomic hydrogen emission lines to quantized electron transitions. Even though it has been occasionally attached to experiment, the proper interest of theoretical development should be emphasized.

Ever since this period, the theoretical work has been pushed further and the possibility of practical implementation of ideas has given a whole new dimension to the field. One of the first manifestations is the implementation of the Hartree-Fock method in the 1930s. The feasible investigations at that period were mostly devoted to atomic systems. Undoubtedly, the evolution of technological possibilities (*i.e.* more efficient processors, larger storage capacities) has allowed for more and more precise calculations and thus a more detailed look at fundamental interactions.

A second evolution has taken place, namely that of the complexity of targeted problems. Besides, the raised feasibility limit has allowed the systems of interest to move closer to those at the center of societal preoccupations (*i.e.* energy production or information storage).

An engineering aspect is obviously present in problematics such as material design. It is however important that the experimental generation and theoretical reproduction of properties goes alongside an understanding of their microscopic origin. Since a majority of observed properties are governed by the electron-electron interaction, its accurate description plays an essential role.

Configuration Interaction (CI) methods have proven to fulfill this role in a very satisfactory manner. They are variational and offer, in contrast to other methods

such as *density functional theory* (DFT), a directly accessible interpretation of effects through the reading of the wave function. Despite technological advances, full configuration interaction (FCI) calculations with a sufficiently large basis set fail principally due to calculation time and memory capacities. This is the reason for the ongoing interest in less expensive methods. In that sense, the development of the *complete active space self-consistent field* method (CASSCF) has to be mentioned as a considerable contribution to the field. It allows for the variational treatment of static correlation, that is, the presence of degenerate or quasi-degenerate electronic configurations within an orbital subspace. On top of the resulting orbital set, a subsequent treatment (*i.e.* CI or perturbative) is necessary to include dynamical correlation, that is, electron-electron repulsion. However, challenges posed by small molecular systems to Hartree-Fock calculations at their time are now posed to the CASSCF by systems such as the family of Prussian Blue Analogues (PBA). A prominent representative of this family of bi-metallic crystalline materials is the CoFe Analogue. The photo-induced magnetization observed in this compound implies simultaneously a spin transition on one site and an electron transfer between the two metal sites. Intermingled effects are thus present within a large orbital subspace containing both Co and Fe 3*d* manifolds and bridging CN ligand π/π^* orbitals. Their inclusion in a CASSCF/CASPT2 treatment is currently impossible due to the size of the necessary complete active space. Furthermore, there is little clarity of the impact of certain chemical factors (*i.e.* crystal vacancies and interstitial alkali ions). As a result, the material is highly complex and its study is challenging both from a chemical and computational point of view.

In this work, the complete problem has been divided into smaller pieces in two ways in order to make it approachable. In a first part of this thesis, I will discuss the exchange interaction in the NiFe PBA (see Chapter 2). It is less complex than its CoFe sister compound, since this is the predominant interaction and no coupling to another phenomenon needs to be considered. In a second part, the study of the CoFe will be rendered feasible by a limitation of the complete active space to the Co site. An accurate treatment of the Co low spin (LS) - high spin (HS) transition in the vicinity of a crystal vacancy will be presented and an implication on the Fe-to-Co electron transfer will be proposed (see Chapter 3).

The ultimate goal remains nevertheless the inclusion of all physical effects of the CoFe PBA in an accurate variational treatment. The program *FRACCIS* has been conceived and implemented. It performs a selective CI calculation in the basis of localized molecular orbitals. In this way, an alternative calculation route is proposed that passes through the rational selection of the reference space and shall (*i*) avoid the costly inclusion of unphysical determinants and (*ii*) provide an analysis tool for the impact of specific determinants. Chapter 4 is devoted to *FRACCIS* development and implementation. The program has been tested on two model systems, namely the dihydrogen dimer, $(H_2)_2$, and 1,3-butadiene, C_4H_6 (see Chapter 5). The results based on FRACCIS have been compared with those from more accurate reference methods and shed a promising light on the proposed approach. The present work

can be considered as a contribution into the field of correlated materials. Despite the considerable evolution in the area, much remains to be done to understand the behaviour in the giant anthill, that is the electron-electron interaction.

2

Existing *ab initio* methods

If the quantum chemist was a carpenter and the Schrödinger equation the wood he was working on, then the ensemble of ab initio methods were the tools in his box. In this chapter I will describe the tools used in this work, and the underlying quantum chemical terms and concepts required to use them properly. Just as the carpenter chooses his tools as a function of the wood he is working with, I will show the basic characteristics of different methods which lead to the choice of one method over another for a particular electronic structure problem. For a more detailed discussion, standard textbooks such as those of Szabo and Ostlund [1] or Helgaker, Jørgensen and Olsen [2] are recommended.

2.1 Generalities

2.1.1 The electronic problem

The quantum chemist deals with different types of chemical systems, all of which can be characterized as interacting systems of N electrons and M nuclei. Such a system is described by the Hamiltonian operator

$$\hat{H} = -\sum_{i=1}^{N}\frac{1}{2}\nabla_i^2 - \sum_{i=1}^{N}\sum_{A=1}^{M}\frac{Z_A}{r_{\mathrm{iA}}} + \sum_{i=1}^{N}\sum_{j>i}^{N}\frac{1}{r_{\mathrm{ij}}} - \sum_{A=1}^{M}\frac{1}{2M_A}\nabla_A^2 + \sum_{A=1}^{M}\sum_{B>A}^{M}\frac{Z_A Z_B}{R_{\mathrm{AB}}} \tag{2.1}$$

where Z_A is the atomic number of nucleus A, r_{iA} the distance between electron i and nucleus A, r_{ij} the distance between electrons i and j, M_A is the mass of nucleus A with respect to the mass of an electron and R_{AB} is the distance between nuclei A and B.

The first three terms of eq. (2.1) concern principally the electrons, namely their kinetic energy, the electron-nucleus attraction and the electron-electron repulsion. The last two terms are analogous terms concerning the nuclei, namely their kinetic energy and the nucleus-nucleus repulsion.

In the non-relativistic time-independent Schrödinger equation

$$\hat{H}\,|\Psi_{\mathrm{tot}}\rangle = E_{\mathrm{tot}}\,|\Psi_{\mathrm{tot}}\rangle \tag{2.2}$$

the operator from eq. (2.1) is applied to a wave function Ψ_{tot} which describes the system. If Ψ_{tot} is an eigenfunction of $\hat{H}$, the energy E_{tot} of the system is the corresponding eigenvalue.

In many cases, such as in this work, the principal interest lies in the electronic structure of a system. Thus, we take advantage of a fundamental approximation in quantum chemistry, namely the *Born-Oppenheimer Approximation*. Nuclei have a much bigger mass than electrons and thus move considerably slower. This allows us, to a good approximation, to neglect their kinetic energy (second to last term in eq. (2.1)) and to consider the nuclear repulsion (last term in eq. (2.1)) as constant.

This reduces the total operator in eq. (2.1) to the electronic operator

$$\hat{H}_{\mathrm{el}} = \underbrace{-\sum_{i=1}^{N}\frac{1}{2}\nabla_i^2 - \sum_{i=1}^{N}\sum_{A=1}^{M}\frac{Z_A}{r_{iA}}}_{\hat{h}_1} + \underbrace{\sum_{i=1}^{N}\sum_{j>i}^{N}\frac{1}{r_{ij}}}_{\hat{h}_2} \tag{2.3}$$

composed of a one-electron and a two-electron operator, $\hat{h}_1$ and $\hat{h}_2$, respectively. The operator $\hat{h}_2$ describes the electron-electron interaction and plays a challenging role in the electronic structure. It is at the heart of most calculation methods and of the following discussions.

Equation (2.2) becomes the electronic Schrödinger equation

$$\hat{H}_{\mathrm{el}}\,|\Psi_{\mathrm{el}}\rangle = E_{\mathrm{el}}\,|\Psi_{\mathrm{el}}\rangle \tag{2.4}$$

where the electronic wave function Ψ depends *explicitly* on the electronic coordinates $\{ r_i \}$ but *parametrically* on the nuclear coordinates $\{ R_A \}$. In this framework, the total energy (excluding the nuclei kinetic) is thus the sum of the electronic energy

and the constant nuclear repulsion for fix $\{ R_{\mathrm{AB}} \}$,

$$E_{\mathrm{tot}} = E_{\mathrm{el}} + \sum_{A=1}^{M} \sum_{B>A}^{M} \frac{Z_A Z_B}{R_{\mathrm{AB}}} \tag{2.5}$$

In the following, the *Born-Oppenheimer Approximation* will always be applied since we only consider the electronic problem and neglect vibrational and rotational degrees of freedom. For the sake of simplicity, I will refer to the electronic Hamiltonian simply as "Hamiltonian" ($\hat{H}$), and write Ψ in a shorthand for Ψ_{el}.

2.1.2 The orbital approximation

A central object providing access to molecular electronic properties is the function Ψ in eq. (2.4) which contains information about the N electrons of the system. With N possibly being quite large, the question is: "How can one conveniently construct Ψ in order to facilitate the resolution of the electronic Schrödinger equation?" One could divide the **one** function Ψ for N electrons into **N** functions $\{\varphi\}$, called *orbitals*, such that each one contains one electron, *i.e.*

$$\Psi(r_1, r_2, \ldots, r_N) \simeq \varphi_a(r_1)\varphi_b(r_2)\ldots\varphi_c(r_N) = \prod_{a=1}^{N} \varphi_a(r_i) \tag{2.6}$$

This is the idea behind the *orbital approximation*. However, a wave-function constructed in this crude manner lacks the important property of indistinguishability of electrons and by consequence anti-symmetry to fulfill the *Pauli Principle*. We shall see in the next section how they are introduced.

Spatial and Spin orbitals

A spatial orbital φ is a function that describes a single electron as a function of its spatial coordinates r. The square $|\varphi(r)|^2$ corresponds to its probability density. Consequently, the expression $|\varphi(r)|^2 dr$ describes the probability of finding the electron within the volume element dr around the point r. The condition of *orthonormality* is frequently imposed on orbitals and can be written as

$$\int dr\ \varphi_i^*(r)\varphi_j(r) = \langle\varphi|\varphi_j\rangle = \delta_{ij} \tag{2.7}$$

where δ_{ij} is the Kronecker symbol

$$\delta_{ij} = \begin{cases} 0 & \text{if } i \neq j \\ 1 & \text{if } i = j \end{cases} \tag{2.8}$$

Orthonormal orbitals fulfill two conditions. The first, *orthogonality*, means that

only projections of an orbital on itself give a non-zero result. Just as the x-axis in a cartesian coordinate system has no projection on the y- or z-axis, an orbital φ has no projection on any other orbital in an orthogonal set. *Normalization* is achieved by preceding φ with an appropriate factor such that the projection on itself yields exactly 1. This requirement is physically reasonable since it corresponds to being sure to find the electron if the search volume is infinite, just like one would be sure to find the needle in the haystack by turning over every straw. The *orthonormality* condition is not always mandatory but it simplifies the calculations to a great extent as shall be seen below.

Spatial orbitals only depend on the spatial coordinates of the electron and lack the important property of spin. In the *spin orbitals* $\chi(x_i)$,

$$\chi(x_i) = \begin{cases} \varphi(r_i)\alpha(\omega) \\ \varphi(r_i)\beta(\omega) \end{cases} \qquad x_i = \{ r_i, \omega \} \tag{2.9}$$

this property is introduced by multiplying the spatial orbital φ with one of the orthonormal functions $\alpha(\omega)$ for spin up ($\uparrow$) and $\beta(\omega)$ for spin down ($\downarrow$). All previous considerations on spin-orbitals still hold only that now the spin orbitals depend both on the spatial (r) and spin (ω) coordinates of the electron, regrouped in the set x. The following notations of the electron i in a spatial or spin orbital are equivalent : $\varphi(r_i) = \varphi(i)$ and $\chi(x_i) = \chi(i)$. The notation of a bar over the spatial orbital is used to distinguish between α and β electrons as

$$\varphi_i\alpha(\omega) = \varphi_i \quad \text{and} \quad \varphi_i\beta(\omega) = \overline{\varphi_i} \tag{2.10}$$

Atomic and molecular orbitals

For the following discussion I will consult the ubiquitous model system H_2. At a large H-H distance, one orbital ϕ_A describes the electron A of H_A and another orbital ϕ_B the electron B of H_B. Since these orbitals are exclusively concerned with the electron of one atom, they are *atomic orbitals* (AOs). However, when H_A and H_B approach each other, their corresponding orbitals start to interact. This interaction is formalized in the *linear combination of atomic orbitals*,

$$\varphi_i = \frac{1}{n} \sum_{j=1}^{N} c_j^i \phi_j \tag{2.11}$$

which proposes to expand *molecular orbitals* (MOs) φ into atomic orbitals ϕ. The participation of the AO ϕ_j in the MO φ_i is described by a coefficient c_j^i and normalization is ensured by a pre-factor $1/n$. In general, as many MOs are defined as there

are interacting AOs. In the case of H_2 in a minimal basis, one obtains the two MOs

$$\varphi_1 = \frac{1}{\sqrt{2(1+S_{AB})}}(\phi_A + \phi_B) \quad \text{and} \quad \varphi_2 = \frac{1}{\sqrt{2(1-S_{AB})}}(\phi_A - \phi_B). \tag{2.12}$$

where S_{AB} represents the overlap between the atomic ϕ_A and ϕ_B orbitals of H_A and H_B. When concerned with molecular orbitals, the bar notation is commonly used to distinguish spin up (φ_1) and spin down ($\overline{\varphi_1}$) since it allows a clear identification of electrons paired in one MO.

2.1.3 Slater determinants

The *antisymmetry principle* states that an N-electron wave function must be antisymmetric with respect to the interchange of the spatial and spin coordinates x of any two electrons, *i.e.*

$$\Psi(x_1, ..., x_j, ..., x_k, ..., x_N) = -\Psi(x_1, ..., x_k, ..., x_j, ..., x_N) \tag{2.13}$$

A wave function constructed as a so-called *Hartree product* of spin orbitals does not satisfy this requirement. To illustrate, a 2-electron wave function in the product form,

$$\Psi(1,2) = \chi_i(1)\chi_j(2)$$

becomes

$$\Psi'(2,1) = \chi_i(2)\chi_j(1)$$

upon interchange of electrons 1 and 2. Since the electrons are indistinguishable, it is clear that $\Psi = \Psi'$ and the wave function needs to be built in a different fashion.

Slater proposed to write the wave function in the form of a determinant, [3]

$$\Psi(x_1, x_2, ..., x_N) = \frac{1}{\sqrt{N!}} \begin{vmatrix} \chi_a(1) & \chi_b(1) & \cdots & \chi_c(1) \\ \chi_a(2) & \chi_b(2) & \cdots & \chi_c(2) \\ \vdots & \vdots & \ddots & \vdots \\ \chi_a(N) & \chi_b(N) & \cdots & \chi_c(N) \end{vmatrix} \tag{2.14}$$

The general expression for N-electron determinants in terms of spin orbitals is

$$|\chi_k \chi_l \cdots \chi_w\rangle = (N!)^{-\frac{1}{2}} \sum_{n=1}^{N!} (-1)^{p_n} \mathscr{P}_n \{ \chi_k(1)\chi_l(2) \cdots \chi_w(N) \} \tag{2.15}$$

where the summation carries over all possible $N!$ permutations of N electrons, generated by the permutation operator $\mathscr{P}_n$. The signature p_n represents the number of electron interchanges necessary to obtain the n^{th} permutation.

In the case of the hydrogen molecule, the wave function has the equivalent expres-

sions

$$\Psi(x_1, x_2) = \frac{1}{\sqrt{2}} \begin{vmatrix} \chi_1(1) & \chi_2(1) \\ \chi_1(2) & \chi_2(2) \end{vmatrix} = \frac{1}{\sqrt{2}} \begin{vmatrix} \varphi_1(1) & \overline{\varphi_1}(1) \\ \varphi_1(2) & \overline{\varphi_1}(2) \end{vmatrix} = |\varphi_1 \overline{\varphi_1}| \tag{2.16}$$

where we have used either spin-orbitals, spatial orbitals or the compact expression containing only the determinant diagonal elements.

Slater's possibly inconspicuous suggestion fulfills the antisymmetry requirement and contains the indistinguishability of the electrons. Furthermore, the probability of finding electron 1 at the same point in space as electron 2 is zero for electrons of the same spin. A certain degree of electron-electron correlation is thus introduced in Slater determinants, so-called Fermi hole.

2.1.4 The Hartree-Fock approximation

Such as presented in eq. (2.14), the wave function is constructed from only one determinant built from a set of spin orbitals $\{ \chi \}$. At the beginning of the 20$^{\text{th}}$ century, *Hartree* and *Fock* proposed a milestone procedure to optimize such a wave function by optimizing the spin orbitals. Although nowadays more sophisticated wave functions can be constructed, the *Hartree-Fock* (HF) approximation remains essential since it constitutes the starting point of most quantum chemical calculations. It is a mean-field method that does not take into account the instantaneous interaction between electrons but rather their average effect in an iterative manner.

The central equation to this approach is the *Hartree-Fock* equation

$$\left[\hat{h}(1) + \sum_{b \neq a} \hat{J}_b(1) - \sum_{b \neq a} \hat{K}_b(1) \right] \chi_a(1) = \epsilon_a \chi_a(1) \tag{2.17}$$

containing the monoelectronic operator $\hat{h}(1)$ and the *coulomb* ($\hat{J}$) and *exchange* ($\hat{K}$) operators dealing with the electron-electron interaction. The coulomb operator,

$$\hat{J}_b(1) = \int dx_2 \chi_b^*(2) \chi_b(2) \frac{1}{r_{12}} \tag{2.18}$$

represents the potential exerted by the charge distribution of electron 2 on electron 1 at r_1. The interaction of the spin orbitals $\chi_a(1)$ and $\chi_b(2)$ through $\hat{J}_b(1)$ is evaluated as,

$$J_{\text{ab}} = \int dx_1 dx_2 \, |\chi_b(2)|^2 \, \frac{1}{r_{12}} \, |\chi_a(1)|^2 \tag{2.19}$$

This so-called *coulomb integral* describes the repulsion of two charge clouds that are a distance r_{12} apart. The summation in eq. (2.17) over all occupied orbitals b other than a gives the effective coulomb potential of the $(N-1)$ electrons acting on electron 1 at r_1. In the previous picture, this corresponds to the repulsion between the charge cloud of electron one and the average charge cloud of the other $(N-1)$

electrons. Different notations, namely the Dirac notation and the chemist notation, are used for the coulomb integral :

$$J_{\text{ab}} = \begin{cases} \langle ab|ab\rangle & = \int dx_1 dx_2 \ \chi_a^*(1)\chi_b^*(2)\frac{1}{r_{12}}\chi_a(1)\chi_b(2) \\ [aa|bb] & = \int dx_1 dx_2 \ \chi_a^*(1)\chi_a(1)\frac{1}{r_{12}}\chi_b^*(2)\chi_b(2) \end{cases} \tag{2.20}$$

In the Dirac bra-ket notation, the complex and real parts of the orbitals are regrouped on the left and right side of the operator while in the chemist notation this separation is done with respect to electron one and two. Evidently, the different notations do not change the physical meaning of the integral. The exchange operator is defined by its effect when acting on a spin orbital $\chi_a(1)$,

$$\hat{K}_b(1)\chi_a(1) = \left[\int dx_2 \chi_b^*(2)\frac{1}{r_{12}}\chi_a(2)\right]\chi_b(1) \tag{2.21}$$

As opposed to the coulomb term, there is no classical interpretation for the exchange term which arises from the antisymmetric nature of the wave function. The corresponding *exchange integral*,

$$K_{\text{ab}} = \int dx_1 dx_2 \chi_a^*(1)\chi_b^*(2)\frac{1}{r_{12}}\chi_a(2)\chi_b(1) \tag{2.22}$$

has the two notations,

$$K_{\text{ab}} = \langle ab|ba\rangle = [ab|ab] \tag{2.23}$$

The result of applying $\hat{K}_b(1)$ on $\chi_a(1)$ depends on the value of χ_a throughout all the space and not just in the point r_1. This is why the exchange operator is called *non local* as opposed to the *local* coulomb operator.

When $b = a$,

$$\left[\hat{J}_a(1) - \hat{K}_a(1)\right]\chi_a(1) = 0 \tag{2.24}$$

and thus the restriction on the sum can be removed and eq. (2.17) be generalized to

$$\left[\hat{h}(1) + \sum_b \hat{J}_b(1) - \hat{K}_b(1)\right]\chi_a(1) = \epsilon_a\chi_a(1) \tag{2.25}$$

The average effect of the $(N-1)$ electrons on electron 1, that is, the combined coulomb and exchange operators, is defined as the *Hartree-Fock potential* $v^{HF}(1)$ which we find in the *Fock operator* $\hat{F}$,

$$\hat{F}(i) = \sum_i^N \hat{h}(i) + \sum_i^N v^{HF}(i) \tag{2.26}$$

A strong resemblance can be noticed when comparing the Fock operator to the electronic Hamiltonian (eq. (2.3)). The first part captures the kinetic and potential

energy of a single electron. However, the explicit electron-electron interaction (r_{ij}^{-1}) term in the Hamiltonian is approximated by the Hartree-Fock potential in the Fock operator. Finally, the initial *Hartree-Fock* (HF) equation becomes

$$f\,|\chi_a\rangle = \epsilon_a\,|\chi_a\rangle \tag{2.27}$$

and seems very similar to the electronic Schrödinger equation eq. (2.4). A crucial difference, however, is found when examining the HF potential $v^{HF}(1)$. It depends on the eigenvectors (*i.e.* the spin orbitals χ) of the very same operator it is part of. Consequently, a direct resolution of the HF equation for the optimal set $\{\chi\}_{HF}$ is impossible and one must resort to an iterative procedure. In practice, an initial guess $\{\chi\}_0$ is used to find the HF potential v^{HF}. Then a new set $\{\chi\}_1$ of spin orbitals is found through resolution of the HF equation 2.27. This is reinjected to find a new HF potential and the corresponding spin orbitals. The optimal set $\{\chi\}_{HF}$ of spin orbitals is found when the potential and orbitals obtained at iteration i coincide with those from iteration $i-1$. In view of the iterative procedure focusing on the field of $N-1$ electrons, the Hartree-Fock method is also called *self-consistent field* (SCF) method. In the following, I will use both terms equivalently.

2.2 Treatment of the electronic correlation

When in a crowded train station, people take a certain path through the crowd because they do not want to bump into fellow travelers. Electrons behave in a similar fashion, that is, the *instantaneous* positions of one electron depends on the *instantaneous* position of all the other electrons and not only their mean position. This instantaneous dependence is called *electronic correlation*. In the Schrödinger equation (eq. (2.4)), it is captured within the r_{ij}^{-1} term and renders its analytic resolution impossible except for hydrogen-like cases.

In general, a distinction is made between two types of electronic correlation. The so-called *dynamical* correlation is an electronic phenomenon that arises from the very electron-electron interaction just described. The *non-dynamical* or *static* correlation has its origin in the presence of degenerate or quasi-degenerate orbitals. The dissociation of H_2 serves as an illustrative example : in the equilibrium geometry and thus in the case of clearly separate σ_g and σ_u MOs, the correlation is *dynamical*. At dissociation limit, on the other hand, the σ_g and σ_u MOs and the corresponding doubly occupied configurations are degenerate and the correlation is *static*. The intermediate region on the dissociation curve exemplifies that both types of correlation can be present simultaneously and that their distinction is not always trivial.

In the following, I will present several methods that share the goal to find the best approximation possible to the wave function Ψ and thus to the electronic correlation.

2.2.1 Configuration Interaction

In the *Configuration Interaction* (CI) approach, the correlation is included in the wave function Ψ,

$$\Psi = c_0\Psi^0 + \sum_{pa} c_a^p \Psi_a^p + \sum_{\substack{a<b \\ p<q}} c_{ab}^{pq} \Psi_{ab}^{pq} + \sum_{\substack{a<b<c \\ p<q<r}} c_{abc}^{pqr} \Psi_{abc}^{pqr} + \dots \tag{2.28}$$

by expanding it into excited electronic *configurations* $\{ \Psi_a^p, \Psi_{ab}^{pq}, \Psi_{abc}^{pqr} \dots \}$ with respect to the reference space Ψ^0. In the singly excited configurations of type Ψ_a^p, for example, an electron from the occupied spin orbital a has been excited to the virtual spin orbital p. Its weight in the wave function corresponds to the square $|c_a^p|^2$ of the coefficient c_a^p, unique for the a, p pair of orbitals. An analogous nomenclature holds for determinants of higher degrees of excitation. The wave function is optimized through the coefficients $\{ c_0, c_a^p, c_{ab}^{pq}, \dots \}$.

In the *full* CI, all possible determinants are included in the expansion of Ψ. The corresponding wave function Ψ^{FCI} has the lowest possible energy $E_{\mathrm{FCI}} = \langle \Psi^{\mathrm{FCI}} | \hat{H} | \Psi^{\mathrm{FCI}} \rangle$ for a given basis set. The wave function thus has two extreme descriptions : either by only *one* determinant (HF) or by *all* possible determinants (FCI). Within a given basis set, the difference between the energies of the two methods is defined as the correlation energy,

$$E_{\mathrm{corr}} = E_{\mathrm{FCI}} - E_{\mathrm{HF}} \tag{2.29}$$

I shall use this definition in the present work even though it differs slightly from other definitions parting from the *exact* energy (*i.e.* FCI in a complete basis set).

Single-reference CI (SRCI)

Ψ^0 in eq. (2.28) represents 1 unique determinant (HF) and the corresponding approach is called single-reference CI (SRCI). One can introduce intermediate descriptions between the two extremes SCF and FCI by increasing the number of excitations in the determinants added in the expansion. The CI of single excitations (CIS) introduces singly excited determinants on top of the HF determinant, the CI of single and double excitations (CISD) adds the singly and doubly excited and so on. In general, the CI expansion in eq. (2.28) is limited to single and double excitations (CISD). Analogous to the FCI energy, the CISD energy $\mathrm{E_{SD}}$, for example, is evaluated as $E_{SD} = \langle \Psi^{\mathrm{SD}} | \hat{H} | \Psi^{\mathrm{SD}} \rangle$.

Multi-reference CI

It is possible to introduce a different reference function Ψ^0 than the mono-determinantal HF wave function in the framework of *multi-reference CI*. The previous considerations concerning the energy evaluation and degrees of excitation in SRCI still hold. Only in this case, excitations are considered with respect to a multi-determinantal reference function.

In the most complete case, the reference function corresponds to a FCI within an orbital subspace. However, this type of treatment is quickly limited by the number of orbitals to be included in the subspace so that a further reduction of the number of determinants might become necessary.

The reference determinants of Ψ^0 can be chosen in different ways. They can be selected based on their perturbation energy contribution [4] or even individually. In this work, the spatial proximity of the orbitals is used to generate the space of reference determinants for an MR-CI treatment.

Difference Dedicated CI

The investigation of magnetic systems has originated the difference dedicated CI (DDCI) method. [5] With respect to the CISD method, DDCI yields a lower computational cost based on the judicious exclusion of a certain class of excitations.

More precisely, the excitations with respect to a reference space are classified with respect to their numbers of holes (h) and particles (p). A hole corresponds to an occupied orbital that loses an electron, a particle to a virtual orbital that gains an electron during an excitation. The orbitals with variable occupation in all of the reference determinants are not considered in this nomenclature. In that sense, an excitation of 2h1p type corresponds to a single excitation from an occupied to a virtual orbital (1h1p) combined to a single excitation to the reference space (1h). Malrieu *et al.* have shown that the energy difference between a ground and excited state remains unaffected by the 2h2p class of excitations at the level of second order of perturbation provided that the environments of the two states are sufficiently close in nature. This is true for magnetic systems since they present a weak spatial redistribution of the electronic density in excited states. Practically, this offers the possibility to use the same orbital set for the considered states. The exclusion of the numerous excitations of the 2h2p class affords thus a considerable reduction of the computational cost without loss of precision.

It should be noted that all CI methods are variational, that is, if the CI space is smaller than the FCI space, its energy will be above that of the FCI (*i.e.* $E_{SD} > E_{\mathrm{FCI}}$).

$$
\begin{array}{c}
 \\
\langle\Psi_0| \\
\langle\Psi_a^p| \\
\langle\Psi_{ab}^{pq}| \\
\langle\Psi_{abc}^{pqr}| \\
\vdots \\
\langle\Psi_N|
\end{array}
\begin{array}{c}
\begin{array}{cccccc}
|\Psi_0\rangle & |\Psi_a^p\rangle & |\Psi_{ab}^{pq}\rangle & |\Psi_{abc}^{pqr}\rangle & \cdots & |\Psi_N\rangle
\end{array} \\
\left[\begin{array}{cccccc}
\langle\Psi_0|\hat{H}|\Psi_0\rangle & 0 & \langle\Psi_0|\hat{H}|\Psi_{ab}^{pq}\rangle & 0 & \cdots & 0 \\
 & \langle\Psi_a^p|\hat{H}|\Psi_a^p\rangle & \langle\Psi_a^p|\hat{H}|\Psi_{ab}^{pq}\rangle & \langle\Psi_a^p|\hat{H}|\Psi_{abc}^{pqr}\rangle & \cdots & 0 \\
 & & \langle\Psi_{ab}^{pq}|\hat{H}|\Psi_{ab}^{pq}\rangle & \langle\Psi_{ab}^{pq}|\hat{H}|\Psi_{abc}^{pqr}\rangle & \cdots & 0 \\
 & & & \langle\Psi_{abc}^{pqr}|\hat{H}|\Psi_{abc}^{pqr}\rangle & \cdots & 0 \\
 & & & & \ddots & 0 \\
 & & & & & \langle\Psi_N|\hat{H}|\Psi_N\rangle
\end{array}\right]
\end{array}
$$

Figure 2.1: Schematic representation of the CI matrix.

$\lvert K\rangle$	$\lvert U\rangle$	$\langle K\lvert\hat{h}_1\rvert U\rangle$
$\lvert\ldots k,l\ldots\rangle$	$\lvert\ldots k,l\ldots\rangle$	$\sum_k^N [k\lvert h\rvert k]$
$\lvert\ldots k,l\ldots\rangle$	$\lvert\ldots u,l\ldots\rangle$	$[k\lvert h\rvert u]$
$\lvert\ldots k,l\ldots\rangle$	$\lvert\ldots u,v\ldots\rangle$	0

Table 2.1: Evaluation of matrix elements of the one-electron operator $\hat{h}_1 = \sum_{i=1}^{N} h(i)$ in terms of spin orbitals k, l, u, v

Evaluation of matrix elements

In the following, we will assume that the set of spin-orbitals is orthonormal. The energy of a CI wave function Ψ as in eq. (2.28) is evaluated by diagonalisation of the CI matrix shown in Fig. 2.1. A set of rules, the *Slater-Condon* rules, [6] formalises the evaluation of the interaction of one determinant $|K\rangle$ with another determinant $|U\rangle$ through the complete electronic Hamiltonian $\hat{H}$.

The value of the hamiltonian integral between two determinants $|K\rangle$ and $|U\rangle$ is governed by the number of spin orbitals by which the two differ. Once they have been put into maximum coincidence, three different cases are considered : the two determinants are the same and the matrix elements correspond to diagonal elements of the CI matrix or they differ by one or two spin-orbitals in the off-diagonal elements. In order to tackle the evaluation of these elements, the Hamiltonian is split into the one- and two-electron operators shown in eq. (2.3).

First, I will discuss elements involving the one-electron operator, $\hat{h}_1$, summarized in Tab. 2.2.1. In the diagonal elements, the two determinants are identical (*i.e.* $|U\rangle = |K\rangle$) and the corresponding matrix element is simply the sum of the one-electron energies of all N electrons.

In the off-diagonal elements, the two determinants can differ by one spin-orbital. If χ_k in $|K\rangle$ is replaced by χ_u in $|U\rangle$, then χ_k is orthogonal to all orbitals in $|U\rangle$. Consequently, the electron 1 described by the operator $\hat{h}(1)$ must be in orbitals χ_k and χ_u and the rest of the spin-orbitals must be identical. Otherwise the integration over the other $N-1$ electrons would yield zero. The element thus reduces to the

$\lvert K\rangle$	$\lvert U\rangle$	$\langle K\lvert\hat{h}_2\rvert U\rangle$
$\lvert\ldots k,l\ldots\rangle$	$\lvert\ldots k,l\ldots\rangle$	$\frac{1}{2}\sum_k^N\sum_l^N [kk\lvert ll] - [kl\lvert lk]$
$\lvert\ldots k,l\ldots\rangle$	$\lvert\ldots u,l\ldots\rangle$	$\frac{1}{2}\sum_l^N [ku\lvert ll] - [kl\lvert lu]$
$\lvert\ldots k,l\ldots\rangle$	$\lvert\ldots u,v\ldots\rangle$	$[ku\lvert lv] - [kv\lvert lu]$

Table 2.2: Evaluation of matrix elements of the two-electron operator $\hat{h}_2 = \sum_{i<j}(r_{ij})^{-1}$ in terms of spin orbitals k, l, u, v

simple integral,

$$[k|h|u] = \int dx_1 \chi_k^*(1)\hat{h}(1)\chi_u(1) \tag{2.30}$$

The off-diagonal elements can also differ by two spin-orbitals ($\chi_k \rightarrow \chi_u$ and $\chi_l \rightarrow \chi_v$). Since the integration over the $(N-1)$ electrons not associated to the operator includes at least one pair of orthogonal spin-orbitals, the matrix element is zero. The same argument holds for determinants that differ in more than two spin-orbitals (see Fig. 2.1).

The reasoning for matrix elements of $\hat{h}_2$ is similar to the previous one. In the diagonal matrix elements the spin-orbitals of all $(N-2)$ electrons, other than 1 and 2 concerned by the operator, must be identical for a non-zero result due to orthogonality. The resulting matrix element,

$$\frac{1}{2}\left(\sum_k^N\sum_l^N [kk|ll] - [kl|lk]\right) = \frac{1}{2}\left(\sum_k^N\sum_l^N J_{\mathrm{kl}} - K_{\mathrm{kl}}\right) \tag{2.31}$$

sums up the possible permutations of electrons 1 and 2 for all unique combinations of spin-orbitals k and l. These are the coulomb and exchange integrals introduced in section sec. 2.1.4,

In the case of determinants that differ in one spin-orbital, the same two terms J and K arise, but the summation is restricted to the spin orbital l shared by the two determinants. In other words, the two distinguishable permutations of electrons 1 and 2 in three spin-orbitals are summed up. Two of the orbitals are different in the two determinants and thus fixed. The third one is varied over all remaining, identical spin-orbitals.

The element is simplified when the determinants are different in two spin-orbitals. Again, orthogonality imposes the two electrons described by $\hat{h}_2$ to be in the spin-orbitals k, l, u, v for a non-zero result. Then, the same two integrals as before are considered.

When more than two spin-orbitals differ between $|K\rangle$ and $|U\rangle$, their two-electron matrix element is zero.

In summary, zero matrix elements are obtained if the two determinants differ by more than one spin-orbital for the one-electron operator and by more than two for the two-electron operator. It becomes clear that the evaluation of the above matrix elements is greatly simplified by the use of orthogonal spin-orbitals. This

property gives a highly appreciable binary character to the integrals between single spin-orbitals.

Brillouin Theorem

The Hamiltonian $\hat{H}$ can be written in terms of the Fock operator $\hat{F}$.

$$\hat{H} = \hat{F} - v^{HF} + \sum_{i<j} \frac{1}{r_{ij}} \tag{2.32}$$

The Fock-operator in eq. (2.32) was stripped down to a mono-electronic operator by removing the mean-field potential v^{HF}. Adding the exact two-electron term r_{ij}^{-1} restores the exact electronic Hamiltonian. The matrix element between the Hartree-Fock ground state Ψ_0 and a singly excited state Ψ_a^p, can be evaluated using the definitions of $\hat{J}$ and $\hat{K}$ known from sec. 2.1.4 and the previously discussed Slater-Condon rules, as

$$\begin{aligned} \langle \Psi_0 | \hat{F} - v^{HF} + \sum_{i<j} \tfrac{1}{r_{ij}} | \Psi_a^p \rangle &= F_{\mathrm{ap}} - \langle \chi_a | v^{\mathrm{HF}} | \chi_p \rangle + \sum_{i<j} \langle \chi_a | \tfrac{1}{r_{\mathrm{ij}}} | \chi_p \rangle \\ &= F_{\mathrm{ap}} - \sum_n \langle \chi_a(1) | \hat{J}_n - \hat{K}_n | \chi_p(1) \rangle \\ &\quad + \sum_n \left([ap|nn] - [an|pn] \right) \end{aligned} \tag{2.33}$$

The last two sums of the coulomb and exchange integrals J and K are identical and thus cancel each other. In other words, the considered matrix element reduces to the off-diagonal element F_{ap} of the Fock matrix,

$$\langle \Psi^{HF} | \hat{H} | \Psi_a^p \rangle = F_{\mathrm{ap}} \tag{2.34}$$

However, the Fock matrix has been diagonalized during the SCF procedure to optimise Ψ^{HF} and the matrix element F_{ap} is consequently zero by definition.

We arrive thus at the *Brillouin theorem*, which states that the HF ground state Ψ_0 and a singly excited determinant Ψ_a^p do not interact directly, *i.e.* their matrix element of the electronic Hamiltonian is zero (see Fig. 2.1),

$$\langle \Psi_0 | \hat{H} | \Psi_a^p \rangle = 0 \tag{2.35}$$

In other words, the single excitations have no energetic effect on the ground state if they are the only ones added to Ψ_0 (*i.e.* CIS). However, from CISD on, they can interact indirectly with Ψ_0 *via* the matrix elements involving double excitations, $\langle \Psi_a^p | \hat{H} | \Psi_{ab}^{pq} \rangle$ and $\langle \Psi_{ab}^{pq} | \hat{H} | \Psi_0 \rangle$. Despite their small effect on the ground state energy, they give access to mono-electronic phenomena (*i.e.* dipole moment, charge transfer) and to a description of excited states.

Size-consistency and size-extensivity

In a chemical system composed of two or more subunits without interaction, it is desirable that the method produces the same energy, no matter if it was calculated in several separate calculations containing one subunit each or in one calculation containing all subunits simultaneously. If the method has this property, it is called *size-consistent*. For a system composed of two subunits A and B, size-consistency is fulfilled if the energy E_{AB} of the whole system can be expressed as the sum of the individual energies E_A and E_B of subunits A and B,

$$E_{AB} = E_A + E_B \tag{2.36}$$

and if the total space $\mathscr{M}_{\mathrm{AB}}$ of the compound system is the direct product of the subunit spaces $\mathscr{M}_{\mathrm{A}}$ and $\mathscr{M}_{\mathrm{B}}$,

$$\mathscr{M}_{\mathrm{AB}} = \mathscr{M}_{\mathrm{A}} \otimes \mathscr{M}_{\mathrm{B}} \tag{2.37}$$

As an example, we shall consider the $(H_2)_2$ system, composed of two non-interacting subunits, $H_2(A)$ and $H_2(B)$. A CI-D calculation on the subunit A includes the ground state and the doubly excited determinant in the wave function,

$$\Psi^{\text{CI-D}}_{\mathrm{H_2(A)}} = c_0 \left|\varphi_1\overline{\varphi_1}\right|_{\mathrm{A}} + c_2 \left|\varphi_2\overline{\varphi_2}\right|_{\mathrm{A}}$$

An analogous calculation on subunit B includes the corresponding determinants on the opposite subunit. Simultaneous double excitations on both subunits leading to $(\varphi_2\overline{\varphi_2})_{\mathrm{A}}(\varphi_2\overline{\varphi_2})_{\mathrm{B}}$ correspond to quadruple excitations and are thus not taken into account in the CI-D wave function. In general, truncated CI methods, in contrast to FCI, do not fulfill the above conditions for size-consistency.

The very similar concept of *size-extensivity* borrows the term extensivity from thermodynamics, where it signifies the proportionality of a property to the number N of particles in a homogeneous system. We can transpose the concept to a system of N interacting subunits. A method is called size-extensive if, in the limit of $N \longrightarrow \infty$, the correlation energy it provides scales linearly with the system size,

$$\lim_{N\to\infty} \frac{E_{\mathrm{corr}}}{N} = constant \tag{2.38}$$

In the case of CI-D calculations, the correlation energy $E^{\text{CI-D}}_{\mathrm{corr}}$ scales as $\sqrt{N}$. Substitution into eq. (2.38) shows that the correlation energy per subunit is not constant and vanishes for large systems. All truncated CI methods present an error of size-extensivity. However, in the case of DDCI this error is reduced with respect to a CISD calculation due to the suppression of the 2h2p excitations.

The *Davidson correction* is a way to take into account the error of size-extensivity

and size-consistency, following the equation

$$E^{\text{Davidson}} = (1 - c_0^2) E_{\text{corr}}^{\text{CI}} \tag{2.39}$$

where the HF wave function carries the coefficient c_0 in the normalized CI wave function and $E_{\text{corr}}^{\text{CI}}$ is the correlation energy calculated with a truncated CI method. The method is approximately valid for relatively small molecules. As an illustrative example, a CISD calculation of an increasing number of non-interacting water molecules is considered. [2] For three water molecules, 84% of the FCI correlation energy recovered by CISD are increased to 95% after application of the Davidson correction. These values before and after correction change to 74% and 89% for eight water molecules. It is clear that the correction is not able to fill the lack of size-extensivity beyond a certain compound system size.

2.2.2 Complete Active Space SCF

The FCI approach is desirable since it delivers the exact energy for a given basis set but is not feasible for problems of considerable size (several tens of orbitals). The *complete active space self-consistent field* (CASSCF) method performs a FCI calculation within a restricted subspace of orbitals and simultaneously optimizes the orbitals following the SCF procedure.

More precisely, the CASSCF wave function Ψ^{CASSCF} is expanded over all determinants Ψ^I that are part of the CAS,

$$\Psi^{\text{CASSCF}} = \sum_{I \epsilon CAS} c_I \Psi^I \tag{2.40}$$

As in the CI expansion, the weight of the determinant Ψ^I in the wave function is given by the square $|c_I|^2$ of its coefficient.

A number of active electrons, n_{actel} and active orbitals n_{actorb} are defined. Both are in most cases considerably smaller than the total number of electrons and orbitals. The complete active space is formed by all possible determinants of n_{actel} electrons in n_{actorb} orbitals that correspond to a given spin multiplicity and spatial symmetry. It is generally noted (n_{actel},n_{actorb}).

All orbitals are distinguished into three different types,

$$\begin{aligned} inactive &: \quad n_{\text{occ}} = 2 \\ virtual &: \quad n_{\text{occ}} = 0 \\ active &: \quad 0 \leq n_{\text{occ}} \leq 2 \end{aligned}$$

depending on their occupation number n_{occ} in all determinants. In other words, all determinants that are part of the CAS share the same sets of occupied *inactive* and vacant *virtual* orbitals.

The molecular orbitals φ^a, elements of the determinants Ψ^I in eq. (2.40), are

expanded over the atomic orbitals ϕ_i with coefficients c_i^a of the AO i in the MO a,

$$\varphi^{\mathrm{a}} = \sum_i c_i^a \phi_i \tag{2.41}$$

Overall, two sets of coefficients are optimized within the CASSCF approach : (*i*) the coefficients $\{ c_i^a \}$ of the AOs in the development of the MOs, and (*ii*) the coefficients $\{ c^I \}$ of the CAS determinants in the development of the wave function.

The nature of the CAS is the keystone of the method since it is capable of capturing the physics of an inspected phenomenon under the condition of it being well-chosen. At present, complete active spaces of around 18 orbitals at most are computationally feasible. It should be noted that the CASSCF calculation is the most expensive when the number of active electrons corresponds to the number of MOs (*i.e.* $n_{\mathrm{actel}} = n_{\mathrm{actorb}}$). Consequently, size limits are reached rather rapidly such as in poly-metallic systems where the number of open-shells increases rapidly.

2.2.3 Perturbative approaches to the second order

A problem that has no exact solution, can be solved approximately by dividing it into two parts; one with a known solution and a perturbation to that solution. In the case of the Schrödinger equation, the complete electronic operator $\hat{H}$ can be divided as

$$\hat{H} = \hat{H}_0 + \hat{V} \tag{2.42}$$

into a part $\hat{H}_0$ with known eigenvectors and eigenvalues and a perturbation $\hat{V}$. The operator $\hat{H}_0$ must be chosen such that it contains the majority of the considered physical effects. Only then the perturbation $\hat{V}$ remains "small" and a perturbative approach is applicable.

The exact energy ε and the exact wave function Ψ can be written as perturbation expansions,

$$E = E^{(0)} + E^{(1)} + E^{(2)} + \cdots \tag{2.43}$$

$$\Psi = \Psi_0 + \Psi^{(1)} + \Psi^{(2)} + \cdots \tag{2.44}$$

where the exponents in parentheses denote the order of perturbation and Ψ_0 the reference function.

The zeroth- and first-order energies, $E^{(0)}$ and $E^{(1)}$, are obtained from the zeroth-order wave function, Ψ_0,

$$E^{(0)} = \langle \Psi_0 | \hat{H}_0 | \Psi_0 \rangle \tag{2.45}$$

$$E^{(1)} = \langle \Psi_0 | \hat{V} | \Psi_0 \rangle \tag{2.46}$$

whereas the second order perturbation energy, $E^{(2)}$,

$$E^{(2)} = \sum_{\mathrm{I} \in \mathrm{FOIS}} \frac{\langle \Psi_0 | \hat{V} | I \rangle \langle I | \hat{V} | \Psi_0 \rangle}{E_0 - E_{\mathrm{I}}} = \sum_{\mathrm{I} \in \mathrm{FOIS}} \frac{|\langle \Psi_0 | \hat{V} | I \rangle|^2}{E_0 - E_{\mathrm{I}}} \tag{2.47}$$

is calculated from the perturbation of the reference function Ψ_0 by the functions $|I\rangle$ and their corresponding energies, E_0 and E_I. Those functions $|I\rangle$ are considered that belong to the *first order interacting space* (FOIS). In general, the FOIS corresponds to the space of determinants that interact with Ψ_0. Different methods can be distinguished by their definition of the FOIS, the reference function Ψ_0 and the reference Hamiltonian $\hat{H}_0$.

Single-reference perturbation theory

If a mono-determinantal reference function describes sufficiently well the considered electronic problem, Ψ_0 can be chosen to be the HF wave function. If, additionally, the operator $\hat{H}_0$ is chosen to be the Fock operator $\hat{F}$ and the perturbation

$$\hat{V} = \sum_{i<j} \frac{1}{r_{ij}} - \sum_{i}^{N} v^{HF}(i) \tag{2.48}$$

restores the complete Hamiltonian, one speaks of *Møller-Plesset-perturbation theory* (MPPT). [7] More precisely, the abbreviation "MP2" is employed for an energy perturbation limited to second order.

In that case, the sum of the zeroth- and first-order energies (eq. (2.45) and eq. (2.46)) corresponds to the HF energy,

$$E^{(0)} + E^{(1)} = \langle \Psi_0 | \hat{H} | \Psi_0 \rangle = E_{\mathrm{HF}} \tag{2.49}$$

and the first correction to the HF energy occurs at the second order in the energy. Based on the Brillouin theorem and the limiting two-electron nature of the perturbation operator, only the doubly excited determinants, Ψ_{ab}^{pq} are included in the FOIS and eq. (2.47) becomes,

$$E^{(2)} = \sum_{\substack{a<b \\ p<q}} \frac{|\langle \Psi_0 | \hat{V} | \Psi_{ab}^{pq} \rangle^2|}{E_0 - E_{ab}^{pq}} \tag{2.50}$$

which can be expressed in terms of the two-electron operator (see Tab. 2.2.1) and the energies $\varepsilon_{a,b}$ and $\varepsilon_{p,q}$ of the occupied and virtual orbitals involved in the double excitation,

$$E^{(2)} = \sum_{\substack{a<b \\ p<q}} \frac{|\langle \Psi_0 | \sum_{i<j} \frac{1}{r_{ij}^{-1}} | \Psi_{ab}^{pq} \rangle^2|}{\varepsilon_a + \varepsilon_b - \varepsilon_p - \varepsilon_q} \tag{2.51}$$

Such an approach includes the dynamical correlation at a lower cost than CISD and is size-extensive. However, it does not incorporate the static correlation and is not variational.

A deficiency in MP2 arises when a perturber state is considered that is close in energy to the reference state. Such an *intruder state* leads to a denominator

in eq. (2.50) that tends to zero and creates thus a divergence of the perturbation expansion.

Multi-reference perturbation theory

In order to incorporate static correlation, the reference function Ψ_0 in eq. (2.44) is chosen to be of CAS (CAS-CI,CASSCF) type in *second order perturbation theory with a CAS reference function* approaches. Two implementations of this kind are CASPT2 [8, 9] and *n-electron valence state perturbation theory* (NEVPT2) [10–13]. The singly and doubly excited determinants with respect to the reference function are partitioned into eight different subspaces of perturber functions according to their numbers of holes and particles analogous to the definition used in DDCI (sec. 2.2.1). In CASPT2, the FOIS spans over all these determinants whereas NEVPT2 follows a contraction scheme to reduce the FOIS down to one interacting function in the strongly contracted variant.

The two methods can be principally distinguished by their choice of the zeroth-order Hamiltonian $\hat{H}_0$. In CASPT2, the Fock operator as in MP2 is used whereas NEVPT2 employs the Dyall Hamiltonian. The latter is mono-electronic in the inactive and virtual spaces but fully bi-electronic in the active space.

2.3 Conclusion

Several methods have been presented in this chapter that all aim at approximating the electronic correlation in the best way possible. They can roughly be categorized in perturbative (MP2, CASPT2, NEVPT2) and variational (SCF, CI, CASSCF) methods. The former ones are computationally less demanding and do not (except CASPT2) present an error of size-consistency. However, they are not variational. The SCF, CI and CASSCF methods present this very advantage but are (except SCF) computationally more demanding.

Bibliography

[1] Szabo, A.; Ostlund, N. S. *Modern Quantum Chemistry*; Dover Publications Inc., New York, USA, 1996.

[2] Helgaker, T.; Jørgensen, P.; Olsen, J. *Molecular Electronic-Structure Theory*; John Wiley and Sons Ltd, West Sussex, England, 2000.

[3] Slater, J. C. *Phys. Rev.* **1929**, *34*, 1293–1322.

[4] Huron, B.; Malrieu, J. P.; Rancurel, P. *The Journal of Chemical Physics* **1973**, *58*, 5745–5759.

[5] Miralles, J.; Castell, O.; Caballol, R.; Malrieu, J.-P. *Chemical Physics* **1993**, *172*, 33 – 43.

[6] Condon, E. U. *Phys. Rev.* **1930**, *36*, 1121–1133.

[7] Møller, C.; Plesset, M. S. *Phys. Rev.* **1934**, *46*, 618–622.

[8] Andersson, K.; Malmqvist, P. A.; Roos, B. O.; Sadlej, A. J.; Wolinski, K. *J. Phys. Chem.* **1990**, *94*, 5483–5488.

[9] Andersson, K.; Malmqvist, P.-A.; Roos, B. O. *J. Chem. Phys.* **1992**, *96*, 1218–1226.

[10] Angeli, C.; Cimiraglia, R.; Malrieu, J.-P. *Chemical Physics Letters* **2001**, *350*, 297 – 305.

[11] Angeli, C.; Cimiraglia, R.; Evangelisti, S.; Leininger, T.; Malrieu, J.-P. *The Journal of Chemical Physics* **2001**, *114*, 10252–10264.

[12] Angeli, C.; Cimiraglia, R.; Malrieu, J.-P. *The Journal of Chemical Physics* **2002**, *117*, 9138–9153.

[13] Angeli, C.; Evangelisti, S.; Cimiraglia, R.; Maynau, D. *The Journal of Chemical Physics* **2002**, *117*, 10525–10533.

3
Magneto-structural relation in the NiFe Prussian Blue Analogue

In many cases, experiment and theory form a fruitful couple when it is a matter of understanding macroscopic material effects on a microscopic level. This chapter is devoted to a member of the family of Prussian Blue Analogues (PBA), namely the NiFe PBA. The electronic interaction in this compound, giving rise to magnetic properties, is investigated at the CAS+DDCI level. More precisely, the impact of a local deformation of the NiFe bi-metallic embedded cluster on the exchange coupling constant J is analyzed. The possibility to generate cation-coupled electron transfer is suggested by the evaluation of the effective hopping parameter. This work has lead to a publication in PCCP (T. Krah et al., 2014).[1]

Prussian Blue has received considerable attention as an inexpensive synthetic pigment ever since its synthesis at the beginning of the 18^{th} century.[2] On the other hand, Prussian Blue Analogues (PBA) owe their ongoing popularity to interesting physical and chemical properties such as spin-crossover, electron transfer or valence tautomerism.[3–5] The possibility to induce a reversible change in their electronic structure has stimulated much experimental and theoretical works with potential applications in information storage devices. A variety of magnetic interactions sprouts from the presence of 3*d* paramagnetic ions connected by cyano bridges, ranging from room-temperature magnets[6, 7] to single-molecule magnets.[8]

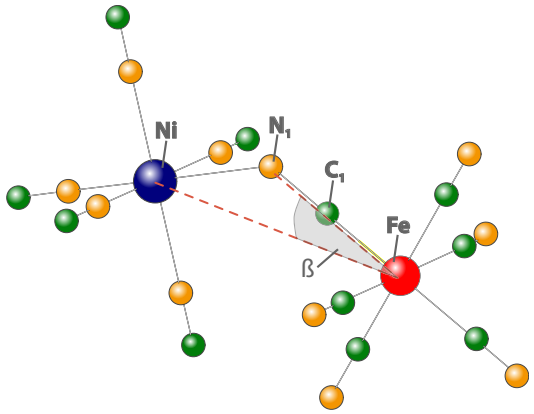

Figure 3.1
Representation of the Ni(II)$(NC)_5$-N_1C_1-Fe(III)$(CN)_5$ cluster. The rotation of the $Ni(NC)_5$ and the rigid $Fe(CN)_6$ unit in opposite directions leads to the opening of the bridging C_1N_1 ligand. This structural deformation is measured by the angle β.

PBAs contain one or two different transition metal centers M and M' bridged by cyanide ligands to form a face-centered cubic lattice structure. It is important to note, that the complexity in PBAs varies significantly with the type of constituent transition metals M and M'. In general, structural modifications within the lattice, electron transfers reactions, and magnetic properties modifications are intermingled. Using state-of-the-art *ab initio* methods, the computational effort necessary to capture all electronic effects, exceeds in certain cases current feasibility limits. In that sense, the Ni(II)-Fe(III) PBA turns out to be a relevant candidate since electron transfer has not been stressed out whereas magnetic interaction between paramagnetic centers is anticipated to be the predominant phenomenon.

Emphasis should also be put on the observation that the NiFe analogue is part of a series of PBA matrices which prove to be remarkable hosts for alkali ions. Indeed, M-CN-M' units have been recently considered as potential cathodes for Na^+-ion based batteries. Compounds of chemical formula $KM[Fe(CN)_6]\cdot zH_2O$ (M,M' = Mn, Fe, Co, Ni, Zn) have demonstrated promising capacities thanks to the large interstitial spaces that offer reversible insertion and mobility.[9–11] The possibility to replace Li^+ ions by Na^+ ions in traditional batteries is of particular importance considering the lithium demand.

The aim of this part of my work has been to investigate the speculated ferromagnetic-to-antiferromagnetic transition in the Ni(II)-Fe(III) PBA by means of wave function-based calculations. Indeed, the relationship between structural deformations (see Fig. 3.1) and the electronic structure is of prime importance in order to understand the resulting macroscopic properties.

3.1 Theoretical Details

The magnetic interactions in the NiFe compound are governed by the overlap of the magnetic orbitals on the Ni and Fe centers and the σ, π and π^* orbitals of the bridging C_1-N_1 cyanide ligand (see Fig. 3.1 for notations). It is known from experiments that the $Fe(CN)_6$ unit is rather rigid[12, 13] whereas distortions are likely to occur around the Ni center. Indeed, X-ray diffraction measurements performed under high pressure conditions have suggested the existence of a weakness in PBAs lattices around the divalent ion, namely Ni(II).[13] During the opening of the bridging C_1N_1 ligand along the angle β (see Fig. 3.1), the $Ni(NC)_6$ unit is forced out its perfectly octahedral coordination while that of the stiff $Fe(CN)_6$ neighbour remains untouched. Therefore, this is a relevant deformation which is expected to modify the orbital overlap, and as a result the exchange interactions between the paramagnetic centers.

A complete *ab initio* treatment of a solid material is obviously out of reach using wave-function based methods. The commonly employed embedded cluster approach allows for accurate wave function calculations on a molecular cluster while still taking into account the leading effects of the actual crystalline surrounding by immersion of the cluster in the so-called *embedding*.[14–18] In this study, the cluster definition comprises the two magnetic sites and their respective first coordination spheres, that is, $Ni(II)(NC)_5$-N_1C_1-$Fe(III)(CN)_5$, called NiFe cluster hereafter. All-electron basis functions were introduced on all atoms of this NiFe cluster. Namely, I used the recently developed atomic natural orbital ANO-RCC basis sets[19, 20] with the following contractions, commonly accepted for studies of magnetic systems:[18] Fe, Ni (5s4p2d); C,N (3s2p1d). The objective of the embedding is to take into account the main effects of the crystal structure onto the cluster. These effects can be separated into a short-range contribution consisting of Coulomb contributions and quantum exchange interactions and a long-range repulsion arising essentially from the Madelung potential generated by the surrounding ions. The short-range interactions are limited to first-shell neighbours of the cluster. In contrast, more distant ions of the crystal environment are considered to contribute only to the Madelung potential. In this case, the short-range embedding (up to the first cluster neighbours) contains 10 total ion pseudopotentials (TIPs) on the Ni(II) and Fe(III) ions that account principally for the Pauli exclusion zones in the actual cluster proximity. Then, formal point charges [Fe(3+), Ni(2+), C(-0.5), N(-0.5)] were used to reproduce the long-range Madelung potential, a critical quantity in ionic[18, 21] and molecular[22] crystals. Using this approach, a rectangular box of approximately 10 Å×10 Å×15 Å containing TIPs and formal point charges was considered around the central NiFe cluster (see Fig. 3.2). The cluster atoms, TIPs and point charges were located at the crystallographic positions reported by Kuwabara *et al.*, [23] associated with the following bond distances : d(Ni-N)=2.03 Å, d(C-N)=1.15 Å and d(Fe-C)=1.93 Å. During the cluster deformation the TIPs and point charges remain on their crystallographic positions. The deformation was carried out by increasing

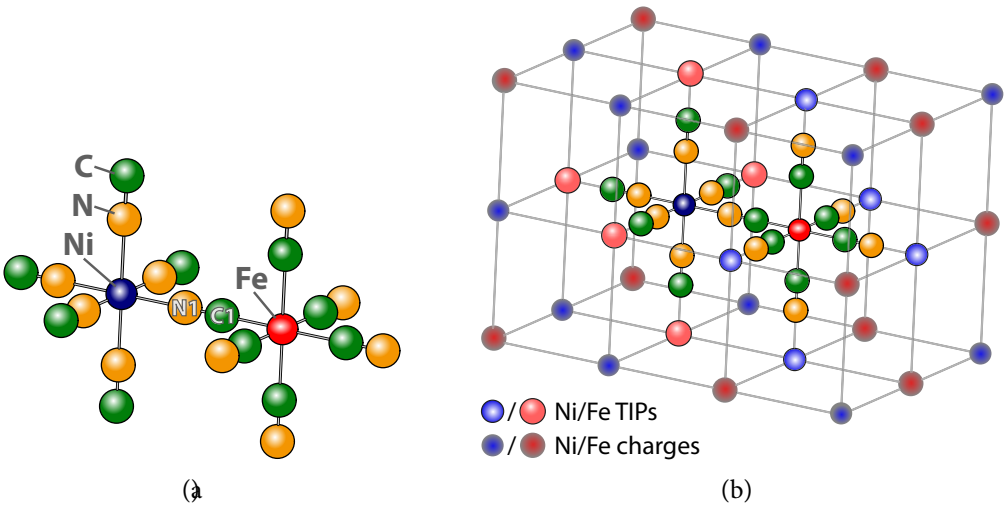

Figure 3.2: (*a*) Ni(II)$(NC)_5$-N_1C_1-Fe(III)$(CN)_5$ cluster used for the DDCI calculations (*b*) embedded cluster in the NiFe PBA lattice. Embedding CN bridges are represented as grey lines for clarity.

the angle β (see Fig. 3.1) from 0 to 25° in 5°-steps. All the Ni(II) and Fe(III) ions were maintained on their crystallographic positions as the two ML_6 units were turned in opposite directions while maintaining a constant angle $\angle(Fe - C_1 - N_1) = 180°$. Consequently, the Ni-$N_1$ bond distance was stretched up to 2.66 Å at the maximum angle value $\beta = 25°$.

Based on this embedded cluster model, the electronic correlation can be divided into static and dynamic contributions. The former results from degenerate or quasi-degenerate electronic configurations while the latter captures the instantaneous electron-electron interactions. The static correlation is introduced by complete active space self-consistent field (CASSCF)[24] calculations using the 7.8 release of the *MOLCAS* package.[25] As expected from the large CN^- crystal field parameter and confirmed experimentally,[26] the Fe(II,d^5) ion is in a low-spin configuration $S_{Fe} = 1/2$ and exhibits one singly-occupied 3d orbital of t_{2g}-type. It should be noted, that in the C_s point group this orbital belongs to a different irreducible representation than the other two quasi-degenerate 3d orbitals. The Ni(II,d^8) ion has two singly occupied 3d orbitals of e_g-type, resulting in $S_{Ni} = 1$. Consequently, a minimal active space consisting of 3 electrons in 3 orbitals (CAS[3,3]) was used (see Fig. 3.3).

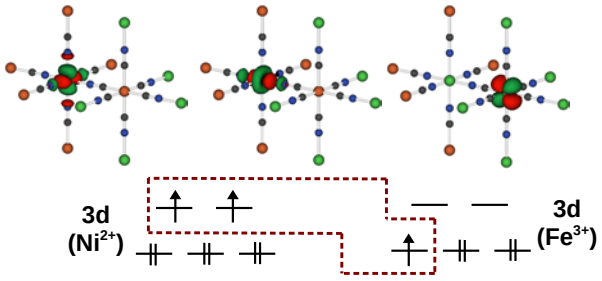

Figure 3.3
The CAS[3,3] (dashed red line) used in the calculations and the corresponding Ni(II) (left) and Fe(III) (right) magnetic orbitals. The represented spin configuration corresponds to a quartet state.

3.2 Exchange interaction

3.2.1 Analytical description

The magnetic behaviour (AFM or FM) can be modeled by parameters such as the hopping integral t, the exchange integral K and the on-site repulsion U. In the following, we will derive this description for the case of the NiFe PBA. The local spins can be either $S_{\mathrm{Ni}} = 1$ or $S'_{\mathrm{Ni}} = 0$ on the Ni center, and $S_{\mathrm{Fe}} = 1/2$ on the Fe site. From the field generated by the cyano ligands, the local singlet state $S'_{\mathrm{Ni}} = 0$ lies much higher in energy. Thus, I assume a local triplet and doublet state on the Ni and Fe centers, respectively. Therefore, the total spin S_{tot} of the model cluster ranges from $|S_{\mathrm{Ni}} - S_{\mathrm{Fe}}| = 1/2$ to $S_{\mathrm{Ni}} + S_{\mathrm{Fe}} = 3/2$. The following derivation will give the analytical expression for the energy difference ΔE between the doublet ($S_{\mathrm{tot}} = 1/2$) and quartet ($S_{\mathrm{tot}} = 3/2$) states (see Fig. 3.3). The magnetic orbitals on the Ni and Fe centers are referred to as a,a' and b, respectively.

In a first step, the consideration is limited to those determinants that preserve the number of electrons on each metal center (*i.e.* "neutral determinants"), namely

$$\phi_N = |aa'\bar{b}|; \quad \phi'_N = \frac{|a\bar{a}'b| + |\bar{a}a'b|}{\sqrt{2}}.$$

In this 2 × 2 space, the energy difference between the doublet and quartet states ΔE_N reads

$$\Delta E_N = 2\sqrt{2}K_{ib} \tag{3.1}$$

where $K_{ib} = (ib, bi) = \langle i\bar{b}|\hat{H}|b\bar{i}\rangle$ ($i = a,a'$) is the exchange integral between the two magnetic sites. We assume here that $K_{ab} = K_{a'b}$.

In a second step, configurations that account for electron hopping from one site to the other (*i.e.* "ionic determinants") are included to enlarge the representation space. Such ionic forms can be written as

$$\phi_I^{Ni1} = |a\bar{a}a'|; \; \phi_I^{Ni2} = |aa'\bar{a}'|; \; \phi_I^{Fe1} = |ab\bar{b}|; \; \phi_I^{Fe2} = |a'b\bar{b}|.$$

The corresponding hopping integrals t_{ab} and $t_{a'b}$ connect neutral to ionic forms as

$$t_{ab} = \langle a\bar{a}a'|\hat{H}|\bar{a}a'b\rangle\,; \quad t_{a'b} = \langle aa'\bar{b}|\hat{H}|ab\bar{b}\rangle\,,$$

One should recall that the amplitude of the hopping integrals is essentially proportional to the overlap between the magnetic orbitals. Following a perturbative treatment of the energies, the inclusion of the above ionic determinants ϕ_I leads to a relative stabilization of the doublet state with respect to the quartet state

$$\Delta E_I = \frac{4\sqrt{2}}{3}(t_{ab}^2 + t_{a'b}^2)\left(\frac{1}{U_a} + \frac{1}{U_b}\right) \tag{3.2}$$

where U_a and U_b stand for the on-site electron-electron repulsion, $U_i = (ii, ii) = \langle i\bar{i}|\hat{H}|i\bar{i}\rangle$. Equations 3.1 and 3.2 can be combined to give rise to the doublet-quartet energy splitting

$$\Delta E = 2\sqrt{2}\,K_{\text{eff}} - \frac{4\sqrt{2}}{3}\,\frac{t_{\text{eff}}^2}{U_{\text{eff}}} \tag{3.3}$$

where $t_{\text{eff}}^2 = t_{ab}^2 + t_{a'b}^2$ and $\frac{1}{U_{\text{eff}}} = (\frac{1}{U_a} + \frac{1}{U_b})$. K_{eff} is the effective exchange integral assumed to be unique whatever a or a'. As expected, two competing contributions can be identified. The first part of eq. (3.3) favours a ferromagnetic coupling between the two sites whereas the second part favours an antiferromagnetic behaviour. The impact of the latter depends on the ratio of the effective hopping integral t_{eff} and the effective on-site repulsion U_{eff}.

The spin-Hamiltonian

$$H = -JS_{\text{Ni}} \cdot S_{\text{Fe}} \tag{3.4}$$

first introduced by Heisenberg [27] and later discussed by Dirac and Van Vleck [28] introduces the so-called exchange coupling constant J.[29] Such model Hamiltonian relies on this single parameter J, and describes the interaction between two spins, $S_{\text{Ni}} = 1$ and $S_{\text{Fe}} = 1/2$ localized on the Ni and Fe centers, respectively. J is uniquely determined by the doublet and quartet states energies and reads

$$J = \frac{1}{3}\left[E(S_{\text{tot}} = 1/2) - E(S_{\text{tot}} = 3/2)\right] \tag{3.5}$$

Besides, J can be split into ferromagnetic (FM) J_{FM} and antiferromagnetic (AFM) J_{AFM} contributions

$$J = J_{FM} + J_{AFM} \tag{3.6}$$

in correspondence to the first and second part of the analytical expression 3.3.

Angle β (°)	J_{CI} (cm^{-1})	J_{DDCI} (cm^{-1})
0	+1.8	+11.4
5	+1.2	+7.4
10	-0.4	-1.1
15	-1.7	-10.0
20	-2.1	-12.4
25	-1.5	-8.5

Table 3.1: CAS-CI (CI) and CAS-DDCI (DDCI) calculated exchange coupling constants (cm^{-1}) with respect to the deformation angle β (°) (see Fig. 3.1). The set of MOs used in the DDCI calculations is the quartet state one (see Fig. 3.3).

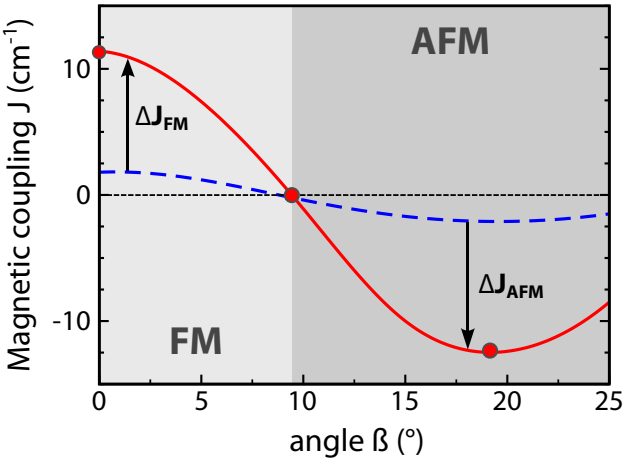

Figure 3.4
Exchange coupling constant J (cm^{-1}) as a function of the deformation angle β (N_1FeNi) at CAS(3,3) (blue, dashed line) and DDCI (red, solid line) level of theory. The ferromagnetic (FM, $J > 0$) and antiferromagnetic (AFM, $J < 0$) regimes are highlighted. Red circles illustrate the positions of particular values used in the text.

3.2.2 Numerical results

The exchange coupling constant J has been calculated following eq. (3.5) as a function of the deformation angle β. The results are summarized in Tab. 3.1 and represented in Fig. 3.4.

I shall first discuss the J_{CI} values in Tab. 3.1. These are obtained from CAS[3,3]-CI calculations using the state-specific CAS[3,3]SCF MOs of the $S = 3/2$ state.

In the $\beta \sim 0°$ regime, the system exhibits ferromagnetic (FM) behaviour (J =+1.8 cm^{-1}). This result is a reflection of the orthogonality between the t_{2g}-like (b) and e_g-like (a, a') MOs localized on the Fe(III) and Ni(II) centers. As mentioned previously, the hopping integral t_{eff} is proportional to the overlap between these orbitals. As expected from Kahn's model, the antiferromagnetic contribution is suppressed with a vanishingly small t_{eff} value, leaving a FM behaviour (see J_{CI} values in Tab. 3.1).

As soon as the cluster is deformed, the magnetic orbital overlap is enhanced and switches on the antiferromagnetic contribution. Therefore, the J value is reduced and spans the FM regime up to a β value of 9.5° (see Fig. 3.4). For this critical value, the Ni-N distance is 2.14 Å as compared to the reported value 2.03 Å.[23] Beyond this critical value, the system exhibits an AFM behaviour up to $\beta = 25°$, with the lowest J value of -2.1 cm^{-1} at $\beta = 20°$.

Now the focus lies on the DDCI set of calculated values. The importance of correlation effects to reach spectroscopic accuracy has been discussed in the literature.[30, 31] First, the *J* value of the non-deformed complex (β =0°, J = +11.4 cm^{-1}) is consistent with the experimental Curie temperature value T_c = 24 K,[26] using the relation between T_c and *J* given by Ruiz *et al.* [32] and therefore validates our embedded cluster DDCI calculations. It is noticeable that the same FM and AFM regimes as for CAS(3,3)CI can be identified at the DDCI level. Since they share a common frontier at β = 9.5°, the qualitative behaviour is not modified. However, the dynamical correlation introduced at the DDCI level greatly amplifies the height of variations, with *J* values ranging from +11.4 cm^{-1} at β = 0° to -12.5 cm^{-1} at β = 19° (see Fig. 3.4). In the FM region, $J_{DDCI} = J_{CI}+\Delta J_{FM}$ with $\Delta J_{FM} > 0$ whereas in the AFM region $J_{DDCI} = J_{CI}+\Delta J_{AFM}$ with $\Delta J_{AFM} < 0$ (see Fig. 3.4). In other words, the correlation effect at the DDCI level seems to stabilize whichever form of magnetic behaviour is dominant in the wave function at the CAS-CI level.

The positive character of ΔJ_{FM} deserves particular attention. It should be recalled that the DDCI space includes the important 2h-1p and 1h-2p sets of excitations. For ferromagnetic systems, the wave functions are essentially represented by neutral forms. Therefore, the AF pathways involving the stabilization of the ionic forms have a negligible contribution. At the DDCI level, the leading contribution effect is not related to the direct interaction of 2h-1p excitations with the valence-bond forms. Their ferromagnetic contribution is associated to more complex pathways involving simultaneously other types of excitations, ligand-to-metal charge transfer (LMCT) forms.[33, 34] As previously reported from selected CI calculations,[34] the presence of the 2h-1p determinants produces an enhancement of the LMCT forms. Besides, the LMCT quartet state is expected to be stabilized as compared to the doublet by Hund's rule. Therefore, the coupling between 2h-1p and the LMCT forms favours the quartet state, and consequently gives rise to a ferromagnetic contribution $\Delta J_{FM} > 0$.

This is to be contrasted with the AFM regime in Fig. 3.4. The calculated $\Delta J_{AFM} < 0$ at the DDCI level is a reflection of the stabilization of the ionic forms which progressively gain weight in the CAS-CI wave function. It is known from the literature that instantaneous charge reorganization (so-called dynamical correlation effects) stabilizes the ionic forms.[30] Such phenomenon is introduced beyond the CASSCF mean field picture and plays a dominant role in the spin states ordering. As a consequence, U_{eff} in Equation 3.3 is reduced by the introduction of dynamical correlation effects, and negative ΔJ_{AFM} are expected.

Finally, from the rigidity imposed to the $Fe(CN)_6$ unit, the Ni-N_1 distance is continuously stretched along the deformation. Therefore, the overlap between the Ni 3d and the bridging π orbitals is reduced, leading to an increase of *J* beyond the minimum value found at β = 19°. It can be seen that such regime is not realistic since the Ni-N_1 distance is stretched by more than 30%.

In order to quantify the effective hopping integral t_{eff} modulation, we finally used the DDCI *J* values calculated for β = 0, 9.5 and 19°, *J* = 11.4, 0 and -12.5 cm^{-1} (red circles in Fig. 3.4). From the value at β = 0°, eq. (3.3) leads to K_{eff} = 4.03 cm^{-1} since

t_{eff} is negligibly small. Due to the strong atomic character of the magnetic orbitals (projections on the 3d atomic orbitals are larger than 0.75 for $0° < \beta < 20°$), the K_{eff} and U_{eff} were assumed to be constant along the deformation. This assumption allows one to concentrate on the modification of the hopping integral parameter. One can easily observe that t_{eff} is increased by a factor 1.5 as the angle β is increased from 9.5 to 19°.

In view of the proven Na^+ mobility in NiFe PBA, a scenario is proposed in which the increase of the hopping integral is coupled to the Na^+ ion diffusion within the matrix. In analogy with "proton-coupled electron transfer" (PCET)[35–37] processes, such a mechanism would correspond to a "cation-coupled electron transfer" (CCET).

3.3 Conclusion

The magnetic interaction in the NiFe Prussian Blue Analogue has been analyzed based on accurate wave function calculations. The comparatively limited complexity in the electronic structure allowed to include relevant magnetic orbitals of both metal sites in a CAS(3,3) treatment followed by DDCI calculations on the embedded $Ni(II)(NC)_5$-$Fe(III)(CN)_6$ cluster. In the case of the non-distorted structure, the result is consistent with the experimental Curie temperature. A rather significant change in the calculated exchange coupling constant (*i.e.*, 23.9 cm^{-1}) revealed a ferromagnetic to antiferromagnetic transition as the local environment of the Ni center is modified away from strictly octahedral geometry. Such a behaviour has been previously proposed to interpret X-ray measurements [13] and can be understood as an increase of magnetic orbital overlap. In that sense, the cluster deformation switches on the effective hopping transfer t_{eff} between the magnetic centers. t_{eff} increases by a factor of ~1.5 over a rather small opening-range of ~10° of the Ni-NC-Fe cyano bridge. A coupling of the increase of the electron hopping integral with the Na^+ ion mobility is suggested that would offer an additional factor tuning the magnetic and conducting properties within this class of materials.

Bibliography

[1] Krah, T.; Amor, N. B.; Robert, V. *Phys. Chem. Chem. Phys.* **2014**, *16*, 9509–9514.

[2] Stahl, G. E. *Experimenta, Observationes, Animadversiones CCC Numero, Chymicae et Physicae* **1731**, 281–283.

[3] Dei, A.; Gatteschi, D.; Sangregorio, C.; Sorace, L. *Accounts of Chemical Research* **2004**, *37*, 827–835.

[4] Evangelio, E.; Ruiz-Molina, D. *European Journal of Inorganic Chemistry* **2005**, *2005*, 2945–2945.

[5] Evangelio, M.-L.; Cabanas, M.; Nakano, M.; Sutter, J.-P.; Dei, A.; Robert, V.; Ruiz-Molina, D. *Chem. A. Eur. J.* **2010**, *16*, 6666–6677.

[6] Mallah, T.; Thiébaut, S.; Verdaguer, M.; Veillet, P. *Science* **1993**, *262*, 1554–1557.

[7] Ferlay, S.; Mallah, T.; Ouahès, R.; Veillet, P.; Verdaguer, M. *Nature* **1995**, *378*, 701–703.

[8] Cho, K. J.; Ryu, D. W.; Kwak, H. Y.; Lee, J. W.; Lee, W. R.; Lim, K. S.; Koh, E. K.; Kwon, Y. W.; Hong, C. S. *Chem. Commun.* **2012**, *48*, 7404–7406.

[9] Lu, Y.; Wang, L.; Cheng, J.; Goodenough, J. B. *Chem. Commun.* **2012**, *48*, 6544–6546.

[10] Wessells, C. D.; Peddada, S. V.; McDowell, M. T.; Huggins, R. A.; Cui, Y. *Journal of The Electrochemical Society* **2011**, *159*, A98–A103.

[11] Moritomo, Y.; Takachi, M.; Kurihara, Y.; Matsuda, T. *Applied Physics Express* **2012**, *5*, 041801.

[12] Yokoyama, T.; Ohta, T.; Sato, O.; Hashimoto, K. *Phys. Rev. B* **1998**, *58*, 8257–8266.

[13] Cafun, J.-D.; Lejeune, J.; Itié, J.-P.; Baudelet, F.; Bleuzen, A. *The Journal of Physical Chemistry C* **2013**, *117*, 19645–19655.

[14] de Graaf, C.; de P. R. Moreira, I.; Illas, F.; Martin, R. L. *Phys. Rev. B* **1999**, *60*, 3457–3464.

[15] Moreira, I. d. P. R.; Illas, F.; Calzado, C. J.; Sanz, J. F.; Malrieu, J.-P.; Ben Amor, N.; Maynau, D. *Phys. Rev. B* **1999**, *59*, R6593–R6596.

[16] de Graaf, C.; Illas, F.; Broer, R.; Nieuwpoort, W. C. *J. Chem. Phys.* **1997**, *106*, 3287–3291.

[17] Illas, F.; Casanovas, J.; Garcia-Bach, M. A.; Caballol, R.; Castell, O. *Phys. Rev. Lett.* **1993**, *71*, 3549–3552.

[18] Krah, T.; Suaud, N.; Zanchet, A.; Robert, V.; Ben Amor, N. *European Journal of Inorganic Chemistry* **2012**, 5777–5783.

[19] Roos, B. O.; Lindh, R.; Malmqvist, P.-A.; Veryazov, V.; Widmark, P.-O. *J. Phys. Chem. A* **2004**, *108*, 2851–2858.

[20] Roos, B. O.; Lindh, R.; Malmqvist, P.-A.; Veryazov, V.; Widmark, P.-O. *J. Phys. Chem. A* **2005**, *109*, 6575–6579.

[21] Le Guennic, B.; Borshch, S.; Robert, V. *Inorganic Chemistry* **2007**, *46*, 11106–11111.

[22] Kepenekian, M.; Le Guennic, B.; Robert, V. *Phys. Rev. B* **2009**, *79*, 094428.

[23] Yamada, S.; Kuwabara, K.; Koumoto, K. *Materials Science and Engineering: B* **1997**, *49*, 89 – 94.

[24] Roos, B. O.; Taylor, P. R.; Siegbahn, P. E. *Chemical Physics* **1980**, *48*, 157 – 173.

[25] Karlström, G.; Lindh, R.; Malmqvist, P.-A.; Roos, B. O.; Ryde, U.; Veryazov, V.; Widmark, P.-O.; Cossi, M.; Schimmelpfennig, B.; Neogrady, P.; Seijo, L. *Comput. Mater. Sci.* **2003**, *28*, 222–239.

[26] Juskzykt, S.; Johansson, C.; Hansont, M.; Ratusmas, A.; Makckill, G. *J. Phys.: Condens. Matter* **1994**, *6*, 5697–5705.

[27] Heisenberg, W. *Z. Phys* **1928**, *49*, 619.

[28] Dirac, P. A. M. *The Principles of Quantum Mechanics*, 3rd ed.; Clarenden, Oxford, 1947; Vol. Chap. IX.

[29] Verdaguer, M.; Robert, V. In *Comprehensive Inorganic Chemistry {II} (Second Edition)*, second edition ed.; Reedijk, J., Poeppelmeier, K., Eds.; Elsevier: Amsterdam, 2013; pp 131 – 189.

[30] Calzado, C. J.; Cabrero, J.; Malrieu, J. P.; Caballol, R. *The Journal of Chemical Physics* **2002**, *116*, 2728–2747.

[31] Calzado, C. J.; Cabrero, J.; Malrieu, J. P.; Caballol, R. *The Journal of Chemical Physics* **2002**, *116*, 3985–4000.

[32] Ruiz, E.; Rodríguez-Fortea, A.; Alvarez, S.; Verdaguer, M. *Chemistry – A European Journal* **2005**, *11*, 2135–2144.

[33] Calzado, C. J.; Angeli, C.; Taratiel, D.; Caballol, R.; Malrieu, J.-P. *The Journal of Chemical Physics* **2009**, *131*, 044327–044340.

[34] Rota, J.-B.; Calzado, C. J.; Train, C.; Robert, V. *The Journal of Chemical Physics* **2010**, *132*, 154702.

[35] Feig, A. L.; Lippard, S. J. *Chem. Rev.* **1994**, *94*, 759–805.

[36] Mayer, J. M. *Annu. Rev. Phys. Chem.* **2004**, *55*, 363–390.

[37] Weinberg, D. R.; Gagliardi, C.; Hull, J.; Murphy, C.; Kent, C.; Westlake, B.; Paul, A.; Ess, D.; McCafferty, D.; Meyer, T. *Chem. Rev.* **2012**, *112*, 4016–4093.

4

A "wool ball" of effects - Photomagnetism in the CoFe Prussian Blue Analogue

This chapter revolves around the CoFe Prussian Blue analogue which reveals an interesting and challenging light-induced magnetization named photomagnetic effect. In this study, the LS-HS transition on the embedded $[Co^{III}(NC)_5(OH_2)]^{2-}$ *cluster has been treated through CAS(10,12)PT2 calculations. A local vacancy-induced deformation is revealed. The latter is very little influenced by the composition of the near-neighbour alkali ion environment. Based on the findings, a scenario for the Fe-Co electron transfer is suggested. The present work has been published in EJIC (T. Krah et al. 2012).[1]*

The predominant effect in the previously discussed NiFe PBA is the interaction between a small number of unpaired electrons in the Ni and Fe 3*d* orbitals leading to so-called magnetic interactions. A simple exchange of one transition metal in the NiFe PBA leads to a much more complex material. More precisely, when exchanging Ni against Co, one obtains the CoFe PBA which bears the same crystal structure as its sister compound (face-centered cubic) but a considerably more complicated electronic structure.

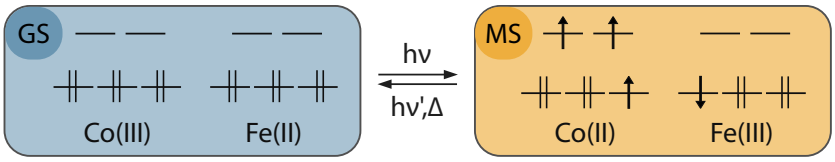

Figure 4.1: Scheme of the light-induced transition from a diamagnetic ground state (GS) to a ferrimagnetic metastable state (MS). The reverse transition can be initiated by light or a thermal treatment.

Sato *et al.* inspected the CoFe PBA experimentally and measured a clear enhancement in magnetization upon irradiation with red light ($\lambda = 660nm$).[2] Without further external stimulus, the increased magnetization persisted for several days at $T = 5K$, but could be switched off partially by irradiation in the blue ($\lambda = 450nm$) and completely by thermal treatment ($T = 150K$). Such a reversible behaviour makes them ideal candidates in the search for tunable bistable compounds with potential applications in information storage. The increase in magnetization is due to a transition from a *diamagnetic* to a *ferrimagnetic* state and has been termed *photo-induced magnetism* or *photomagnetic effect* (PME). [2, 3] The diamagnetic - ferrimagnetic transition can then be written as

$$\mathrm{Co}(\mathrm{t}_{2g}^6)\text{-NC-Fe}(t_{2g}^6) \longrightarrow \mathrm{Co}(\mathrm{t}_{2g}^5 e_g^2)\text{-NC-Fe}(t_{2g}^5)$$

Two effects are involved to give rise to the global transition, namely an Fe→Co electron transfer and a low-spin (LS) - high-spin (HS) transition on the Co(III) site (see Fig. 4.1).

Since the discovery of Sato *et al.*, a considerable effort has been put into the experimental inspection of the CoFe PBA (*i.e. via* X-ray, magnetic, IR and UV-vis measurements). Owing to an overall neutral compound, $[Fe(CN)_6]^{4-}$ vacancies and alkali ions A^+ (A=Rb, K, Cs) are present after synthesis of the CoFe PBA (see Fig. 4.2(a)).[4] It has been shown that the $[Fe(CN)_6]^{4-}$ vacancies are filled with water molecules leading to the modification of the short-range ligand environment of the neighbouring Co(III) sites. The experimentally observed increase of the lattice constant ($\Delta a_0 = 0.17$Å) has been linked to the occupation of the anti-bonding e_g orbitals during the photomagnetic process (see Fig. 4.1). This dilatation of the Co coordination sphere is supposed to create too strong crystal strains in a vacancy-less PBA for the phenomenon to occur. In contrast, the presence of a PME in materials doted with vacancies is supposedly owed to their capacity to attenuate such crystal strains.[3, 5] Recent DFT+U calculations in Prussian Blues have shown that the controversy about the impact of the vacancies, initially emphasized, is ongoing.[6]

Several studies also attribute an important role to the alkali ions, present in the interstitial tetrahedral sites. The investigation of a thermally induced electron transfer has shown that Cs^+ ions are responsible for a local deformation around the T_d site.[7] Furthermore, comparative measurements have shown that the derivative

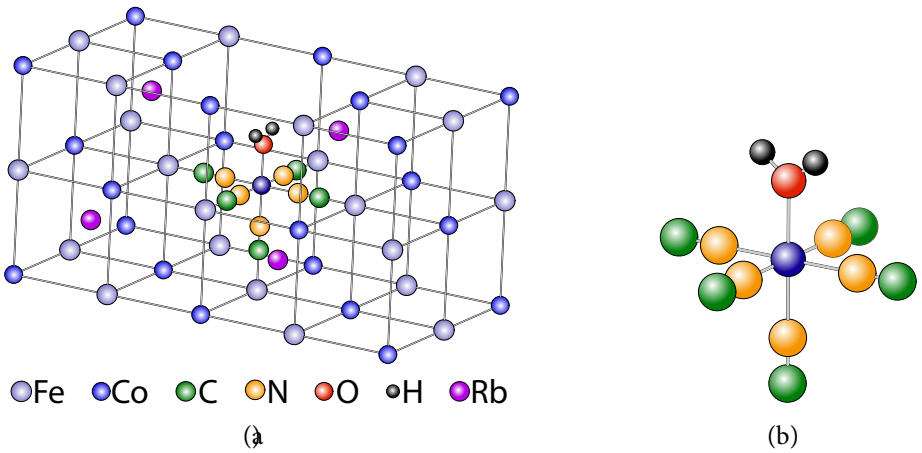

Figure 4.2: (a) The elementary lattice of the CoFe PBA. Only selected counter ions are shown for the sake of clarity. (b) Local $[Co^{III}(NC)_5(OH_2)]^{2-}$ species generated by the presence of a vacancy.

containing Rb^+ ions (RbCoFe in the following) displays a particularly pronounced photomagnetic effect.[5] In this compound, an average of one cyano ligand in the coordination sphere of Co is replaced by a water ligand and the Rb^+ ions occupy in average *ca.* 1/4 of the tetrahedral sites.

Despite the considerable experimental findings, the interplay between short-range (*i.e.* alkali ions, vacancies) and long-range (*i.e.* cooperative crystal environment) effects remains somewhat of a tangled "wool ball" based on currently available information. A theoretical study could provide helpful insight to the discussion, but is for now out of computational reach for the complete bi-metallic unit, $[Co^{III}(NC)_4(OH_2)]$-NC-$[Fe(CN)_5]$. Indeed, one could not limit the active space to a small number of 3*d* metal orbitals as was done in the NiFe analogue. On the contrary, the presence of an electron transfer in this compound would demand the inclusion of *all* Co and Fe 3*d* as well as π and π^* orbitals on the bridging CN ligand. However, considering the experimental observation, that the $\{Fe(CN)_6\}$ unit undergoes minimal structural changes during the formation of the CoFe PBA and the subsequent photo-induced phenomenon, one can anticipate that the properties of CoFe PBAs can be mostly attributed to structural changes in the vicinity of the Co ions immersed in the crystal matrix. In that sense, the present study focuses on the $[Co^{III}(NC)_5(OH_2)]^{2-}$ unit (see Fig. 4.2(b)). In a contributive effort to untangle the wool ball of effects, I investigated the energetic and structural influence of the short- and long-range environments on the Co(III) LS-HS transition.[1]

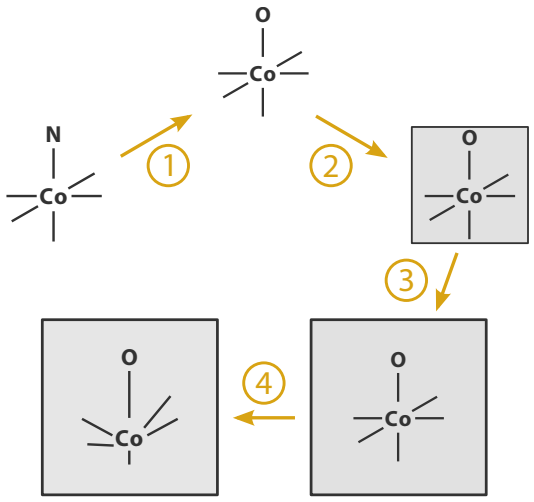

Figure 4.3
Schematic representation of the 4-step strategy used to take into account the presence of a vacancy in the ideal crystal (step 1). The crystal effects were considered through the construction of an appropriate embedding (grey square in step 2). The amplitudes of the deformations were simulated by applying a totally symmetric breathing mode to the entire crystal (step 3) and finally a local deformation in the frozen optimized environment (step 4).

4.1 Theoretical Details

The commonly employed embedded cluster approach has been followed to build the environment around the $[Co^{III}(NC)_5(OH_2)]^{2-}$ cluster.[8–11]

A 4-step strategy has been used in order to assure a proper characterization of the electronic and structural effects in the CoFe PBA (see Fig. 4.3). After the substitution of a cyano by a water ligand in the ideal $\{Co(NC)_6\}$ structure (step 1), the long- and short range embedding was constructed around the central $[Co^{III}(NC)_5(OH_2)]^{2-}$ unit adapted from the crystal structure (step 2). An optimization was then carried out with respect to two different types of structural deformation. First, a fully symmetrical breathing mode concerning both the short- and long-range environments (step 3) was investigated. Finally, the long-range environment was frozen and a local relaxation of the cluster was carried out (step 4).

In the present work, the long-range interactions were reproduced by using formal charges as point charges for the distant Fe, Co, C and N ions. As mentioned previously, experimental studies have revealed the average occupation of 2 of the 8 tetrahedral sites surrounding the Co metal by Rb^+ ions. Nevertheless, their distribution within the tetrahedral sites is not accessible from experiment. Thus, the distant alkali counter ions were treated in an average manner (see Tab. 4.1) by placing point charges of +0.25 in each tetrahedral site. Depending on the electronic configuration of the Co ion (d^6 or d^7) of the cluster model, the surrounding iron and cobalt point charges were modified to reproduce the electronic redistribution within the CoFe units. Nevertheless, the atomic positions were not modified and correspond to the ones of a perfect Co(III)-Fe(II) structure, (see (a) in Figure 1), neglecting the possible presence of other $Fe(CN)_6$ vacancies. Concerning the short-range contributions arising from the crystal, the ions up to the first-shell neighbours were treated using total ion pseudo-potentials (TIPs). [12, 13] A last consideration in the embedding optimization was dedicated to the potential generated by the nearest-neighbour

Table 4.1: Point charges used to generate the Madelung potential acting on the cluster. The charges located on the Co and Fe positions are shown for the two electronic configurations Co(d^6)-Fe(d^6) / Co(d^7)-Fe(d^5).

Co	Fe	C	N	Rb
+3 / +2	+2 / +3	-0.5	-0.5	+0.25

alkali ions. It is experimentally known but not fully understood that the nature of the cation should have an influence on the electron transfer and photomagnetic properties. First, a TIP with a +0.25 point charge was placed in each tetrahedral site to reproduce the average short-range effects arising from two Rb^+ ions in the elementary lattice. Later on, the construction of this short-range Rb^+ ion embedding will be discussed in more detail.

All calculations were performed at the CASSCF/CASPT2 [14, 15] level of theory with the 7.2 release of the *MOLCAS* package [16], using the recently developed atomic natural orbital ANO-RCC basis sets. [17, 18] These basis sets provide an improved description of the correlation of the semi-core electrons. A comparison of several different contractions was carried out and lead to the conclusion that a combination of $6s5p3d2f1g$, $4s3p2d$ and $3s2p1d$ upon the Co atom, second row elements (C,N, and O) and the H atoms, respectively, is a very satisfactory compromise between accuracy and calculation efforts. The transitions between magnetic states, as treated in the previous chapter, imply a much smaller redistribution of the electronic density than do spin transitions. The latter case thus demands more extended basis sets to properly account for the rearrangements within the metal 3d orbitals.[19, 20] To avoid intruder states, all CASPT2 calculations were performed using a level shift of 0.50 a.u. (atomic units). [21, 22] The default IPEA shift of 0.25 a.u. has been used. Scalar relativistic effects were included using a Douglas-Kroll Hamiltonian. [23, 24] As reported in the literature, [19, 25] a 10 electron/12 orbital active space is required for the electronic description of a d^6 ion using a CASPT2 approach (see Fig. 4.4). Starting from the valence-based active space (6 electrons/5d-type MOs for Co(III)), a second set of d-type metal-centered virtual orbitals with an extra radial node (*i.e.* $3d'$) is traditionally included in the active space to account for the so-called "double-shell effect". [26–29] The importance of this second d shell has been much debated previously in the context of spin crossover compounds. [13, 19, 30, 31] An active space without these $3d'$ orbitals underestimates the importance of dynamical correlation effects and charge-transfer excitations. Indeed, these charge transfers (CT) can only be well-described when the wave function is flexible enough to account for the orbital relaxation. To complement the description of CT excitations, two σ-bonding ligand orbitals were added to properly account for the non-dynamical correlation effects associated with covalent metal-ligand interactions. [32] These σ-type ligand orbitals are correlated with the antibonding (e_g-type in O_h or D_{4h}) cobalt $3d$ orbitals that are essentially empty in a LS (S = 0) configuration but become occupied in the HS (S = 2) one. The above considerations finally lead to the use of a CAS(10,12).

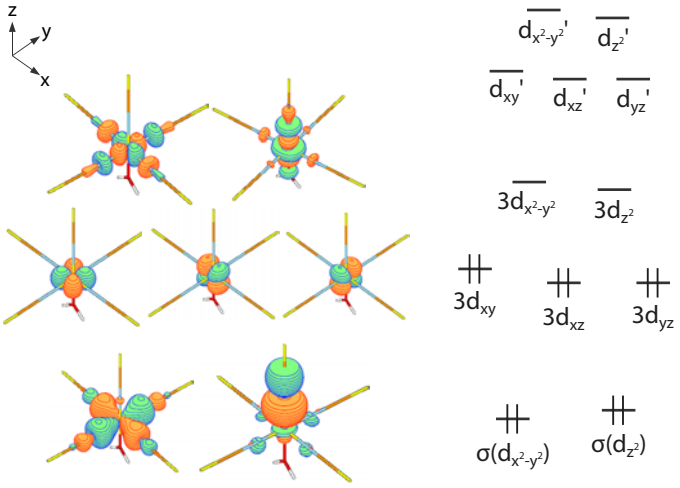

Figure 4.4
CAS(10,12) active space and selected active orbitals for the CASSCF and subsequent CASPT2 calculations on the d^6 $[Co^{III}(NC)_5(OH_2)]^{2-}$ cluster. $3d$- and σ-character orbitals are sketched for clarity.

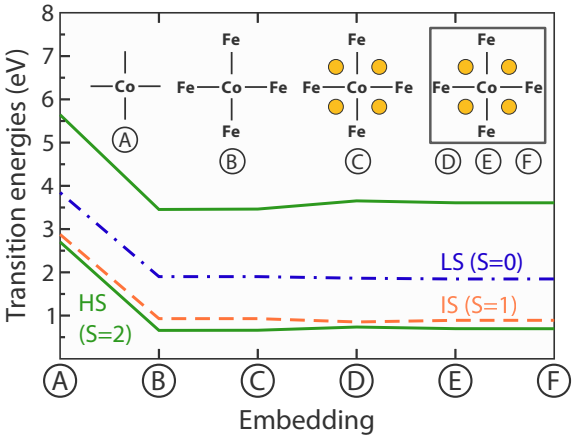

Figure 4.5
Calculated CASPT2 excitation energies (eV) from the S=0 ground state of the Co(III) cluster (A) using different embedding baths. Next-neighbour iron centers (B), average Rb ions (C) and a point charge environment (square - (D) 10 Å, (E) 20 Å, (F) 40 Å) are progressively added. Only selected states are represented for clarity (HS states (green solid lines), IS state (red dashed line), LS state (blue dashed/dotted line)).

4.2 Influence of the long-range environment

4.2.1 Dimension of the embedding

The embedding extension was defined by examining the convergence of the excitation energies involving all the S=0 (LS), S=1 (intermediate-spin, IS) and S=2 (HS) spin states arising from six electrons in five 3d orbitals. The embedding of the cluster model was progressively extended using the TIPs and point charges located on the crystallographic positions. As seen in Fig. 4.5, nearest-neighbor Fe ions play a major role in the spectroscopy definition since the LS-HS energy difference is reduced by *ca.* 2 eV as compared to the gas phase. In contrast, the presence of the alkali ions in the vicinity of the cluster does not greatly modify the energy differences. Therefore, their distribution is not relevant at this stage but this particular issue will be looked into in the following. The excitation energies are considered converged for a point charge cube of ≈ 40Å dimension in addition to the TIPs placed in proximity of the central cluster. This dimension corresponds to four times the experimentally found

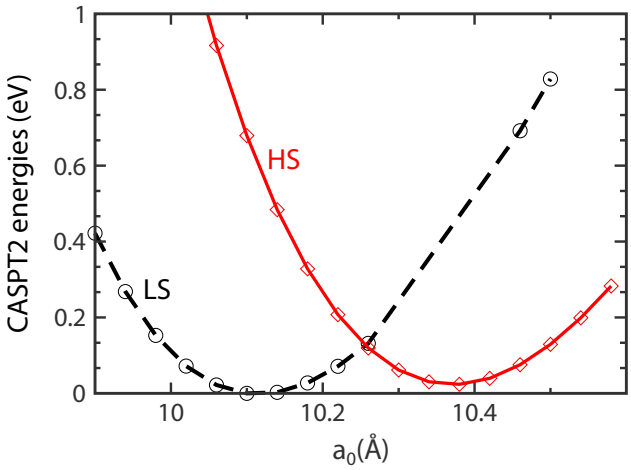

Figure 4.6
CASPT2 energy (eV) variations of the embedded $[Co^{III}(NC)_5(H_2O)]^{2-}$ LS (black, dotted line) and HS (red, solid line) states as a function of the lattice constant a_0 (Å). The reference energy is the LS state minimal energy.

lattice constant (a_0 = 9.96 ± 0.05Å). The following steps of the investigation will be based on such an environment.

4.2.2 Investigation of the lattice constant a_0

It has been experimentally observed that the $\{Fe(CN)_6\}$ units undergo only negligible structural changes during the photo-magnetic process. They can be considered as rigid octahedral units with the following bond lengths all along the transition : d(Fe-C)=1.93Åand d(C-N)=1.15Å. In that sense, the lattice constant a_0 is defined by the Co-ligand bond lengths d(Co-N) and d(Co-O). Starting from the previously converged environment, these distances were modified in the $[Co^{III}(NC)_5(H_2O)]^{2-}$ cluster as well as in the embedding in order to optimize a_0 while keeping d(Fe-C) and d(C-N) at their mentioned values. The local Co environment was in a first phase assumed to be perfectly octahedral (*i.e.* d(Co-N)= d(Co-O)). A derivation from this structure will be discussed later on. This fully symmetrical breathing mode corresponds to step 3 in Fig. 4.3. The potential energy curves of the LS (S=0) and HS (S=2) states of the $[Co^{III}(NC)_5(OH_2)]^{2-}$ cluster are shown as a function of the lattice constant in Fig. 4.6. The energy minima of the embedded cluster LS and HS states were found at a_0 = 10.11Å (d(Co-ligands)=1.97Å) and a_0 = 10.37Å (d(Co-ligands)=2.11Å), respectively. Their difference shows a 0.26Å increase in the lattice parameter during the spin transition, in good agreement with the observed experimental increase during the photomagnetic process (0.33Å).[3, 33] Furthermore, the LS and HS states are almost degenerate in their respective environments (the adiabatic LS-HS energy difference is calculated as ≈ 0.02eV). Together with the small activation energy separating the two spin states (≈ 0.1eV), this supports a reversible phenomenon in this type of material. In the following, the influence of the short-range environment will be discussed. Since the CoFe PBA is experimentally excited from a LS Co(III) center, I chose to carry out the local distortions of the LS and HS state in the above described optimal LS environment.

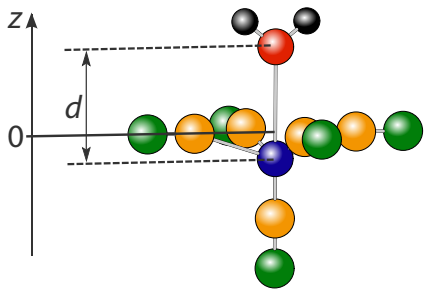

Figure 4.7
Structural parameters d and z used to examine the stability of the $Co^{III}(NC)_5(OH_2)$ cluster in the presence of a vacancy (H_2O in white and red) in the crystal structure.

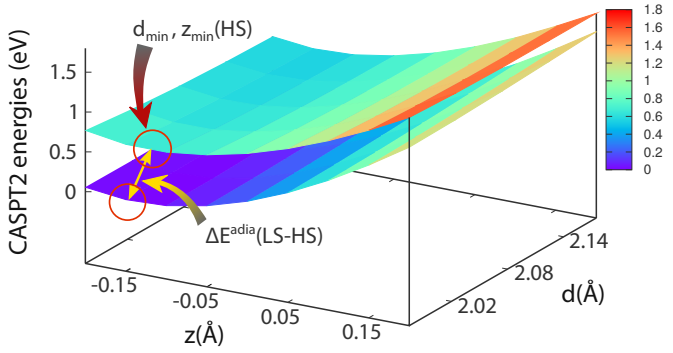

Figure 4.8
LS (bottom) and HS (top) Co(III) (a_0=10.11 Å) CASPT2 PES (eV) with respect to the structural parameters d and z (Å). The reference is the LS minimal energy. The two circles indicate the energy minima positions.

4.3 Influence of the short-range environment

4.3.1 Vacancy-induced asymmetric deformation

The $[Fe(CN)_6]^{4-}$ vacancies in the RbCoFe PBA are filled with water molecules modifying (*i*) the composition of the Co coordination sphere and (*ii*) supposedly the capacity of the crystal to attenuate crystal strains due to the Co coordination sphere dilatation. In this part of the study (step 4 in Fig. 4.3), these two points are explored by looking into a local cluster deformation along the Co-O axis. More precisely, the energies of the LS and HS states have been calculated as a function of two structural parameters shown in Fig. 4.7 : the Co-O bond length (d) and the amplitude (z) of the Co ion displacement with respect to the equatorial plane taken as a reference $z = 0$. The typical CASPT2 potential energy surfaces (PES) are shown in Fig. 4.8. The inspection of the minima of the PES allowed to identify $z_{\min}$ and $d_{\min}$, the optimal position of the Co atom and Co-O bond length, respectively. Additionally, the energetics $\Delta E^{\text{adia}}_{\text{LS-HS}}$ and structural changes as measured by the mean Co-ligand distance $\langle d \rangle$ are reported in Tab. 4.2. The increase of $\langle d \rangle$ by 0.05Å represents the dilatation of the coordination sphere most of which is due to an elongation of the Co-O bond by 0.15Å. In the HS state, the oxygen is loosely bound to the cobalt (d = 2.27Å). More surprisingly, the Co^{3+} ion is displaced away from the equatorial plane towards the axial CN ligand by -0.15Åcorresponding to *ca.* 10% of the initial Co-N bond length. Such an unexpected phenomenon is evidently a consequence of the introduction of a water molecule into the coordination sphere. In an electrostatic interpretation, an asymmetric charge distribution along the (H_2O)-(Co^{3+})-(NC^-)

Table 4.2: Optimized values of the d and z parameters (Å) defined in Fig. 4.7 for the LS (S=0) and HS (S=2) states of the embedded Co(III) cluster. A +0.25 point charge along with the TIP is placed in all the tetrahedral sites.

	z_{min} [Å]		d_{min} [Å]		$\langle d \rangle$ [Å]		$\Delta E^{\text{adia}}_{\text{LS-HS}}$ [eV]
	LS	HS	LS	HS	LS	HS	
8 $Rb^{+0.25}$	−0.15	−0.15	1.97	2.27	1.95	2.00	−0.53

axis provokes the displacement of the Co^{3+} cation towards the CN^- anion.

Finally, the extent to which the nearest-neighbour alkali cation environment influences this displacement has been looked into.

4.3.2 Alkali Cation Influence - Numbers and Positions

The importance of alkali counter ions for structural and electronic properties of PBAs, has been previously emphasized.[5, 7, 34, 35] Indeed, the existence of a PME has been found to depend on the type of ion present in the material.[5] The focus of this part of the study has been on the number and distribution of the Rb^+ ions within the 8 tetrahedral sites neighbouring the cluster.

The previous deformations of the Co ion coordination sphere are relevant as long as the local environment is of C_2-symmetry. Thus, starting from the previous distribution (*i.e.* full occupancy of the tetrahedral sites by +0.25 charges and TIP), specific positions were imposed to the nearest-neighbor alkali ions to fulfill this C_2-symmetry requirement (see 4.9 (a)-(g)). One additional alkali distribution (see 4.9 (h)) was also investigated since it minimizes the resulting Coulomb repulsion between the two alkali ions. Depending on the number of nearest-neighbor Rb ions in the elementary lattice (n = 2, 4 and 8), their charge was adjusted as to reproduce an overall contribution of +2 per unit cell (+1.0, +0.5 and +0.25, respectively), in accordance with the experimental average. In the presence of such alkali distributions in the vicinity

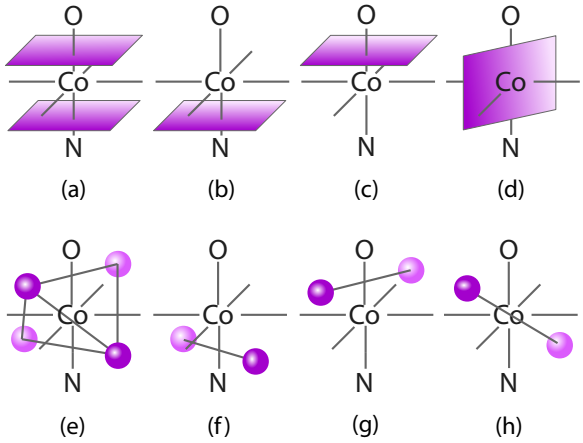

Figure 4.9
Different distributions of the nearest-neighbor alkali ions used to generate the embedding bath. Darker colors represent Rb ions in the forefront, one square represents 4 counter ions. Distributions (a)-(g) preserve the local C_2-symmetry of the Co ion. (a) corresponds to the full occupancy of the tetrahedral sites. (h) minimizes the Coulomb repulsion between 2 alkali ions.

of the cluster model, the energetics of $[Co^{III}(NC)_5(OH_2)]^{2-}$ was investigated as a

Table 4.3: Optimized values of the d and z parameters (Å) defined in 4.7 for the LS (S=0) and HS (S=2) states of the embedded Co(III) cluster (a_0 = 10.11Å). Different distributions (a)-(h) of the Rb ions as defined in Fig. 4.9 were inspected.

		z_{min} [Å]		d_{min} [Å]		$\langle d \rangle$ [Å]		$\Delta E^{\text{adia}}_{\text{LS-HS}}$ [eV]
		LS	HS	LS	HS	LS	HS	
8 $Rb^{+0.25}$	(a)	-0.15	-0.15	1.97	2.27	1.95	2.00	-0.53
	(b)	-0.10	-0.10	1.92	2.12	1.95	1.98	-0.59
4 $Rb^{+0.5}$	(c)	-0.15	-0.20	2.07	2.42	1.97	2.02	-0.48
	(d)	-0.15	-0.15	1.97	2.27	1.95	2.00	-0.60
	(e)	-0.15	-0.15	1.97	2.27	1.95	2.00	-0.59
	(f)	-0.10	-0.10	1.97	2.12	1.96	1.98	-0.63
2 $Rb^{+1.0}$	(g)	-0.15	-0.25	2.02	2.72	1.97	2.07	-0.35
	(h)	-0.15	-0.15	1.97	2.27	1.95	2.00	-0.58

function of the d and z parameters. The resulting structural and energetical values are shown in Tab. 4.3. For both spin states and all distributions of alkali ions, values of $z_{min} < 0$ are observed. This means, that the displacement of the Co^{3+} ion is qualitatively independent of the number and position of the alkali ions. From a quantitative point of view, a majority of LS distributions (c-e,g,h) lead to $z_{min} = -0.15$Å, a value observed for the average distribution of $8Rb^{+0.25}$ ((a) in Tab. 4.3). Previously, this displacement was explained as the result of an asymmetric charge distribution around Co(III). In contrast, the amplitude of displacement is reduced down to $z = -0.10$Å for both spin states as soon as the alkali cations (either 2 or 4) are placed close to the axial CN ligand (b,f). With respect to the average distribution, this is seen as a consequence of the reduced Coulomb repulsion between Co^{3+} and Rb^{+} ions close to the H_2O ligand. However, the Coulomb repulsion is increased when the alkali ions are concentrated close to the H_2O ligand, as reflected by the increased values of $|z|$ in the HS state (c : $z_{min} = -0.20$Å, g : $z_{min} = -0.25$Å). Indeed, the distribution of $2Rb^{+}$ in vicinity of the the axial CN^{-} ligand (f) leads to the smallest absolute energy of the LS state.

An expansion of the coordination sphere is again found in the values of $\langle d \rangle$. The LS state is more stabilized than the HS state, as reflected by the values of ΔE_{adia} ranging from −0.63 to −0.35 eV. These values are considerably larger than ΔE_{adia} previously found upon variation of the lattice constant a_0 (0.02eV). A combination of the short- and long range environment modifications seems to lead to a pronounced stabilization of the LS with respect to the HS state.

As the ultimate interest lies in the structural effects which are likely to trigger electron transfer in the CoFe PBA, I felt that a similar inspection of the $[Co^{II}(NC)_5(OH_2)]^{3-}$ unit would be desirable. Therefore, the d and z parameters (step 4 in 4.3) were evaluated in the most stable 2 Rb^{+} environment (f) following exactly the same strategy

Table 4.4: Optimized values of the d and z parameters (Å) defined in Fig. 4.7 for the LS (S=1/2) and HS (S=3/2) states of the embedded $[Co^{II}(NC)_5(OH_2)]^{3-}$ cluster.

	z_{min} [Å]		d_{min} [Å]		$\langle d \rangle$ [Å]		$\Delta E^{adia}_{LS\text{-}HS}$ [eV]
	LS	HS	LS	HS	LS	HS	
2 Rb^+	0.00	0.00	2.17	2.12	2.01	2.00	0.45

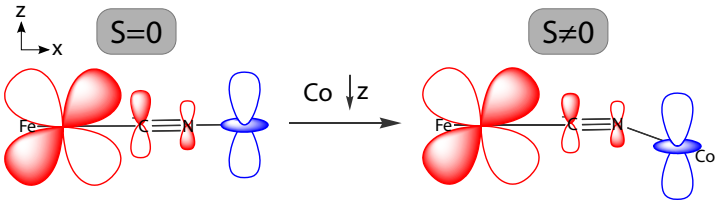

Figure 4.10
A possible vacancy-induced scenario for electron transfer in the CoFe PBA. S is the orbital overlap between the fragments orbitals.

as before. Considering the electron transfer time scale, the environment of the cluster was assumed to remain unchanged. The calculated structural parameters and energetics of the Co(II) S=3/2 (*i.e.* HS) and S=1/2 (*i.e.* LS) are shown in Tab. 4.4. As expected, practically no increase in the coordination sphere expansion $\langle d \rangle$ is observed since the responsible e_g anti-bonding orbitals are occupied in both spin states of Co(II). Furthermore, a value of $\Delta E^{adia}_{LS\text{-}HS}$ = 0.45eV indicates that the HS state is more stable than the LS one. Astonishingly, the distortions along the z mode do not bring any energy stabilization, in contrast with the results obtained for the Co(III) cluster. Thus, the photomagnetic reduction of the Co(III) ion into a Co(II) ion is accompanied by a simultaneous breathing of the coordination sphere (*ca.* 1.97 Å→ 2.0 Å) and the lift of the cobalt ion back into the equatorial pocket.

In the light of these findings on the monomer Co unit, a possible scenario for electron transfer process between the Fe and Co sites is suggested. The structural changes resulting from the presence of a vacancy might be combined with orbital considerations based on the {Fe(CN)} and {Co} fragments (see Fig. 4.10). In the absence of any displacement of the Co(III) ion along the z direction, the coupling between the localized states Co(II)-Fe(III) and Co(III)-Fe(II) through the bridging cyano π^* orbital is zero for symmetry reasons (see Fig. 4.10, left). As demonstrated in the vibronic PKS model,[36] no intervalence charge transfer band is predicted. This orthogonality has been used to rationally prepare ferromagnetic molecular systems by quenching the super-exchange mechanisms which favour the LS states over the HS ones.[37] A superexchange-based model Hamiltonian has been proposed to describe the electron transfer in symmetric homonuclear compounds.[38, 39] Nevertheless, the out-of-plane drift of the Co(III) ion in the presence of the water molecule lifts the symmetry constraint and results in a non-zero effective overlap (see Fig. 4.7, right). As a consequence, the electron transfer is triggered by such displacement and a reduction into Co(II) is likely to occur. Then, the Co(II) ion

recovers the equatorial position. The final reverse electron transfer Co(II)-Fe(III) → Co(III)-Fe(II) is thus hindered for symmetry reasons and needs to be initiated by an external stimulus.

4.4 Conclusion

Wave function CASPT2 calculations were performed on a model cluster $Co(NC)_5(OH_2)$ extracted from the CoFe PBA. Such building block is known to undergo valence tautomerism along the photomagnetic process. The aim of this work was primarily to investigate (*i*) the influence of the short- and long-range environments, and (*ii*) the structural and spectroscopic impact of an apical vacancy. The cluster was placed in a previously optimized embedding. The number and positions of the alkali ions were found to influence to a small extent the Co(III) structural properties. The results suggest that the local environment of the Co(III) ion is distorted whereas the Co(II) ion remains within the equatorial plane of the cyanide ligands. In view of our structural results, we suggest a possible scenario governing electron transfer within the photomagnetic CoFe Prussian blue family. The vacancy-induced displacement of the Co(III) ion is likely to trigger the Fe(II) → Co(III) electron transfer process since it switches on the Fe(d)-CN(π^*)-Co(d) orbital overlap. Once the Co(II) is lifted into the equatorial position, this overlap vanishes and another structural phenomenon should take place to trigger the Co(II) → Fe(III) reverse electron transfer. Based on our demanding calculations, we suggest that the water molecule plays an important role in the CoFe PBA photomagnetic process.

Bibliography

[1] Krah, T.; Suaud, N.; Zanchet, A.; Robert, V.; Ben Amor, N. *European Journal of Inorganic Chemistry* **2012**, 5777–5783.

[2] Sato, O.; Iyoda, T.; Fujishima, A.; Hashimoto, K. *Science* **1996**, *272*, 704–705.

[3] Cartier dit Moulin, C.; Villain, F.; Bleuzen, A.; Arrio, M.-A.; Sainctavit, P.; Lomenech, C.; Escax, V.; Baudelet, F.; Dartyge, E.; Gallet, J.-J.; Verdaguer, M. *J. Am. Chem. Soc.* **2000**, *122*, 6653–6658.

[4] Yokoyama, T.; Ohta, T.; Sato, O.; Hashimoto, K. *Phys. Rev. B* **1998**, *58*, 8257–8266.

[5] Bleuzen, A.; Lomenech, C.; Escax, V.; Villain, F.; Varret, F.; Cartier dit Moulin, C.; Verdaguer, M. *J. Am. Chem. Soc.* **20Oo**, *122*, 6648–6652.

[6] Wojdel, J. C. *J. Mol. Model.* **2009**, *15*, 567–572.

[7] Bleuzen, A.; Escax, V.; Ferrier, A.; Villain, F.; Verdaguer, M.; Münsch, P.; Itié, J.-P. *Angew. Chem. Int. Edit.* **2004**, *43*, 3728–3731.

[8] Lepetit, M.-B.; Suaud, N.; Gelle, A.; Robert, V. *The Journal of Chemical Physics* **2003**, *118*, 3966–3973.

[9] Bastardis, R.; Guihéry, N.; Suaud, N.; de Graaf, C. *J. Chem. Phys.* **2006**, *125*, 194708–194717.

[10] Suaud, N.; Gaita-Ariño, A.; Clemente-Juan, J. M.; Marín-Sánchez, J.; Coronado, E. *J. Am. Chem. Soc.* **2002**, *124*, 15134–15140.

[11] Suaud, N.; Lepetit, M.-B. *Phys. Rev. B* **2000**, *62*, 402–409.

[12] Barandiaran, Z.; Seijo, L. *J. Chem. Phys.* **1988**, *89*, 5739–5746.

[13] Sadoc, A.; de Graaf, C.; Broer, R. *Phys. Rev. B* **2007**, *75*, 165116.

[14] Andersson, K.; Malmqvist, P. A.; Roos, B. O.; Sadlej, A. J.; Wolinski, K. *J. Phys. Chem.* **1990**, *94*, 5483–5488.

[15] Andersson, K.; Malmqvist, P.-A.; Roos, B. O. *J. Chem. Phys.* **1992**, *96*, 1218–1226.

[16] Karlström, G.; Lindh, R.; Malmqvist, P.-A.; Roos, B. O.; Ryde, U.; Veryazov, V.; Widmark, P.-O.; Cossi, M.; Schimmelpfennig, B.; Neogrady, P.; Seijo, L. *Comput. Mater. Sci.* **2003**, *28*, 222–239.

[17] Roos, B. O.; Lindh, R.; Malmqvist, P.-A.; Veryazov, V.; Widmark, P.-O. *J. Phys. Chem. A* **2004**, *108*, 2851–2858.

[18] Roos, B. O.; Lindh, R.; Malmqvist, P.-A.; Veryazov, V.; Widmark, P.-O. *J. Phys. Chem. A* **2005**, *109*, 6575–6579.

[19] Kepenekian, M.; Robert, V.; Le Guennic, B.; de Graaf, C. *J. Comput. Chem.* **2009**, DOI: 10.1002/jcc.21236.

[20] Pierloot, K.; Vancoillie, S. *The Journal of Chemical Physics* **2006**, *125*, –.

[21] Ghigo, G.; Roos, B. O.; Malmqvist, P.-A. *Chem. Phys. Lett.* **2004**, *396*, 142–149.

[22] Forsberg, N.; Malmqvist, P.-A. *Chem. Phys. Lett.* **1997**, *274*, 196–204.

[23] Douglas, M.; Kroll, N. M. *Ann. Phys.* **1974**, *82*, 89–155.

[24] Hess, B. A. *Phys. Rev. A* **1986**, *33*, 3742–3748.

[25] De Graaf, C.; Sousa, C.; Ordejon, B. *J. Am. Chem. Soc.* **2008**, *130*, 13961–13968.

[26] Dunning Jr., T. H.; Botch, B. H.; Harrison, J. F. *J. Chem. Phys.* **1980**, *72*, 3419–3420.

[27] Botch, B. H.; Dunning Jr., T. H.; Harrison, J. F. *J. Chem. Phys.* **1981**, *75*, 3466–3476.

[28] Andersson, K.; Roos, B. O. *Chem. Phys. Lett.* **1992**, *191*, 507–514.

[29] Roos, B. O.; Andersson, K.; Fülscher, M. P.; Malmqvist, P.-A.; Serrano-Andrès, L.; Pierloot, K.; Merchàn, M. In *Advances in chemical Physics: New Methods in Computational Quantum Mechanics*; Prigogine, I., Rice, S. A., Eds.; John Wiley & Sons: New York, 1996; Vol. 93; p 219.

[30] Pierloot, K.; Vancoillie, S. *J. Chem. Phys.* **2008**, *128*, 034104.

[31] Bolvin, H. *J. Phys. Chem. A* **1998**, *102*, 7525–7534.

[32] Pierloot, K. *Computational Organometallic Chemistry*; Dekker: New York, 2001.

[33] Escax, V.; Bleuzen, A.; Itié, J. P.; Munsch, P.; Varret, F.; Verdaguer, M. *J. Phys. Chem. B* **2003**, *107*, 4763–4767.

[34] Bleuzen, A.; Escax, V.; Itié, J.-P.; Münsch, P.; Verdaguer, M. *C. R. Chim.* **2003**, *6*, 343 – 352.

[35] Cafun, J.-D.; Champion, G.; Arrio, M.-A.; Cartier dit Moulin, C.; Bleuzen, A. *J. Am. Chem. Soc.* **2010**, *132*, 11552–11559.

[36] Piepho, S. B.; Krausz, E. R.; Schatz, P. N. *Journal of the American Chemical Society* **1978**, *100*, 2996–3005.

[37] Verdaguer, M.; Bleuzen, A.; Marvaud, V.; Vaissermann, J.; Seuleiman, M.; Desplanches, C.; Scuiller, A.; Train, C.; Garde, R.; Gelly, G.; Lomenech, C.; Rosenman, I.; Veillet, P.; Cartier, C.; Villain, F. *Coordination Chemistry Reviews* **1999**, *190–192*, 1023 – 1047.

[38] Bolvin, H. *The Journal of Physical Chemistry A* **2003**, *107*, 5071–5078.

[39] Bolvin, H. *Inorganic Chemistry* **2007**, *46*, 417–427, PMID: 17279820.

5
A selective approach - the *FRACCIS* method

"You can't always get what you want, but if you try sometimes, you get what you need." Applied to CI, this songtext translates into : the desired FCI is unreachable but with a wise choice of determinants a good approximation can be obtained. This is the approach of the "FRAgmented Contracted CI of Single excitations" (FRACCIS) method. In this chapter, I will give some motivation for the method development and some technical details of the implementation. Two applications will be presented in Chapter 6.

5.1 Motivation and Aim

In Chapter 2, we have seen that multi-reference CI (MR-CI) methods offer a more accurate description of the wave function than do single-reference (SR-CI) methods. At the same time, their cost is considerably lower than that of the full CI (FCI) and this combination makes them an attractive calculation strategy. An initial consideration is dedicated to the choice of the multi-determinantal reference space. The latter will be the subject of the following discussion and the present implementation.

The reference space serves as basis for the subsequent inclusion of dynamical correlation through a CI, in most cases limited to single- or double-excitations on

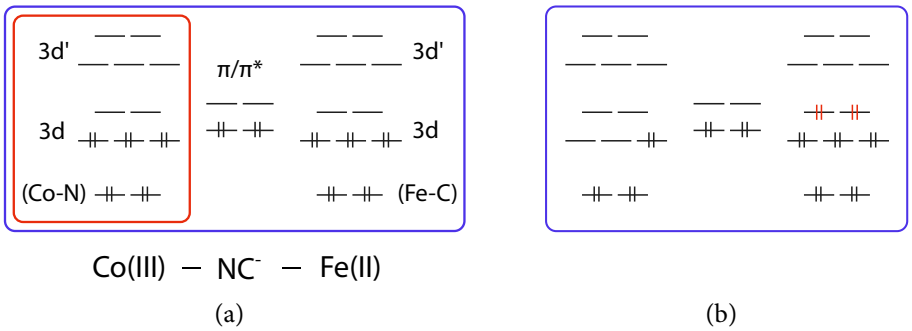

Figure 5.1: (a) Illustration of the CAS(10,12) (red square), used for the inspection of the Co(III) spin transition. An extension to a CAS(24,18) is necessary to include the phenomenon of Fe(II)-to-Co(III) electron transfer. The orbital occupation corresponds to the HF ground state. (b) Example of a determinant included in the CAS(24,18) despite its vanishing probability.

top of the reference. Frequently, a multi-configuration self-consistent field (MC-SCF) function is chosen as the reference function since it includes static correlation effects (see chap. 2).

A prominent implementation of this family uses a complete active space (CAS). Since it includes all possible electron distributions of the active electrons within the active orbitals (that obey a given spatial symmetry and spin multiplicity) the choice of configurations is transformed into a choice of active electrons and orbitals. The two previous chapters show examples for the numerous systems whose study has been enabled by this approach. However, currently the method is technically no longer feasible as soon as the active space comprises more than *ca.* 18 active orbitals. The previously examined CoFe PBA is such a case and shall be briefly discussed here for illustrative purposes. In order to inspect the Co(III) spin transition, a CAS(10,12) has been used that included antibonding metal 3d, 3d' and bonding σ-like (Co-ligand) orbitals (seeFig. 5.1(a)). In contrast, the electronic rearrangements associated to the Fe(II)-to-Co(III) electron transfer demand an extension of such an active space towards the Fe site. The Fe(II) orbitals of the same type as previously on the Co(III) site should now also be comprised as well as the π/π^* orbitals on the bridging CN^- ligand. Finally, these considerations lead to a CAS(24,28) ($\approx 10^9$ determinants), impossible since it exceeds the technical limits posed by calculation power and storage capacity. One would like to render such systems approachable by providing a reference space that is considerably reduced in size and does nonetheless not lack the physical effects of a given problem. This is one of the principal motivations of the present development.

A door-opening observation in that sense is that the CAS contains a large number of unphysical determinants. As an illustration, we shall consider the CoFe ground state, approximated by Co(d^6)-NC-Fe(d^6). For example, the simultaneous transfer of four electrons from the Co to the Fe site, as represented by Co(d^2)-NC-Fe(d^{10})

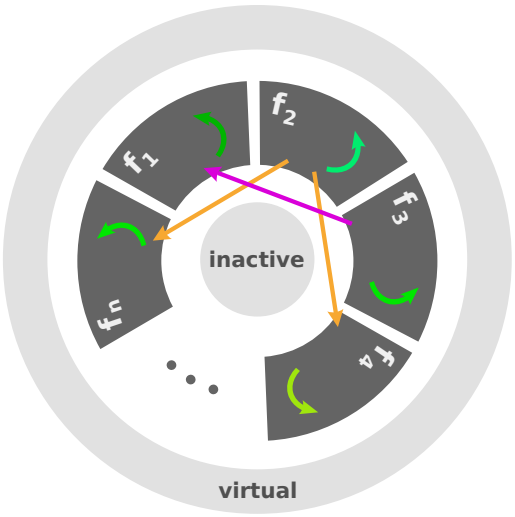

Figure 5.2
Scheme of the FRACCIS method starting from a set of n fragments containing each a subset of LMOs. Individually chosen excitation limits within each fragment (bent arrows) and between different fragments (straight arrows) define the determinants to be included in the reference CI space.

(see Fig. 5.1(b)) seems highly unlikely in view of the enormous charge redistribution over a large distance.

Despite their presumably vanishing contribution, determinants of this type are included in the active space. Since they are very numerous, their elimination provides a promising route towards size reduction of the reference space.

The central question in such a reduction remains which determinants to eliminate from the complete reference space. Among other criteria, the contribution of a given determinant depends on the distance between the excited electrons, as shown in the above example. In view of the local nature of the electronic correlation spatial considerations seem to be a reasonable guideline to decide upon inclusion or exclusion of determinants. In that sense, localized molecular orbitals (LMOs) provide a very well-suited basis thanks to their limited spatial extension in one molecular or atomic region.

FRACCIS uses LMOs as a basis for a selected CI method in order to achieve two important aims : (*i*) reducing significantly the number of determinants in the reference space, and (*ii*) analyzing systematically the energetic contribution of different types of excitations and thus deducing their physical importance in the inspected molecular system.

An illustration of the procedure is given in Fig. 5.2. First, an arbitrary number of fragments according to the physical characteristics of the system is defined. Each one contains a subset of LMOs and together they constitute the active orbitals. Then, two different types of restrictions are imposed in the form of maximum excitations *within* each fragment and *between* them. The two value sets allow for the definition of the fragment reference determinants which are finally combined to give the molecular reference determinants.

It should be clarified that, in the present implementation, the space of single excitations on top of the reference space is treated in the traditional manner. The novelty of *FRACCIS* lies in the manner to generate the LMO-based determinants

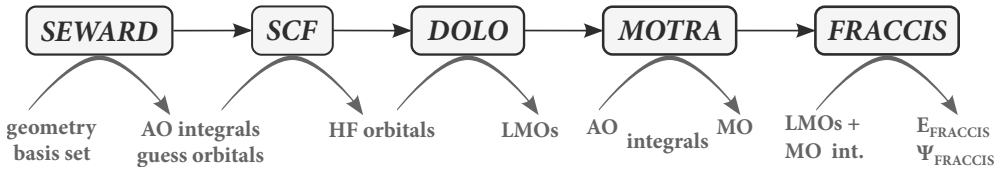

Figure 5.3: Overview of the calculations preceding *FRACCIS*. The input and output objects of a given code are presented in gray.

included in the reference space.

It should be mentioned that other methods such as the "generalized active space" (GAS)[1] or the "occupation-restricted multiple active space" (ORMAS)[2, 3] follow the same philosophy. In contrast to the present approach however, these methods do not take profit of localized molecular orbitals as a basis for a systematic determinant selection.

5.2 Preceding calculations and input format

Several calculations preceding *FRACCIS* are carried out by the *MOLCAS* [4] and the *COST* program suites. The transition from *MOLCAS* to *COST* is assured by the *COST* interface program molcost and will be implicit in the following whenever such a transition is mentioned. The localization procedure of Maynau *et al.* [5] has been chosen since it can provide not only localized occupied orbitals but also localized virtual orbitals. It is important to mention, that this procedure can be based on SCF or CASSCF orbitals. However, it is exactly a costly CASSCF step that shall be avoided in the present approach and thus SCF or CASSCF calculations with a small CAS are preferable.

In the first two steps, the *MOLCAS* programs *SEWARD* and *SCF* are executed in order to generate one- and two-electron atomic integrals and to calculate a set of HF orbitals, respectively. The subsequent localization of MOs is carried out by the *COST* program *DOLO*. It creates local orbitals by diagonalizing blocks of density matrices of the concerned molecular or atomic region in the basis of orthogonalized atomic orbitals (OAO). Since the resulting local orbitals are not optimized they are projected on the set of SCF orbitals. Finally they are hierarchically orthogonalized to obtain an orthogonal LMO set of SCF quality.

An integral transformation is necessary since the subsequent calculations demand orthonormal molecular instead of atomic orbital integrals. This step is carried out by the *MOLCAS* program *MOTRA*. In summary, a set of LMOs and integrals in these LMO basis are necessary to run *FRACCIS*. An overview of the preceding runs is given in Fig. 5.3, an example of a complete input file can be found in the appendix.

In the following, I will describe an example *FRACCIS* input (see Tab. 5.1), formally divided into three parts. A first part concerns the general data, such as the number of fragments, spin multiplicity and spatial symmetry. A second part is devoted to

Table 5.1: Example input file for the *FRACCIS* code. The intra-fragment excitations correspond to those illustrated in Fig. 5.2.

	input	description

I - general data	`& fraccis`
	`prefix=' '`
	`nfrag=...`
	`is0=...`
	`ms2=...`
		
		prefix of input and output files
		total number of fragments
		desired spatial symmetry
		double of the desired spin projection

II - INTRA-fragment data	`FRAGMENT 1`
	`1 3 5 8 10 11 14`
	`2220010 exc=2`
	`2211100 exc=1`
	`FRAGMENT 2`
	⋮
	`FRAGMENT n`
	`end`
		
		numbers of the LMOs of fragment 1
		list of generator determinants (LMO occupations and corresponding max. degree of exc. `exc`)
		input analogue to fragment 1

III - INTER-fragment data	`interfrag`
	`3 1 1`
	`2 n 1 2 4 2`
	`end`
		
		excitation format :
		(dep. fragment) (arr. fragment) (`interexc`)

the definition of each fragment. Finally, a third part deals with the inter-fragment excitation limits.

I - The first part of the input contains data concerning the wave function (*i.e.* spatial symmetry, spin multiplicity) and several code variables (*i.e.* file prefix, number of fragments, overall maximum excitation degree).

II - For each fragment, one or multiple generator configurations are given, each one associated with an excitation limit `exc`. Starting from a given generator determinant, all excited determinants up to `exc` are generated. As an example, let fragment 1 contain a σ and a σ^* orbital (LMOs 1 and 2, respectively) associated to `exc = 2`. If one starts from the $(\sigma)^2$ generator determinant, the two determinants $(\sigma\sigma^*)$ and $(\sigma^*)^2$ are generated by the input :
`FRAGMENT 1`
`1 2`
`20 exc=2`. This corresponds to a local FCI within the σ/σ^* subspace.

III - The input for the inter-fragment excitations follows the electronic transfer. More precisely, a maximum number of electrons (`interexc`) is transferred from a departure fragment ($\mathtt{f}_{\text{from}}$) to an arrival fragment ($\mathtt{f}_{\text{to}}$). These three variables are given as ($\mathtt{f}_{\text{from}}$ $\mathtt{f}_{\text{to}}$ `interexc`) in the input and generate the following set of determinants : $\{\mathtt{f}_{\text{from}}^{(-i)}\ \mathtt{f}_{\text{to}}^{(+i)}\}$ ($i = 1, \ldots,$ `interexc`). Here, the number of lost electrons are noted as a negative superscript, the number of gained electrons as a positive superscript. The dihydrogen dimer, $(H_2)_2$, depicted in a minimal basis set, shall illustrate this input. Let the four LMOs (σ and σ^* on each molecule) be divided into four fragments (see Fig. 5.4). The input `1 2 2`, for example, creates the singly- and doubly excited determinants $(\sigma_1\sigma_1^*)$ and $(\sigma_1^*)^2$ that can be formalized as local excitations on the first H_2 unit, $H_2(1)$. The same holds for the excitations between the two dihydrogen units $H_2(2) \longrightarrow H_2(1)$ created by the input `3 2 2`. They lead to $(\sigma_1)^2\sigma_2\sigma_1^*$ and $(\sigma_1)^2(\sigma_1^*)^2$.

It is also possible to combine several input data sets on the same line. In that case, the two excitations are generated simultaneously. In the above example system, the input `1 4 1 3 4 1` associates the charge transfer excitation $\sigma_1 \longrightarrow \sigma_2^*$ (`1 4 1`) to the σ repolarization $\sigma_2 \longrightarrow \sigma_2^*$ (`3 4 1`).

Finally, the input `1 2 2 3 4 2` associates the previously mentioned local single- and double excitations. The resulting four excitations are of dispersive type and include one double-, two triple- and one quadruple excitation.

It is clear from the above illustration that different excitation types can be generated with an adapted definition of fragments and excitations. The equivalent of a FCI space (as in the above example) or a truncated CI space can be easily obtained. Depending on the inspected problem, different input approaches can be favorable. When a

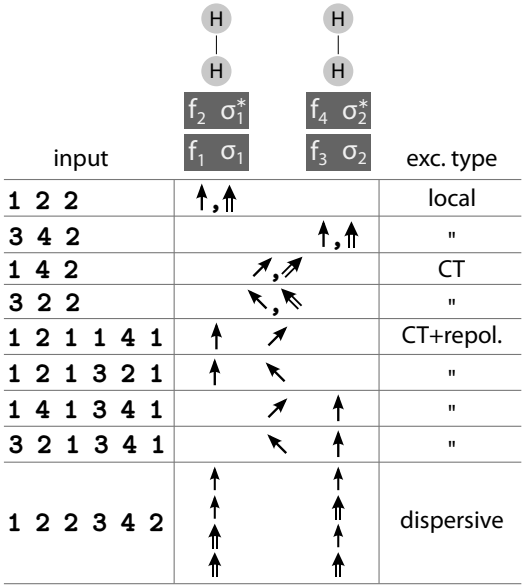

Figure 5.4
Illustration of the input format for inter-fragment excitations for the case of the minimal basis $(H_2)_2$, divided into four fragments. Single and double excitations are shown as single and double arrows, respectively. The comma indicates that excitations are generated separately.

considerable number of determinants within an LMO subspace (*i.e.* transition metal 3*d* orbitals) is necessary, the definition of large fragments and attached `exc` can be advantageous. On the other hand, the isolation of a small number or even single LMOs in one fragment and the use of inter-fragment data can be more laborious but allows for the generation of well-targeted excitations.

5.3 Construction of the reference Hamiltonian matrix

The objective of the code is to build the Hamiltonian matrix, in the basis of the reference determinants constructed from the input data. The present implementation proceeds in three general steps :

1. generate reference determinants and their corresponding addresses
2. read integrals in MO basis
3. find all matrix elements as combinations of address 1, address 2 and their integral value

After a brief description of the manner to store determinants, I will describe the details of steps 1) and 3). I will note in lower or upper case those variables that concern the fragment or molecular determinants, respectively.

5.3.1 Determinant storage

Throughout the present implementation, the LMO occupation is stored as a pair of integers. In the case of fragment determinants, the two integers $a1$ and $a2$ are stored separately. Their binary format represents the open-shell (OS) and closed-shell (CS) occupation of the fragment LMOs, as shown as follows (corresponding integers in parentheses),

LMO occupation :	220010
$a1$:	000010 (16)
$a2$:	110000 (3)

This format facilitates storage and addressing steps. The fragment integers $a1$ and $a2$ are calculated as $a_{1,2} = \sum_{i=1}^{\texttt{noac}} 2^{i-1}$ ($i \in occ$) where `noac` is the number of active orbitals in the fragment and i concerns the indexes of singly- and doubly-occupied LMOs for $a1$ and $a2$, respectively. For the occupation shown above, $a1 = 2^{4-1} = 16$ and $a2 = 2^{(1-1)} + 2^{(2-1)} = 3$. Even though it is technically possible to define large fragments (up to `noac` = 32) the spirit of the present approach should rather encourage the user to the definition of smaller, well-defined fragments.

The previous fragment occupations $a1$ and $a2$ are now linked to represent molecular occupations $A12$, as before in binary format. The following series of bits, built from three fragments, shall illustrate this format of molecular determinants (the previous fragment $a1$ and $a2$ in red) :

$$\overbrace{\underbrace{\underbrace{\overbrace{000010}^{a1(f_1)}\,\overbrace{0010}^{a1(f_2)}\,\overbrace{010010}^{a1(f_3)}}_{A1}\,\underbrace{\overbrace{110000}^{a2(f_1)}\,\overbrace{0100}^{a2(f_2)}\,\overbrace{100001}^{a2(f_3)}}_{A2}}}^{A12}$$

The number of bits necessary to represent $A12$ corresponds to ($2 * \texttt{NOAC}$) where `NOAC` is this time the number of active orbitals in the whole molecular system (*i.e.* the sum of the active orbitals in all fragments). In the above case, `NOAC` = 6 + 4 + 6 = 16. If the number of active orbitals in the whole system does not exceed 16, the occupation can be represented by one integer $A12$ of 32 bits. Formally, $A1 = a1(f_1)a1(f_2)\cdots a1(f_n)$ and $A2 = a2(f_1)a2(f_2)\cdots a2(f_n)$ can be distinguished that contain the molecular OS and CS occupation. In contrast to the fragment determinants, where the two different occupations are systematically stored in two variables, the single variable $A12$ unites both of them as the combination of $A1$ and $A2$.

class	fragments					
	1	2	3	4	⋯	n
1	0	-1	0	0	⋯	1
2	0	-2	0	1	⋯	1
3	0	-3	0	2	⋯	1

Table 5.2: *class_frag* array of fragment excitations for the example input
`2 n 1`
`2 n 1 2 4 2`

In the case of `NOAC` > 16, the bit series is cut into blocks of 32 bits. In the following example, `NOAC` = 8 + 5 + 6 = 19, and thus the first integer is exceeded by 6 bits :

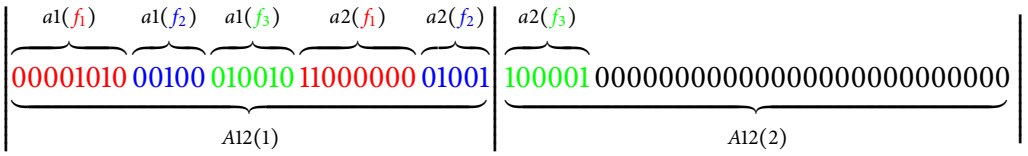

In summary, the OS and CS occupation in fragments is contained in two separate integers $a1$ and $a2$. The molecular occupations are represented by 1 or more integers $A12$, depending on the number of active orbitals.

5.3.2 Generation of the reference determinants

A clarification is necessary at the beginning of this section. As previously discussed, the determinants are technically represented by series of bits. Even though they do obviously not contain any of the associated physical properties, the term "determinant" shall still be used in the following.

The code proceeds in three steps to generate the space of reference determinants. First, starting from the generator determinants, the fragment reference determinants are found. These determinants are subsequently combined to give the molecular reference determinants for the whole system. Finally, the different spin combinations are introduced.

For a given generator determinant, all excitations up to the corresponding maximal excitation degree `exc` are carried out. The same treatment of all the other generator determinants leads to a first set of *occupation-based internal determinants* (`oid`) based on *intra*-fragment data. The label *occupation-based* signifies that the determinants only contain information about the occupation of the LMOs (2, 1, or 0) and not about the spin of the electrons.

Subsequently, the *inter*-fragment data is stored in the array *class_frag* where each class represents numbers of electrons removed from or added to each fragment (see Tab. 5.2). In order to generate determinants based on inter-fragment excitations, one needs to know how many electrons a fragment can lose and gain at most due to all inter-fragment excitations (`maxrem` and `maxadd`, respectively). These values correspond simply to the smallest and largest values in one column of `class_frag`. Starting from the `oid` set of determinants, all possible excitations of n electrons (`maxrem` < n < `maxadd`) are carried out. The resulting set of determinants is noted

occupation-based external determinants (`oed`). Together with the set `oid`, they constitute the fragment reference determinants (occupation-based reference determinants, *ord*).

These determinants take into account the restrictions per fragment given by `exc` and `interexc`. However, not all of their combinations respect the requirements on molecular determinants and several condition are therefore imposed.

A first obvious condition is that the total number of electrons in the system must be preserved. This translates into demanding a zero-sum over all inter-fragment excitations in a given combination of fragment determinants,

$$\sum_{i=1}^{nfrag} exc(f_i) = 0$$

For example, the molecular determinant ($f_1^{(-4)}\ f_2^{(+1)}\ f_3^{(+2)}$) is not allowed since the above sum yields –1. In other words, the system would lose one electron.

Second, the distribution of electrons in fragments must correspond to a given fragment excitation class (see Tab. 5.2). In other words, there must exist a row in the array `class_frag` whose entries coincide with the exponents of a given determinant, otherwise it is rejected. The determinant ($f_1^{(-1)}\ f_2^{(-2)}\ f_3^{(0)}\ f_4^{(+2)} \ldots f_n^{(+1)}$) preserves the number of electrons but coincides with no class in `class_frag`. On the other hand, the combination ($f_1^{(0)}\ f_2^{(-3)}\ f_3^{(0)}\ f_4^{(+2)} \ldots f_n^{(+1)}$) is accepted since it corresponds to class 3.

Third, the spatial symmetry of a given combination has to correspond to that given in the data. A selection with respect to the desired spin projection will be performed in the addressing step.

The fourth and final condition is optional and arises if a maximal excitation degree `maxtot` on all the fragments is imposed. A chain of n minimal basis dihydrogen molecules, $(H_2)_n$, shall serve as an illustrative example. Let there be n fragments, each one containing the σ/σ^* LMOs of one H_2 molecule. If a single excitation within each fragment is allowed (`exc`= 1), then the highest excited determinant with respect to the HF ground state is the n-fold excited $(\sigma\sigma^*)_n$. If `maxtot`= 4, the overall excitation degree is limited to 4, leading to four simultaneous single excitations at most. The variable `maxtot` makes thus available an overall restriction on the excitation degree. If it is not set at all, no limitation is imposed.

The ensemble of fragment determinants that fulfill all the above conditions when combined, constitute the set of *occupation-based reference determinants* (`ORD`). As shall be discussed further below, the electronic spin is introduced for a given determinant *via* all possible distributions of unpaired electrons that coincide with the desired spin projection.

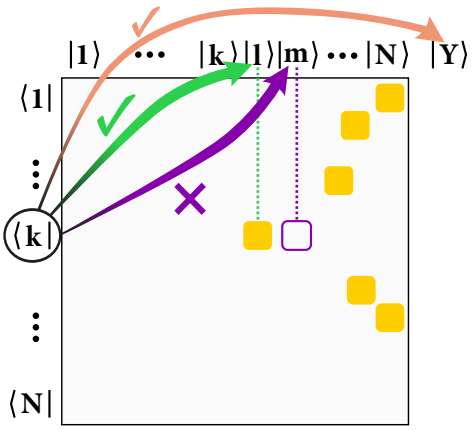

Figure 5.5
Scheme of the access to reference matrix elements for their evaluation. Single- and double excitations allow to avoid zero-value elements (violet) and address directly non-zero (orange) elements. An excitation might lead to a determinant outside the reference space (Y).

5.3.3 Addressing procedure - why and how?

Once the list of reference determinants is generated, the goal is to evaluate the matrix elements,

$$H_{ij} = \langle det_i | \hat{H} | det_j \rangle \tag{5.1}$$

The matrix element H_{ij} shall ultimately be stored in the array H with three types of entries, two describing det_i and det_j and one for the associated integral value. A large number of such elements are zero due to an excess of orbital differences between det_i and det_j as given by the Slater-Condon rules (chap. 2). In order to avoid such elements, the pairs det_i/det_j are found through excitations that are limited to single- and double-excitations (see Fig. 5.5). The number of unnecessary excitations to determinants outside the reference space is small compared to the number of zero-value elements avoided by such an approach.

The single- and double-excitations give access to the occupation of the two determinants as stored in the integers *A*12 (sec. 5.3.1). However, their size makes it impossible to use *A*12 directly in the storage of H. This is why a smaller variable, namely the *address* has to be used.

Since the determinants are stored in a binary format, two bits are necessary to describe the closed- and open-shell occupation of one active LMO. For a given number NOAC of active orbitals, the number of possible bit combinations is 2^{NOAC*2}. However, when one bit in *A*1 and the corresponding bit in *A*2 carry simultaneously the value 1, the bit combination does not represent a physical determinant since one LMO cannot be simultaneously singly- and doubly-occupied. If this type of bit combination is taken out of the complete 2^{NOAC*2} set, only a small number of combinations representing actual determinants remains. For $NOAC = 10$, this proportion represents only $\approx 6\%$ of all bit combinations. Among this proportion, an even smaller number is included in the reference space (ORD, see Fig. 5.6). The list of all reference determinants is stored in memory after their generation. Finally, the address of a given determinant is simply its position in this list, represented by an integer ranging from 1 to N, the total number of molecular reference determinants.

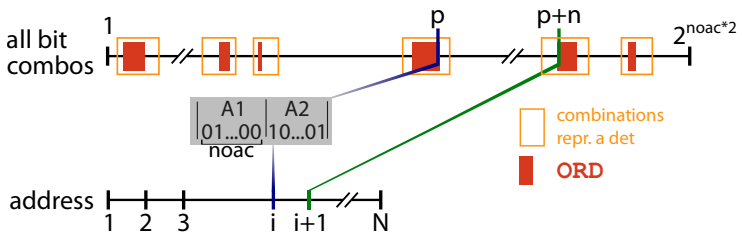

Figure 5.6: Among all imaginable $2^{\mathrm{NOAC*2}}$ bit combinations, only a small part can represent a possible determinant (orange, hollow rectangles). An even smaller proportion is included in the reference set ORD (red, solid rectangles). The address of a given determinant corresponds to its position in the continuous list of ORD and compacts the gaps in ORD. N is the total number of molecular reference determinants.

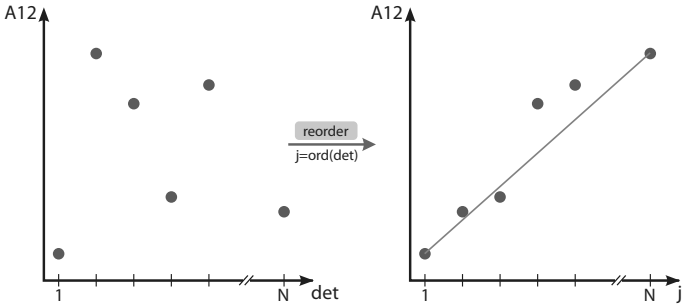

Figure 5.7
The non-ordered determinants are ordered by increasing value of $A12$ and a linear interpolation of the form $j(A12) = \mathtt{b} \times A12 + \mathtt{c}$ is found. N is the total number of reference determinants.

In that sense, using the addresses is a way of closing the considerable gaps in the determinant list.

As sketched in Fig. 5.6, the address of a reference determinant and its occupation represented by $A12$ are related in a univocal manner. Indeed, there exists a function $f(adr) = A12$ $(1 < adr < N)$ giving access to $A12$ parting from an arbitrary address. However, the inverse function $f^{-1}(A12) = adr$ that yields directly the address of a given determinant is impossible to build. Consequently, the following question remains : how can one find the address of a given determinant without running an expensive loop over the entire list and comparing with every entry? The addressing procedure discussed in the following proposes an efficient way of finding this couple determinant $\longrightarrow$ address.

Practically, the list of disordered determinants is sorted by increasing values $A12$ (Fig. 5.7), such that the x-axis contains the continuous address integers $j = 1, \ldots, N$, where N is the number of molecular reference determinants. The y-axis represents the determinant occupations as given by $A12$ (see sec. 5.3.1). Then, the equation of a linear interpolation through all points,

$$j(A12) = \mathtt{b} \times A12 + \mathtt{c} \tag{5.2}$$

is found through the coefficients $\mathtt{b}$ and $\mathtt{c}$. Equation (5.2) gives an approximate correspondence $A12 \rightarrow j$ and is used to provide a starting point for the incremental research of a given determinant address. An example run shall illustrate the pro-

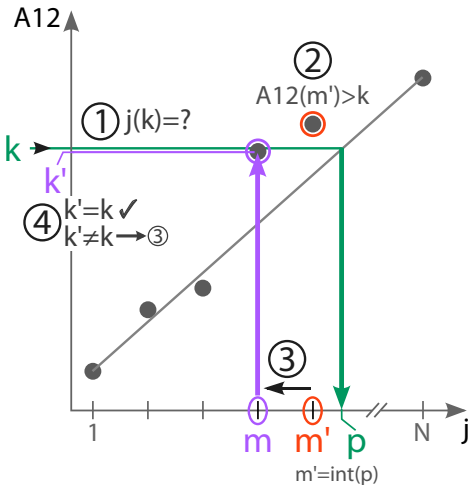

Figure 5.8
Illustration of the addressing procedure. To find the address j of a given determinant with $A12 = k$, 4 principal steps are performed. (1) Use the straight line equation to find a guess address m′. (2) Compare the stored determinant value $A12(m')$ with k. (3) Since $A12(m') > k$, decrease m′ to m. (4) Compare the new value $k' = A12(m)$ with k. If $k' = k$, address found is m. If $k' \neq k$, decrease m further. Steps 3 and 4 follow the same principle if $A12(m') < k$.

cedure. The corresponding schematic representation is given in Fig. 5.8. In the following, we shall assign concrete numbers in addition to generic letters to the variables for the sake of clarity in the explanation. Let the determinant whose address we want to find be represented by an integer value $k = 90$. Furthermore, let the coefficients in eq. (5.2) be $b = 1/30$ and $c = 2$. By inserting k into eq. (5.2) with the latter coefficients we obtain a guess address $m' = 5$ (step 1 in Fig. 5.8). On a side note, eq. (5.2) works with real type coefficients and its direct result is thus a real number p. Since the subsequent steps use integer types the transformation of the real p to an integer as $m' = int(p)$ is necessary. In any case, step 1 returns an integer guess address m' for a search determinant k through eq. (5.2). Then, the guess address m' is incremented positively or negatively. The search direction is determined by a comparison of the determinant value $A12(m')$ stored at position m' and the sought $k = 90$ (step 2 in Fig. 5.8). If the determinant value is higher than that of the searched one (*i.e.* $A12(m') > k$), check the previous determinant in the list, that is, decrease m'. In the opposite case (*i.e.* $A12(m') < k$), increase m' to check the next determinant. In the illustrative example, let $A12(5) = 98$ and since 98 is greater than the searched 90, decrease m' to $m = m' - 1$, that is, from 5 to 4. This corresponds to step 3 in Fig. 5.8. Finally, the determinant value stored at the new address, $k' = A12(m)$, is compared with the search value k (step 4). If $k' = k$, we have found the address m of the determinant k. This is the case in the present example where $A12(4) = 90$. Otherwise, if $k' \neq k$, one has to return to step 3 and further increment the address until $k' = k$.

In the above example two principal simplifications have been made with respect to the actual procedure for the sake of clarity in the explanation. The first one concerns the incrementation of m' to m. The step from $m' \rightarrow m$ are not fixed at 1. Indeed, just like in the search of avalanche victims, it is more efficient to perform big steps at the beginning in order to quickly reach the target zone. Subsequently, a reduction of the step length, or even a reversal of direction is necessary for the final search.

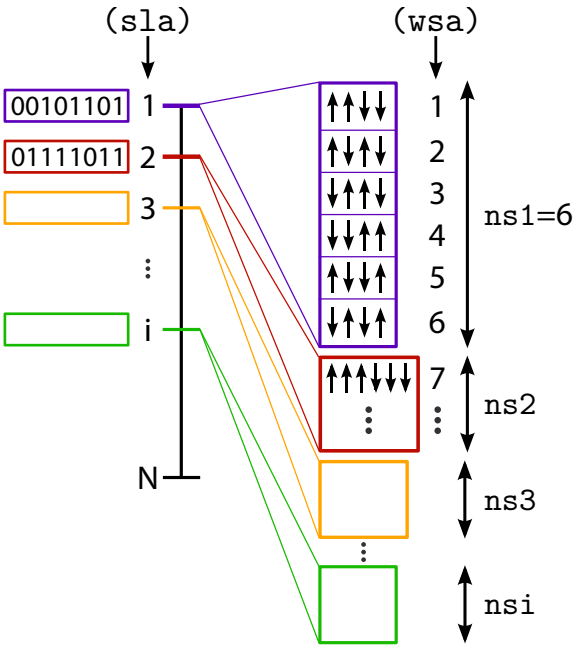

Figure 5.9
Scheme of the transition from spin-less addresses (sla) to with-spin addresses (wsa) of desired total spin projection $S_z = 0$. Two determinants containing four and six open shells, respectively, are represented. The wsa corresponds to the address within the spin distributions ns for a given determinant, shifted by the sum of all previous distributions, *i.e.* up to sla − 1. Note that ns2 > ns1.
$\mathtt{wsa1} = rank(\mathtt{ns1})$
$\mathtt{wsa2} = rank(\mathtt{ns2}) + \mathtt{ns1}$
$\mathtt{wsai} = rank(\mathtt{nsi}) + \sum_{k=1}^{i-1} \mathtt{nsk}$
$= rank(\mathtt{nsi}) + F(i)$
$F(i)$ is stored in memory.

The second simplification has been made in the construction of the linear interpolation. The only function of the first two steps is to find a guess address and the direction of research for the following incrementation steps. It is the latter incremental comparison that is the most time-consuming. Since the number of increment steps depends on the distance between the guess and the actual address, a guess of good quality ensures an efficient addressing procedure. For this reason, the single interpolation above is in reality cut into linear segments, each one with the same type of equation as eq. (5.2). In consequence, the interpolation is more exact and a more accurate guess address can be obtained. In practice, less than 20 iterations (steps 3 and 4) are usually necessary before finding the address. It should be emphasized that even for a large number of segments the associated cost is small since only two coefficients per segment (eq. (5.2)) have to be stored and read. Also, the additional preliminary step to identify the segment corresponding to an injected determinant k demands a negligible effort.

The above procedure allows one to find efficiently the spin-less addresses (sla). Finally, the sla are transformed into with-spin addresses (wsa) by introducing a shift according to the number of spin distributions ns respecting a given spin projection (see Fig. 5.9). For a given determinant i, the sum of spin distributions of the $i-1$ previous spatial determinants is taken as a basis. This quantity

$$F(i) = \sum_{k=1}^{i-1} \mathtt{nsk}$$

is previously calculated for all reference determinants and stored in memory. To

obtain the `wsa` of a spin determinant originating from the spatial determinant i,

$$\texttt{wsai} = rank(\texttt{nsi}) + F(i)$$

its rank within the spin distributions `nsi` is added to $F(i)$.

The number of determinants including spin is significantly higher than that without spin. In the interest of minimizing the generation ad addressing steps, the spin is introduced as the very last determinant property.

5.4 Conclusion

The MC-SCF development has known a well-merited success in electronic-structure calculations since the efficient implementation of Roos *et al.*. It avoids a costly CI calculation while still taking into account important multi-configurational effects in a pertinent part of the system. Nevertheless, such an approach has difficulties to cope with larger systems (*i.e.* multiple transition metals) and several developments have been conducted that introduce various active spaces and excitation limits.[1–3] This same philosophy is extended in the present work by combining LMOs with a great liberty in the definition of excitation restrictions. It should be noted that the price to pay for a large number of restrictions imposed to reduce the complete space is a more complicated implementation that needs to include a considerable number of verification steps to ensure the conformity to the desired restrictions. This is the reason why a code for truncated CI calculations (*i.e.* CI-SD) is more efficient than a selected CI code for a similar number of determinants. However, the computational effort is compensated by the advantages to enlarge the system size and to analyze systematically the energetic contribution of different determinants to the wave function.

Bibliography

[1] Olsen, J.; Roos, B. O.; Jorgensen, P.; Jensen, H. J. A. *The Journal of Chemical Physics* **1988**, *89*, 2185–2192.

[2] Ivanic, J. *J. Chem. Phys.* **2003**, *119*, 9364–9376.

[3] Ivanic, J. *J. Chem. Phys.* **2003**, *119*, 9377–9385.

[4] Karlström, G.; Lindh, R.; Malmqvist, P.-A.; Roos, B. O.; Ryde, U.; Veryazov, V.; Widmark, P.-O.; Cossi, M.; Schimmelpfennig, B.; Neogrady, P.; Seijo, L. *Comput. Mater. Sci.* **2003**, *28*, 222–239.

[5] Maynau, D.; Evangelisti, S.; Guihéry, N.; Calzado, C. J.; Malrieu, J.-P. *J. Chem. Phys.* **2002**, *116*, 10060–10068.

6

Validation of *FRACCIS* on two model systems : the dihydrogen dimer and butadiene

This chapter deals with the application of FRACCIS to two model systems, namely the dihydrogen dimer, $(H_2)_2$, and the butadiene molecule, C_4H_6. The dissociation energy D_e of $(H_2)_2$ and the cis/trans rotational barrier D_{rot} of C_4H_6 are calculated based on CI spaces which contain systematically chosen determinants. A comparison with FCI and CAS(4,36)CI reference values shows a promising outcome of FRACCIS. In the case of D_e, 90% are recovered using ≈3% of the full space. The CI space in the case of D_{rot} could be reduced down to less than 1% while keeping the accuracy up to 97%. The work presented here has been published in JMMO (T.Krah et al., 2014).[1]

6.1 Introduction

In the following, *FRACCIS* is applied to two 4-electron parent systems, namely the dihydrogen dimer, $(H_2)_2$, and the butadiene C_4H_6 molecule. Dispersive interactions are the predominant element in the $(H_2)_2$ binding and a great number of excitations are necessary for their proper description. This type of system seems to be an ideal candidate for a selected CI approach since the contribution of the different numerous excitations can be analyzed systematically. The butadiene can be seen here as a covalent 4-electron sister compound when considering only the π system. It is furthermore a model representative of the interesting family of more extended carbon systems (*i.e.* polyenes, graphenes).

Full CI calculations within all orbitals or a large orbital subset are accessible for the model systems using double zeta + polarization basis sets. They provided the reference for the examination of van der Waals interactions of $(H_2)_2$ and the rotational barrier of C_4H_6.

6.2 Generation of CI spaces

The here-proposed strategy takes advantage of the generation of localized molecular orbitals (LMOs). Such a procedure, reported in the literature [2–5], has been applied for example to the accurate description of spin-coupled magnetic systems [6–8]. In this work, the localization procedure of Maynau *et al.* [2] is chosen since it generates occupied as well as virtual LMOs. The method produces either CASSCF or *Hartree-Fock* LMOs, and the latter were used in this work. Let us recall that the present approach bases the determinant inclusion/exclusion on considerations concerning the spatial distribution of electrons in the molecular structure. This is why LMOs are highly valuable for the present purpose. They offer a clear, valence-bond-type picture, impossible within the delocalized MOs framework [9, 10] (see Fig. 6.1).

First of all, let us clearly identify the framework of *FRACCIS*. Since the method is based on the use of localized orbitals, its limitations are related to the quality of these LMOs on one hand, and, on the other hand, to the average coordination number of the system. Concerning the quality of LMOs, they will be more local for covalent systems than for metallic ones. Concerning the coordination number, it increases with the dimensionality of the system. The dimensionality can take values of 1 (1D, *i.e.* hydrogen, H_n, or polyene chains), 2 (2D, *i.e.* graphene, nanotubes, fullerenes) or 3 (3D, *i.e.* diamond, metallic clusters). 1D systems present the lowest coordination number and thus the most favorable case to take advantage of the locality, 3D systems are the least favorable ones.

Similarly, if too large basis sets are employed, diffuse orbitals are included that have, after localization, important tails on neighbouring subunits. In that case, an analysis in terms of local excitations, as presented in this work, would be impossible, and one would not benefit from this kind of approach. The study of $(H_2)_2$ with a very

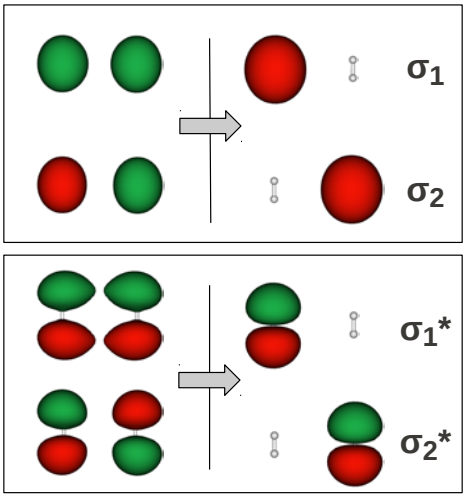

Figure 6.1
$(H_2)_2$ - Representation of the first four MOs (left) and LMOs (right). In contrast to the original MOs, the LMOs can be clearly identified as σ and σ^* orbitals on each H_2 molecule.

large basis set as in Reference [11] would be possible with this approach, but probably with no efficiency gain. *FRACCIS* is clearly devoted to large systems with basis sets not larger than double or triple zeta with polarisation which already correspond to a large domain of interest.

Let us recall that we pursue two important goals : (*i*) reducing significantly the number of determinants in the reference space, and (*ii*) analyzing systematically the calculated energy as a function of the CI space composition. In this way, the physical importance of successively appended determinants in the inspected molecular system can be deduced. We take thus advantage of the localized nature of the MOs to concentrate the numerical effort on physically relevant contributions to the CI expansion.

The strategy is exemplified on the analysis of the interaction energy within the H_2 dimer and then used to calculate the *cis*/*trans* rotational barrier of C_4H_6. At this stage, let me stress that the goal is not to obtain accurate quantitative results, such as reproducing the $(H_2)_2$ potential energy surface of Ref. [11], but rather to demonstrate the robustness of our approach on two 4-electron parent systems. However, we will see below that in the case of C_4H_6 an accurate value for the *cis*/*trans* rotational barrier could be obtained that compares well with values in the literature [12]. In the following, we consider both systems to be composed of two subunits. In the case of $(H_2)_2$, each subunit contains one of the two H_2 molecules. For the C_4H_6 molecule, each subunit contains one of the two C-C double bonds. Based on this practical division, we can split the excitations with respect to the Hartree-Fock ground state present in the FCI space into three major categories : (*i*) local correlation, *LC* (*e.g.* local FCI spaces on each subunit), (*ii*) dispersion excitations, *D* (*e.g.* simultaneous single excitations on each subunit), and (*iii*) single and double charge transfer excitations (*1CT* and *2CT*) from one subunit to the other. In section 6.3, I will show how our approach can be used to investigate the energetic impact of the three different types of excitations.

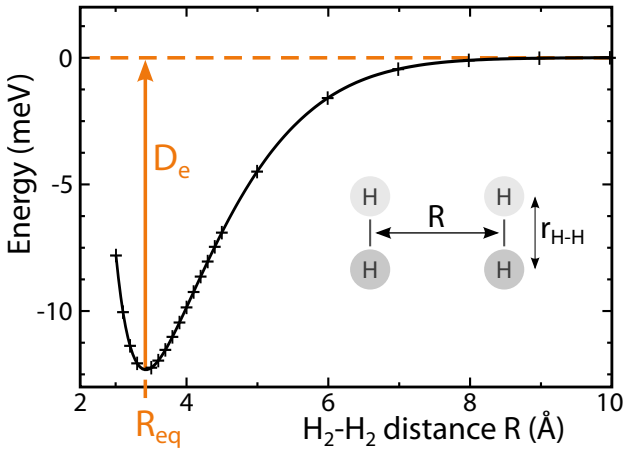

Figure 6.2
FCI energy (meV) of $(H_2)_2$ as a function of the inter-molecular distance R (Å). The intra-molecular distance r_{H-H} is kept constant at 0.74 Å.

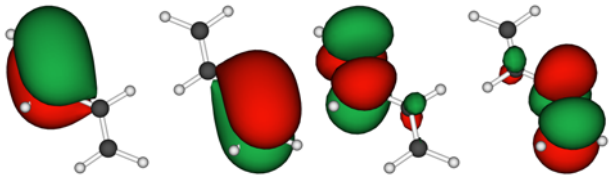

Figure 6.3
The π/π^* LMOs in *trans*-butadiene. The *cis*-conformer LMOs are very similar and not represented for simplicity.

All reference calculations were carried out within the 7.8 release of the *MOLCAS* package [13] using Large Atomic Natural Orbital (ANO-L) type basis sets [14]. The contractions were chosen in order to allow for full CI reference calculations and systematic inspections.

Van der Waals interactions in the H_2 dimer

The intra-molecular H-H distance was kept constant at a generally accepted value r_{H-H}=0.74 Å while the inter-molecular H_2-H_2 distance *R* was varied between 3.0 and 20.0 Å (see Fig. 6.2). All $(H_2)_2$ calculations were carried out within the C_1 point group using 2s1p contractions.

Cis/trans rotation barrier in butadiene

In strong analogy to the σ MOs in $(H_2)_2$, the π delocalized MOs of C_4H_6 can be transformed into an LMOs set (see Fig. 6.3) to trace its *cis*/*trans* rotation barrier D_{rot}. We used the C-C and C-H distances of Feller and Craig [12]. Since these distances differ only slightly between the *trans* and *cis* conformations, we investigated the rotation barrier with respect to the dihedral angle θ (see 6.4). All butadiene calculations were carried out in the C_s point group using 3s2p1d and 2s contractions on C and H atoms, respectively. Neither C core, nor σ(C-H) and σ(C-C) orbitals were correlated.

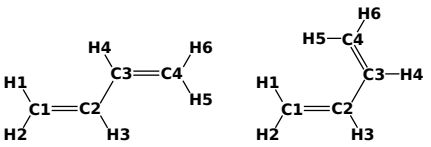

Figure 6.4
The two inspected *trans*- and *cis* conformers of butadiene corresponding to dihedral angle ($C_1C_2C_3C_4$) values $\theta = 180°$ and $\theta = 0°$.

CI space	1	2	3	4	FCI
nb. dets	18	14050	32050	929	36100
% dets(FCI)	0.1	39	89	3	100.0
D_e (meV)	2.1	8.0	12.2	11.2	12.3
% D_e(FCI)	17	65	99.7	90	100
R_{eq} (Å)	4.0	3.7	3.4	3.5	3.4

Table 6.1: $(H_2)_2$ - Dissociation energy D_e (meV) and equilibrium distance R_{eq} (Å) for different CI spaces 1-4 and the reference FCI.

6.3 Results and Discussion

6.3.1 Van der Waals interactions in the H_2 dimer

The reference values of the dissociation energy D_e=12.3 meV and the equilibrium distance R_{eq}=3.4 Å were obtained by a *full configuration interaction* (FCI) calculation. Different fragmentation strategies of the system were considered (CI spaces 1-4). The corresponding results are summarized in Tab. 6.1. In the minimal CI space 1, two fragments were defined - each of them containing the $\sigma/\sigma^\star$ orbitals of one H_2 molecule (a in Fig. 6.5). None of the other orbitals are included in this CI space. Following an intuitive picture of London type interactions, local correlation (*LC*) and dispersion contributions (*D*) were taken into account. More precisely, all determinants corresponding to the FCI calculation on each H_2 molecule were considered (*LC*). In addition, simultaneous single excitations on each molecule were carried out (D). The resulting values of D_e=2.1 meV and R_{eq}=4.0 Å are far from the FCI reference value D_e =12.3 meV and R_{eq} =3.4 Å. An extension of the CI space is obviously necessary.

Therefore, in CI space 2, the 2s and 2p virtual orbitals were included in each fragment (b in Fig. 6.5). The same type of excitations as in CI space 1 were used (*i.e.* those corresponding to a FCI on each molecule and dispersive excitations coupling the two). The significant shifts in the dissociation energy, D_e=8.0 meV, and equilibrium distance, R_{eq}=3.7 Å show that these orbitals bring about important local radial and angular correlation contributions.

At this stage, all determinants defining the FCI space are included in the calculation except those corresponding to the charge transfers between the two subunits. In a first step, only single charge transfer (*1CT*) excitations corresponding to H_2^+-H_2^- electronic distributions are added (CI space 3). The resulting equilibrium distance and dissociation energy are in excellent agreement with the reference values (D_e=12.2 meV, R_{eq}=3.4 Å). The ultimate step, that is the addition of double charge transfer (*2CT*) excitations, would restore the FCI space. The dissociation energy curves both of the above described CI spaces and the FCI are shown in Fig. 6.6.

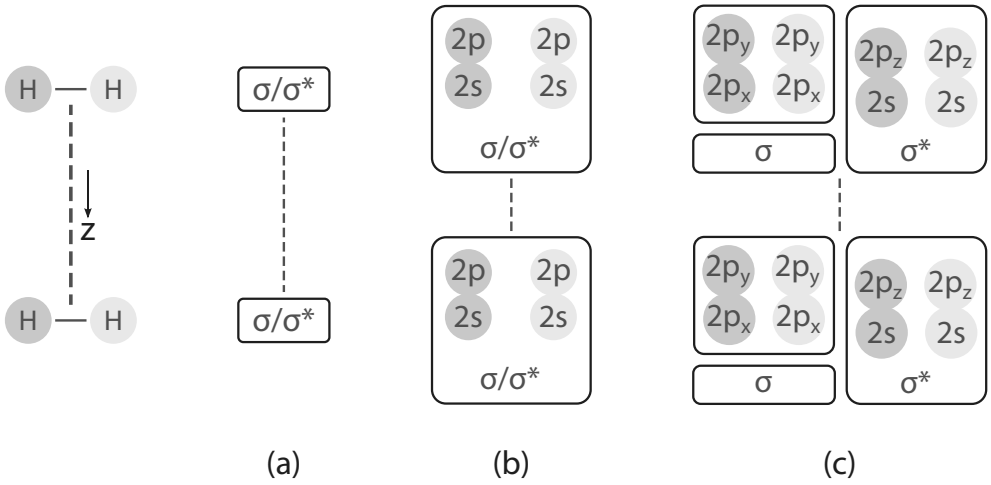

Figure 6.5: The fragmentation of the LMOs of $(H_2)_2$ using a 2s1p atomic basis set. The generation of CI spaces is based on fragmentation (a) for CI space 1, (b) for CI spaces 2 and 3, (c) for CI space 4.

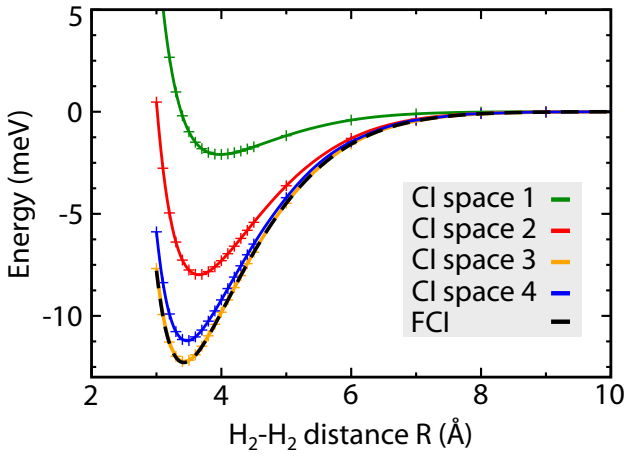

Figure 6.6
$(H_2)_2$ - Dissociation energy (meV) as a function of the inter-molecular distance R (Å) for different CI spaces 1-4 (see table 6.1) and the FCI reference calculation.

From this inspection based on 2 fragments we can conclude that the $2CT$ excitations can be neglected without significant loss of accuracy. Based on the corresponding CI space 3, 99.7% of the reference D_e are recovered. However, even when excluding all excitations of this type, the dimensions of the CI space with respect to the FCI space remain large (89 %).

Up to this point, all LMOs were divided into 2 fragments, each containing the LMOs of one H_2 molecule. In the following, our objective will be to gain a more differentiated insight and identify the orbitals that contribute most to the above-mentioned excitations. Therefore, a refined partitioning of the orbitals was considered by constructing smaller fragments. The σ orbitals were isolated in order to allow for specific excitations departing from these sets. Furthermore, the 2p manifold was split into the $2p_z$ and $(2p_x,2p_y)$ components since one can assume the behaviour of the $2p_z$ orbitals, pointing towards one another, to be different from that of the $2p_x$, $2p_y$

orbitals, parallel to one another (see Fig. 6.5). The $2p_z$ were gathered into separate fragments together with the remaining spherical type orbitals. These considerations lead to a partitioning into 6 fragments, 3 on each H_2 molecule (c in Fig. 6.5).

We took advantage of the distinction between the $2p_x/2p_y$ and the $2p_z$ orbitals in order to analyze the participation of the *1CT* and dispersive excitations along the x/y and z directions separately.

Based on the previous conclusions, all *2CT* excitations were excluded in CI space 4. Furthermore, two separate local FCI spaces were still considered. Finally, dispersive-like and *1CT* excitations were limited to the fragments containing $2p_z$ orbitals. This is the intuitive picture of dynamical correlation effects mostly occurring along the H_2—H_2 direction. Based on this CI space the equilibrium distance is slightly stretched to R_{eq}=3.5 Å (0.1 Å longer than the FCI value) and the dissociation energy is D_e=11.2 meV. In other words, 90 % of D_e is recovered based on a significant CI space reduction down to 3 %. Besides this considerable removal of deadwood determinants, we can easily apprehend the van der Waals interaction in the dihydrogen dimer with respect to the orbital orientation. More precisely, all orbitals are necessary to correctly describe the local correlation of each individual H_2 molecule. In contrast, the interaction between the two molecules can be mostly attributed to dispersion and charge transfer mechanisms involving spherical type orbitals (σ,σ^*,2s) and those pointing towards the respective neighbouring molecule ($2p_z$).

6.3.2 Cis/trans rotation barrier in butadiene

After the inspection of dispersive interactions in $(H_2)_2$, the focus was turned towards a covalently bound system, namely 1,3-butadiene. Evidently, the present strategy is expected to be particularly attractive for delocalized and extended π networks where a CAS approach becomes rapidly unmanageable. The targeted quantity in this compound is the *cis/trans* rotation barrier $D_{rot} = E_{\text{cis}} - E_{\text{trans}}$ for which a reference value of 14.7 kJ/mol was obtained from a CI calculation within a (4,36) subspace. The latter comprised the four π/π^* and the virtual 3p and 3d LMOs on each carbon atom. For this reference calculation as well as in the selected spaces presented below, the σ-type orbitals remain strictly doubly occupied. The reference energy compares very well with the one found by Feller and Craig [12] (14.6 kJ/mol).

In the following, the number of determinants and the *cis*/*trans* rotational barrier given by *FRACCIS* will be compared to the CAS(4,36)-CI reference values. Since our objective is not only to reproduce a reference energy difference but also to correctly treat the electronic correlation in the respective *cis*/*trans* conformations, its proportion $\%E_{corr}$ for both conformers will be added to the observed quantities.

In the quest of a pertinent CI space, the butadiene molecule was considered as resulting from two distinct subunits C_1C_2 and C_3C_4, each one containing the π/π^* and 3p/3d LMOs of the respective carbon atoms ((a) in Fig. 6.7). These orbitals were partitioned in a fashion similar to that in $(H_2)_2$. Namely, the π LMOs were isolated to allow for specific excitations and the π^* and atomic virtual 3p and 3d LMOs were

Table 6.2: Height of the *trans*/*cis* rotation barrier D_{rot} (kJ/mol) of butadiene, number of determinants and percentage of the correlation energy (%E_{corr}) for CI spaces 1-4 and the reference FCI(π/3p/3d).

CI space	1	2	3	4	FCI
nr. dets	676	868	1252	1636	198765
% dets(FCI)	0.3	0.4	0.6	0.8	100
D_{rot} (kJ/mol)	13.4	13.4	13.9	14.3	14.7
% D_{rot}(FCI)	91	91	95	97	100
% E_{corr}(*trans*)	89.5	90.4	91.3	92.5	100.0
% E_{corr}(*cis*)	90.4	91.2	91.9	92.8	100.0

also placed in distinct fragments, resulting in 12 fragments (*i.e.* 6 on each subunit as seen in Fig. 6.7). Four CI spaces were tested and the corresponding results are summarized in Tab. 6.2.

The first CI space contains the minimal excitations necessary to describe the full π system and both subunits. More precisely, CI space 1 consists of FCI spaces within (*i*) each subunit, and (*ii*) the π network (*i.e.* CAS(4,4)), discarding all excitations between those subspaces ((a) in Fig. 6.7). This CI space reproduces 91% of D_{rot} and roughly 90% of the individual correlation energies using 0.3% of the reference space.

In CI space 2, determinants corresponding to single charge transfer excitations (*1CT*) between the subunits are added to CI space 1. They correspond to charge distributions such as [subunit 1]$^+$–[subunit 2]$^-$ and are of two types. The first type consists of single excitations from the π LMOs to the 3p/3d LMOs of their first neighbour in the opposite subunit. In the second type, those charge transfer excitations are associated to single π/π^* excitations in order to take into account part of the repolarisation resulting from the charge transfer ((b) in Fig. 6.7). The addition of these excitations to CI space 1 does not improve the value of D_{rot} (91%) and slightly improves the description of electron correlation (%E_{corr}) in a differential manner (*ca.* 1% for both conformers). This indicates that these excitations play a similar role in both conformers.

Subsequently, different double-, triple- and quadruple excitations are included that resemble the dispersive type in the previous system since they couple excitations on opposite subunits. We shall recall the input format discussed in the previous chapter (*i.e.* $\texttt{f}_{\text{from}}$ $\texttt{f}_{\text{to}}$ `interexc`) to detail these excitations. One illustrative representative is given by the input data [π(1) π^*(1) 2 π(2) 3p(2) 2] where numbers in parenthesis represent the subunit to which the respective orbital belongs. One can see that such an input creates four couples (see Fig. 5.4) based on $\pi \rightarrow \pi^*$ excitations on the first, and $\pi \rightarrow$ 3p excitations on the second subunit. They are not only performed to the 3p but also to the 3d orbitals. The symmetric couplings (*i.e.* exchange of the subunit numbers in the above input) are also included. However, since these excitations incorporate the potentially numerous virtual orbitals, they were in a first step restricted to nearest-neighbour in the opposite subunit (CI space 3, Fig. 6.7 (c)).

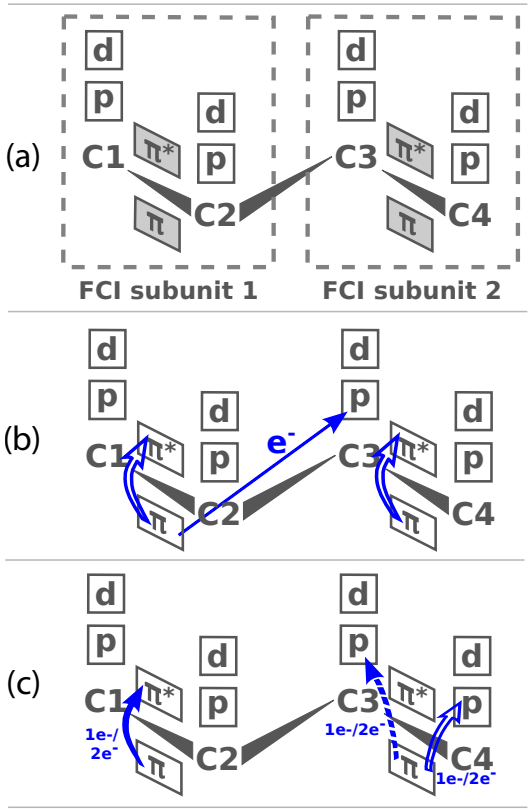

Figure 6.7: Fragmentation of the LMOs of C_4H_6 in 12 fragments contained in two practical subunits. Schemes of the different excitation types progressively included in CI spaces 1-4. (*a*) CI space 1 : FCI subunit 1 + FCI subunit 2 + FCI π/π^*. (*b*) CI space 2 : single charge transfers (*1CT*) including excitations of type $[\pi_{C1C2} \rightarrow (3p/3d)_{C3}]$ and $[\pi_{C1C2} \rightarrow (3p/3d)_{C3} \otimes \pi_{C1C2} \rightarrow \pi^*_{C1C2}]$ (central arrow and hollow left arrow) and $[\pi_{C1C2} \rightarrow (3p/3d)_{C3} \otimes \pi_{C3C4} \rightarrow \pi^*_{C3C4}]$ (central arrow and hollow right arrow) (*c*) dispersive-like excitations; CI space 3 : $[\pi_{C1C2} \rightarrow \pi^*_{C1C2} \otimes \pi_{C3C4} \rightarrow (3p/3d)_{C3}]$ (full and dashed arrow), CI space 4 : $[\pi_{C1C2} \rightarrow \pi^*_{C1C2} \otimes \pi_{C3C4} \rightarrow (3p/3d)_{C4}]$ (full and hollow arrow). For CI spaces 2-4 (figures (*b*) and (*c*)), the symmetric excitation types, obtained by exchanging atomic indices of subunit 1 and subunit 2, are not shown for clarity, but are also included.

In contrast to the previous *1CT* excitations, these dispersive-like excitations seem to play a differential role. That is, passing from CI space 2 to CI space 3, more correlation energy is recovered for the *trans* conformer (*ca.* 0.9%) than for the *cis* one (*ca.* 0.7%) indicating their slightly more important role in the *trans* conformation. This leads to an improved value of D_{rot} of 13.9 kJ/mol representing 95% of the reference value using 0.6% of the reference space.

Finally, the range of the previous dispersive-like excitations is extended up to the second neighbour in the opposite subunit (CI space 4, Fig. 6.7 (c)). Here as well, the *trans* conformer is more stabilized than the *cis* one (1.2 % *vs.* 0.9 % improvement with respect to previous CI space 3), leading to a value of D_{rot} of 14.3 kJ/mol, thus 97% of the reference value based on just 0.8% of the reference space. The dispersive-like excitations added in CI spaces 3 and 4 are distance dependent. Consequently, their contribution in the *trans* conformer is more important due to its shorter C_2-C_3 bond.

6.4 Conclusion

Two model systems, namely the weakly bound dihydrogen dimer, $(H_2)_2$, and the covalently bound butadiene, C_4H_6, have been chosen to test the FRACCIS approach. The systematic inclusion of determinants based on localized molecular orbitals has allowed a significant reduction of the CI space. For the H_2 dimer, the CI space is reduced down to 3 %, keeping the accuracy up to 90 % in the binding energy. For C_4H_6, the reduction of the CI space is even larger since less than 1 % of the determinants are kept within accuracy of 97 % in the *cis/trans* rotational barrier.

It seems that the case of C_4H_6 is more favourable than that of $(H_2)_2$. This phenomenon is probably due to the better locality of the *3p* orbitals of carbon than *2s* of hydrogen atoms, due to the larger spatial extension of the hydrogen 2s orbital. In spite of a larger distance between the two subunits, it was more difficult to reduce the size of the CI space and to maintain relevant results in the case of $(H_2)_2$. Indeed, trials with a larger basis set did not give satisfactory results since the localization tails are too important to allow for an efficient partitioning into fragments.

In contrast, covalent assemblies as represented here by C_4H_6 seem more appropriate. The best $(H_2)_2$ result is based on 3 % of the reference CI space. However, the worst result in the covalent C_4H_6 is already reasonably satisfactory [91 % of D_{rot}(FCI(π/3p/3d))] and demands only 1% of the reference CI space.

An upscaling in system size to hydrogen dimer chains (*i.e.* $(H_2)_2 \longrightarrow (H_2)_n$) and polyenes (*i.e.* $C_4H_6 \longrightarrow C_nH_{n+2}$) should be an interesting sequel of the present study. In those systems, the above mentioned problems would be present only between neighbouring H-H or C=C units, respectively. Furthermore, the above results for C_4H_6 show the expected distance dependence of dispersive excitation types (CI space 3 *vs.* 4). In the case of C_nH_{n+2}, the use of localized independent FCI spaces (*i.e.* including one C=C subunit each) in combination with some supplementary excitations to a small number of respective near neighbours is likely to give promising results.

Indeed, for large values of n, a linear scaling behaviour is expected. Furthermore, this approach should be relevant for large π systems like organic ligands in metal ion complexes.

In summary, the obtained results confirm that, in standard CI calculations such as FCI, but also CI of single and double excitations or other truncated CI method, a large majority of determinants have a vanishing contribution and play a non-significant role. This fact is not new, and has been an argument in favour of selected CI methods. However, these methods are difficult to manage as the development of efficient computational codes is a hard task, so that it is cheaper to use standard truncated CIs. A large number of unnecessary determinants are taken into account but, actually, the computation is less demanding in spite of the much larger dimension of the CI. The methodology presented in this work can be viewed as a step towards an efficient and systematic selected CI method thanks to the division of the system into fragments.

Bibliography

[1] Krah, T.; Ben Amor, N.; Maynau, D.; Berger, J.; Robert, V. *Journal of Molecular Modeling* **2014**, *20*.

[2] Maynau, D.; Evangelisti, S.; Guihéry, N.; Calzado, C. J.; Malrieu, J.-P. *J. Chem. Phys.* **2002**, *116*, 10060–10068.

[3] Boys, S. F. *Rev. Mod. Phys.* **1960**, *32*, 296–299.

[4] Edmiston, C.; Ruedenberg, K. *Rev. Mod. Phys.* **1963**, *35*, 457–464.

[5] Angeli, C.; Evangelisti, S.; Cimiraglia, R.; Maynau, D. *The Journal of Chemical Physics* **2002**, *117*, 10525–10533.

[6] Rota, J.-B.; Calzado, C. J.; Train, C.; Robert, V. *The Journal of Chemical Physics* **2010**, *132*, 154702.

[7] Oms, O.; Rota, J.-B.; Norel, L.; Calzado, C. J.; Rousselière, H.; Train, C.; Robert, V. *European Journal of Inorganic Chemistry* **2010**, *2010*, 5373–5378.

[8] Calzado, C. J.; Maynau, D. *The Journal of Chemical Physics* **2011**, *135*, 194704.

[9] Bories, B.; Maynau, D.; Bonnet, M.-L. *J. Comput. Chem.* **2007**, *28*, 632–643.

[10] Le Guennic, B.; Ben Amor, N.; Maynau, D.; Robert, V. *J. Chem. Theo. Comput.* **2009**, *5*, 1506–1510.

[11] Patkowski, K.; Cencek, W.; Jankowski, P.; Szalewicz, K.; Mehl, J. B.; Garberoglio, G.; Harvey, A. H. *The Journal of Chemical Physics* **2008**, *129*, –.

[12] Feller, D.; Craig, N. C. *The Journal of Physical Chemistry A* **2009**, *113*, 1601–1607.

[13] Karlström, G.; Lindh, R.; Malmqvist, P.-A.; Roos, B. O.; Ryde, U.; Veryazov, V.; Widmark, P.-O.; Cossi, M.; Schimmelpfennig, B.; Neogrady, P.; Seijo, L. *Comput. Mater. Sci.* **2003**, *28*, 222–239.

[14] Widmark, P.-O.; Malmqvist, P.-Å.; Roos, B. O. *Theoretica chimica acta* **1990**, *77*, 291–306.

7
Conclusion and Perspectives

The first part of this thesis is devoted to the inspection of Prussian Blue Analogues (PBAs) using established *ab initio* methods. In the NiFe Analogue, the interaction between 3d electrons, modeled by the exchange coupling constant J, has been calculated at CAS+DDCI level following the embedded cluster approach. The results show that a local deformation provokes a ferromagnetic to antiferromagnetic transition of considerable amplitude (ΔJ = -23.9 cm^{-1}). Furthermore, an increase in the electron hopping integral of ≈1.5 is observed over a small deformation range. In view of recent results confirming the high mobility of Na^+ ions in NiFe PBA, a coupling of ion mobility and increased hopping integral has been suggested.

Then, the attention has been turned to the CoFe PBA, known to exhibit a photomagnetic effect (PME), that is, an increase in magnetization upon red-light irradiation. In view of the complexity in this compound, the study has been focused on the spin transition on the Co(III) site, one of the ingredients in the PME. A vacancy-induced deformation has been evidenced by embedded cluster CASPT2 calculations. The Co(III) ion in the $[Co(III)(NC)_5(H_2O)]^{2-}$ cluster is displaced away from the equatorial plane towards the axial CN^- ligand. This deviation from the strictly octahedral symmetry is suggested to trigger the other PME component, namely the Fe-to-Co electron transfer. The treatment of the bi-metallic unit for an explicit inclusion of the metal-to-metal charge transfer is not part of this thesis but remains the ultimate goal. Particular attention in such a study should be paid to the mobility of the Rb^+ counter ion which is likely to stabilize the MMCT state.

The second part is dedicated to the development and implementation of the selected CI code *FRACCIS*. The approach works in the basis of localized molecular orbitals and seeks to render systems such as the CoFe PBA approachable by excluding physically irrelevant determinants from the reference space. In this way, the complete

space can be reduced down to a small number of physically vital determinants that built the basis for further inclusion of dynamical correlation. The code as for now does not compete with the computation time of existing FCI or truncated CI algorithms but comparative tests after the current development stage will be necessary to ultimately evaluate the performance. In any case, selected CI approaches demand per se more costly verification steps than standard truncated CIs. However, this is counterbalanced in the present approach by the fact that complicated architectures (*i.e.* numerous open-shells), currently inaccessible to a CASSCF treatment, come into reach. Furthermore, it shall be emphasized that the code offers the possibility to deduce, from their energetic impact, the physical significance of certain excitations or excitation classes in the system under study.

Within this work, the implementation of *FRACCIS* has been completed and tested on two model systems, namely the dihydrogen dimer, $(H_2)_2$, and the butadiene molecule, C_4H_6. The results are promising. In the case of $(H_2)_2$, the systematic inclusion of excitation classes (*i.e.* local, charge transfer, dispersive) indicates the negligible impact of double charge transfer excitations on the obtained dissociation energy. Furthermore, a directional preference of single charge transfer and dispersive excitations is observed. Most of all, 90% of the FCI reference value have been reproduced using only 3% of the full space. An even more significantly reduced CI space (1% of the CAS(4,36)CI reference space) has been sufficient to recover 97% of the *cis/trans* rotation barrier of C_4H_6. These results encourage the study of more extended systems such as polyenes, C_nH_{n+2}, work in that direction is under way. In such low-dimensional systems, one could adopt a strategy that moves closer to physics site-oriented approaches. More precisely, the computational effort could be focused on individual C=C units and then be supplemented by restricted excitations between them.

In the above applications, *FRACCIS* has been successfully employed to select the determinants for a CI calculation. An optimization of the orbitals has just recently been included in the implementation and has allowed first reproduction of CASSCF results.

At short term, this MC-SCF version of the code, already available, shall be used to analyze small systems. One possible targeted problem are small Beryllium chains, Be_n (n=3,4,5) that demand a multi-determinantal treatment and constitute a challenge for quantum chemical method. It has been shown that small active spaces are insufficient but when large active spaces are used severe limitations to the size of the chain that can be treated are imposed. Excitations could be focused on neighbouring atoms to gain in efficiency and insight.

Currently, it is technically necessary to divide all orbitals of the system (inactive, active, virtual) into fragments. However, since the maximum number of treatable total orbitals is 256, reasonable MC-SCF spaces are already possible at this stage. Work is in progress to extend the available active space further by placing inactive and virtual orbitals outside the fragments.

At long-term, the initial target system CoFe PBA shall be analyzed. In this case,

a division into ten fragments is likely to be a useful starting point : on each metal, the σ-type, t_{2g}, e_g and 3d' orbitals are placed in 4 respective fragments. The bridging ligand π and π^* orbitals are added in 2 separate fragments, as represented below.

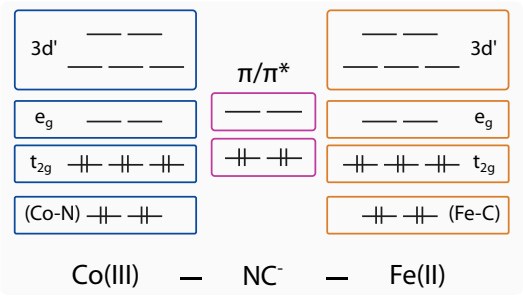

Such a partitioning would allow for a thorough treatment of each metal site and the addition of individual excitations between them. Besides, recent studies in the CASSCF framework quantify the substantial improvement of excitation energies based on a (quasi-)state-specific description of excited states compared to state-average results. The here-proposed method could open a route towards an improved description of excited states, such as the MMCT state in CoFe PBA, by generating adapted starting orbitals based on well-suited MC-SCF spaces.

Finally, a wide range of intriguing properties in molecular systems can be traced back to the underlying electron-electron interaction. In view of its fundamental role, the accurate description of the instantaneous interaction and the careful decryption of the resulting effects are indispensable. However, the physical and computational difficulty grows with more and more Gordian targets. The current work can be seen as a contribution to the ongoing efforts towards a rational analysis of electron correlation in complex systems.

Appendix

Complete input example for a *FRACCIS* calculation of the $(H_2)_2$ divided into two fragments. The different preceding runs are separated by horizontal lines.

```
Project='H22'
CurrDir=$PWD
WorkDir=$TMP
export PATH=$PATH:/home/krah/cost2/bin
export Project WorkDir CurrDir
cd $WorkDir
echo "Workdir="$WorkDir
echo "CurrDir="$CurrDir
```

```
molcas $CurrDir/sewin > $CurrDir/output
```

```
molcas $CurrDir/scfin » $CurrDir/output
cp $WorkDir/$Project.scf.molden $CurrDir
molcost « EOF » $CurrDir/output
 &cost prefix='H22.',ymo=t /
EOF
cp H22.ScfOrb $CurrDir
cp H22.ScfOrb INPORB
```

```
dolo » $CurrDir/output
proj_scf « EOF » $CurrDir/output
 &pscf prefix='H22.',calcul='SCF',scf='H22.ScfOrb' /
EOF
cp NONORLOC_scf NONORLOC
schmudort « EOF » $CurrDir/output
 &ort /
EOF
cp LOCORB INPORB
```

```
molcas $CurrDir/../../DOLO_MOTRAIN » $CurrDir/output
molcost « EOF » $CurrDir/output
```

```
 &COST
 prefix='H22.'
 FROZEN= 0,
 DELETE= 0,
 FERMI= 2,
 /
EOF
casdint « EOF » $CurrDir/output
 &casdint prefix='H22.'  /
EOF
```

```
fraccis « EOF > $CurrDir/out.fraccis
 &fraccis prefix='H22.',nfrag=2,is0=1,ms2=0,nodist=t /
FRAGMENT 1
1 3 5 6 9 10 13 14 17 18
2000000000 exc=2
FRAGMENT 2
2 4 7 8 11 12 15 16 19 20
2000000000 exc=2
end
interfrag
1 2 2
2 1 2
end
EOF
```

List of Figures

List of Tables

Remerciements

Je ne savais pas à quoi m'attendre avant de commencer cette thèse. Un nouvel endroit, un sujet en partie nouveau, des nouveaux collègues. Il y avait évidemment les deux cotés de la médaille : excitant et inquiétant. Le fait que cette aventure est devenue une expérience très riche à la fois au niveau scientifique et humain est grâce aux personnes que j'aimerais remercier ici.

Tout d'abord, j'aimerais remercier Vincent Robert, Nadia Ben Amor et Daniel Maynau qui m'ont guidé, soutenu, motivé et nourrit scientifiquement pendant ce travail. Merci, Chef-ele, pour tes explications pédagogiques grâce auxquelles j'ai souvent vu des connections entre différents sujets que je n'avais pas forcément vu avant. Merci, Nadia, pour ta patience, ton enthousiasme et bien sûr tout un monde de programmation que j'ai découvert grâce à toi à la base. Merci, Daniel, d'avoir pris mes questions plus ou moins pertinentes toujours avec un esprit ouvert (je me rappellerai toujours de ton constat : "La physique, c'est de savoir ce qui est important."). Et bien sûr merci à vous trois pour tout les moments et toutes les discussions en dehors de la science !

"Dank je wel", "Merci", "Gracias" et "Dangge" à Arjan Berger, Nicolas Suaud, Alex Domingo et Benjamin Meyer avec qui j'ai eu le plaisir de travailler directement et discuter à Toulouse et à Strasbourg.

Le travail, ce n'est pas uniquement les collaborateurs immédiats mais aussi tous les collègues autour. L'ambiance de travail dans les deux labos étaient très agréable. Que ce soient les pique-niques du mardi à Toulouse ou les bières à la cafète à Strasbourg, nous avons partager des bons moments. Merci à tous !

Je tiens également à mentionner Sylvie et Paola, qui étaient toujours là, prêtes à aider quand il y avait besoin de quelque chose... merci !

Et le travail, ce n'est pas tout... merci beaucoup à Thiago, Samy, Clio pour tout ces moments sportifs et non-sportifs que nous avons pû partager.

Je später die Danksagungen... meinen Eltern habe ich viel von der Neugier, Ruhe, und Ausdauer zu verdanken, die für eine Doktorarbeit nötig sind. Vor allem habt ihr mir beigebracht, mich nicht von etwas neuem abschrecken zu lassen und mir das sichere Gefühl gegeben, dass ich mich immer auf euch verlassen kann. Dafür danke ich euch von ganzem Herzen.

Un grande "Grazie" anche a il mio fratello Nils e la mia cognata Ilaria. Grazie a voi so che la gioia della vita è piu importante che il sonno !

Mein letzter Dank geht an meine liebste Iza. Du hast mich immer getragen.

Tim KRAH

Développement et application d'une méthode d'Interaction de Configurations sélectionnées : des interactions dispersives au magnétisme photo-induit dans les Analogues du Bleu de Prusse

Résumé

Dans une première partie, la structure électronique de deux membres de la famille des Analogues de Bleu de Prusse (ABP) a été inspectée à l'aide de méthodes basées sur la fonction d'onde. Dans l'ABP NiFe, un changement du couplage magnétique a été mis en évidence lors d'une déformation structurale locale. Basé sur les résultats obtenus pour l'ABP CoFe, un rôle clé dans le processus photomagnétique observé dans ce matériau est attribué aux lacunes cristallines.

Dans une deuxième partie, un développement méthodologique a été mené jusqu'à l'implémentation de la méthode *FRACCIS* (FRAgmented Contracted Configuration Interaction of Single excitations). Elle permet de concentrer l'effort numérique sur un petit nombre de déterminants physiquement importants. De plus, elle constitue un outil d'analyse pour mesurer l'importance de certaines excitations dans le système inspecté. L'application à $(H_2)_2$ et C_4H_6 montre qu'une réduction majeure de l'espace d'IC est possible en gardant une bonne précision par rapport aux valeurs de référence. Ce travail contribue aux efforts vers l'analyse rationnelle de la corrélation électronique.

Mots clés : Corrélation électronique, Interaction de Configurations sélectionnées, MC-SCF, Photomagnétisme, Analogues du Bleu de Prusse, Dispersion

Résumé en anglais

In the first part, the electronic structure of two members of the family of Prussian Blue Analogues (PBA) has been inspected using wave function-based methods. The NiFe PBA exhibits a change of the magnetic coupling under a local structural deformation. Based on the results obtained for the CoFe PBA, a key role in the photomagnetic process observed in this material is attributed to the crystal vacancies.

In a second part, a methodological development has been carried out and has lead to the implementation of the *FRACCIS* method (FRAgmented Contracted Configuration Interaction of Single excitations). It allows to concentrate the numerical effort on a small number of physically relevant determinants. Furthermore, it constitutes an analysis tool to measure the importance of certain excitations in the inspected system. The application to $(H_2)_2$ et C_4H_6 shows that a major reduction of the CI space is possible while keeping good accuracy with respect to reference values. This work contributes to the efforts towards a rational analysis of electronic correlation.

Keywords : Electronic correlation, Selected Configuration Interaction, MC-SCF, Photomagnetism, Prussian Blue Analogues, Dispersion